UNIVERSITY OF CALGARY

MULTIPHASE SIMULATIONS WITH LATTICE BOLTZMANN SCHEME

by

Alexandr Kuzmin

A THESIS

SUBMITTED TO THE FACULTY OF GRADUATE STUDIES

IN PARTIAL FULFILLMENT OF THE REQUIREMENTS FOR THE

DEGREE OF DOCTOR OF PHILOSOPHY

DEPARTMENT OF MECHANICAL AND MANUFACTURING ENGINEERING

CALGARY, ALBERTA

December, 2009

UNIVERSITY OF CALGARY

FACULTY OF GRADUATE STUDIES

The undersigned certify that they have read, and recommend to the Faculty of Graduate Studies for acceptance, a thesis entitled "Multiphase simulations with Lattice Boltzmann Scheme" submitted by Alexandr Kuzmin in partial fulfillment of the requirements for the degree of Doctor of Philosophy.

Supervisor, Dr. A.A. Mohamad
Department of Mechanical and Manufacturing Engineering

Dr. O. Vinogradov
Department of Mechanical and Manufacturing Engineering

Dr. L. Sudak
Department of Mechanical and Manufacturing Engineering

Dr. J. Azaiez
Department of Chemical Engineering

External Examiner, Dr. S. Mitra
Department of Mechanical Engineering
University of Alberta

Date

Abstract

This work thoroughly analyzes one of the most popular multiphase models, the Shan-Chen model, for the lattice Boltzmann equation. The advantages and disadvantages are presented. This work extends the applicability of the Shan-Chen model to simulate different phenomena and presents alternatives to some of disadvantages. The model's stability limit is improved by applying the Multiple-Relaxation Time (MRT) collision operator. The surface tension effect is decoupled from the equation of state with the help of the multirange potential. A few schemes for the multirange potential are presented, which perform better with the rotational isotropy. Thus, the spurious current effects are decreased, which improves the stability. The generalized Shan-Chen model allows one to incorporate anisotropic phenomena with different momentum flux pressures. The model is able to simulate the ferro-fluidics. Finally, the work is concluded with suggestions as to how to use the Shan-Chen model.

Acknowledgements

This work couldn't have been accomplished without the help of many people. I would never be able to fully express my gratitude to my wife and my daughter, who were helpful, supportive and allowed me to spend some extra time on my studies. The same goes to my friends and the small Russian community in our office and even outside the office. I'd like to mention Victor Prosolin who opened for me a new world called Linux. His patience to explain all the things to a Linux dummy was excessive.

My thanks go to Dr. Mohamad, who was all the time supportive during my studies. His willingness to help whenever I had problems are fascinating. In fact, Dr. Mohamad is a great problem solver. His advice was very helpful.

My special thanks go to Dr. Succi and his team, including Dr. Sbragaglia and Dr. Falcucci, who helped me substantially in a few key moments, especially in the beginning of my studies. The collaboration with them was always joyful and productive.

My thanks go to Dr. Ginzburg, whose genius inspired me to begin the research on stability. Our communication includes a thousand questions and answers, and she was always keen to help me understand a few more things about LBM. Her patience to explain some issues was unbelievable, taking into account the fact that she sometimes explained the same thing five times in row.

The Alberta Ingenuity Fund supported me through all my studies. Without their financial support I wouldn't have been able to meet all the wonderful people in the lattice Boltzmann community. NSERC is also acknowledged for their financial support.

My final thanks go to all the people, whom I don't mention here due to space requirements (it can be ten pages of names). There are many of them who are actively involved in my life and stay behind it.

Table of Contents

List of Tables

List of Figures

Nomenclature

$\boldsymbol{\mathcal{H}}$	The Hermite polynomials tensor
$\boldsymbol{\mathcal{P}}$,$\boldsymbol{P}$	The momentum flux tensor used in the Navier-Stokes equation
$\boldsymbol{\xi_i}$	The velocity abscissae
$\boldsymbol{\xi}$	The microscopic velocity associated with the distribution function $f(\boldsymbol{r}, \boldsymbol{\xi}, t)$ used for the Hermite polynomial expansion
$\boldsymbol{a}$	The Hermite polynomials series expansion coefficient tensor
$\boldsymbol{c_i}$	The non-dimensional velocity abscissae to match the rectangular grid
$\boldsymbol{F}$	The local force
$\boldsymbol{r}$	The space coordinates vector
$\boldsymbol{u}$	The local macroscopic velocity
$\boldsymbol{v}$	The microscopic velocity associated with the probability distribution function $f(\boldsymbol{r}, \boldsymbol{v}, t)$
ϵ	The Knudsen number
$\omega = \frac{1}{\tau}$	The non-dimensional relaxation rate
ψ	The pseudopotential for the Shan-Chen model
ρ	The density recovered from the distribution function
ρ^{eq}	The density recovered from the equilibrium distribution function
τ	The non-dimensional relaxation time

θ	The non-dimensional temperature
ε	The local macroscopic energy
A_{ij}	The MRT matrix
a_{ij}	The weight coefficient for the discretization schemes
Bo	The Bond number
D	The space dimension
f	The probability distribution function
f^{eq}	The equilibrium distribution function
G	The temperature-like parameter for the Shan-Chen model
k	The Navier-Stokes compliant surface tension
M	The mass source
Ma	The Mach number
w_i	The weight associated with the velocity $\boldsymbol{c_i}$

Chapter 1

Introduction

The Lattice Boltzmann method (LBM) was first introduced by McNamara and Zanetti in 1988 to overcome the shortcomings of cellular automata (McNamara and Zanetti, 1988; Wolfram, 1986). Since then, the method reached maturity and has been widely used in industrial and academic works (Succi, 2001). The LBM is originally based on the lattice gas automata (Higuera and Jimenez, 1989) and only being able to capture the hydrodynamics effects (Luo, 2003). Since then, the lattice Boltzmann method has become a powerful computational fluid dynamics (CFD) competitor with the ability to simulate not only hydrodynamics but also thermal flows (Ansumali et al., 2003; Yuan and Schaefer, 2006b; Zhang and Chen, 2003), micro-flows (Ansumali et al., 2006; Wu et al., 2008; Yu et al., 2007), ferrofluids (Flament et al., 1996; Lavrova et al., 2004; Rosensweig, 1997), multiphase flows (Luo, 1998; Rothman and Keller, 1988; Shan and Chen, 1994; Swift et al., 1995). In the presence of complex physical effects such as turbulence, multi-phase flows, flow of oil and gas through porous material, flow around surfaces with complex geometries or blood flow with deformable particles, the solution of the basic Navier-Stokes equations becomes difficult or impractical. For example, on a micro-scale level with the Knudsen number order of unity, the continuous mechanics approach is not appropriate. On the other hand, the micro-scale calculations for such systems based on the Molecular Dynamics approach (MD) are computationally extremely demanding. The Lattice Boltzmann Method (LBM), which focuses on the meso-scale, may be the best choice for such complex flow problems, being able to capture macro- and micro-flows.

LBM utilizes particles based on the probability density function values. All particles are moving in certain directions, needed to restore the macroscopic picture. For exam-

ple, in the simplest two-dimensional case, only six directions are required to recover the Navier-Stokes equations with satisfactory accuracy. The particles propagate and interact with each other in specified nodes organized in a rectangular grid. It is extremely interesting that such a simple approach at the meso-scale can restore the Navier-Stokes equation including the non-linear advection term which plays a dominant role in fluid dynamics, especially for turbulent flows.

The LBM utilizes the probability distribution function to find a particle at a certain time and at a certain location. Therefore, the method tracks not a separate molecule, as in MD simulations, but a whole ensemble of molecules, resulting in the probability distribution function. The integration of the probability distribution function in velocity space readily provides macroscopic variables such as: density, velocity or shear stress. The LBM can be interpreted as a particle method in comparison with the continuity methods, though being able to restore continuity macroscopic variables. The method is the bridge between continuity approaches as in all conventional CFD methods, and computationally demanding MD simulations. In Molecular Dynamics Simulation (MD), the microscopic scale of simulations is visible only for extremely small systems due to computer resource demands. It is impractical to apply MD for macro-scale problems. On the other hand, it is very difficult to use conventional computational fluid dynamics for complex flow problems due to the difficulties of tracing moving boundaries, modeling interaction between phases, handling surface tension at the macro-scale level, etc. The LBM covers the region between the micro and macro worlds (the so-called mesoscopic world) and takes advantage of both previously mentioned methods. This allows the combination of the best of both methods: the geometrical flexibility of particle methods with the large-scale resolution of continuum methods. Also, the kinetic nature of the LBM simplifies the incorporation of many physical phenomena into the LBM because they can be always described on the molecular level.

Nowadays, the LBM has all the attributes common for highly developed CFD methods, as the ability to simulate multiphase models (Luo, 2003; Nourgaliev et al., 2003), pressure-velocity (Zou and He, 1997) and off-lattice boundary conditions (Chun and Ladd, 2007; Ginzburg and d'Humières, 2003; Yu et al., 2003), turbulence simulations with LES method (Krafczyk et al., 2003), refined grid and multigrid approaches (Tölke et al., 2006), GPU based simulations (Tölke and Krafczyk, 2008), ferrohydrodynamics (Dellar, 2005; Falcucci et al., 2009), colloids (Adhikari et al., 2005; Nash et al., 2008), even the fusion with different CFD methods, such as the level set method (Thömmes et al., 2007), the finite volume method (Xi et al., 1999), etc.

However, despite the many advantages and simplicity, there are many questions in LBM that are still open. There is no fully developed theory for energy transfer, compressible flows, or combustion. The main disadvantage of the LBM is that the lattice Boltzmann equation is able to simulate the hydrodynamics in a slightly compressible limit (Yu et al., 2003), though some modifications are established (Shan et al., 2006) to extend the limit of compressibility. Many multi-phase flows simulations cannot perform calculations for the large gas-liquid density ratios or reproduce the proper dynamic contact angle behaviour. LBM multi-phase model cannot simulate the systems with large viscosity ratio fluids. Also, there are many unresolved problems for delivering LBM as a computational tool for applications. Often LBM fails in terms of robustness and stability when it is applied to real industrial problems simulations. That certainly restricts the application of LBM for industrial problems. During the last few years many milestone steps were taken to resolve these issues, nevertheless a few questions remain to be solved.

This research addresses one of these issues and is mainly concentrated on the multiphase phenomena and problems related to it. First, we give the literature review for the lattice Boltzmann equation (LBE) and its current stage of development, followed by the literature review on multiphase phenomena. Then we state problems associated

with multiphase simulations in the LBM. One of the most popular multiphase models (Shan-Chen model) is examined, and the improvements for stability and gas-liquid ratio through the Multi-Relaxation Time (MRT) model are presented. Also, a few extensions of the Shan-Chen model are proposed in this work. The generalized Shan-Chen model is able to simulate the anisotropic phenomena, usually presented in ferro-fluidics. The multirange model is able to separate the equation of state from the surface tension term, which are coupled in the original Shan-Chen model. The model gives the opportunity to simulate multiphase phenomena with controlled interface thickness. Also, it is based on a better numerical stencil and improves stability. Few findings are presented, such as the MRT force incorporation, and the consistent approach to construct the equilibrium distribution function.

Chapter 2

Literature review

The Lattice Boltzmann method originated from cellular gas automata (Wolfram, 1986), which is originally based on boolean logic. A new version of the lattice Boltzmann method was introduced by McNamara and Zanetti (1988) and was based on the probability function. This allowed one to overcome most problems associated with staggered invariants, non-Galilean invariance, stability simulation sensitivity (Succi, 2001). It was found that LBM can be obtained by two approaches - from discretizing the kinetic equation through the Bogolubov scheme and prescribing the conservation laws by Gauss quadrature integration (He and Luo, 1997; Shan et al., 2006) or by considering the finite difference equation, which LBE appears to be, and prescribing macroscopic quantities to the equilibrium distribution function. The role of the LBE is in the so-called mesoscopic range, where the method is able to capture discontinuous phenomena, where the Knudsen number is close to unity, without involving high computational resources as Molecular Dynamics (MD) does, and continuous mechanics and hydrodynamics (Knudsen number is less than unity). In fact, the method doesn't compete with the two well-established methods (CFD and MD) but bridges the gap between them.

2.1 Single Relaxation Time (SRT) and Multi-Relaxation Time (MRT)

The Lattice Boltzmann Equation (LBE) is divided into two parts: streaming and collision. While streaming is the same for all possible methods, and involves moving the particle from one lattice node to another, the collision operator can be modified and brings advantages and disadvantages for the method.

The Bhatnagar-Gross-Krook (BGK) method known as the Single-Relaxation Time method, was introduced by Qian et al. (1992), the latter being based on the original idea of Bhatnagar et al. (1954). The method is easy for understanding and comprehension, and is still the most popular among the LBM community. The method utilizes only one relaxation time parameter, ω, in the collision operator. The disadvantage of the formulation is that the macroscopic parameters depend on ω and the lattice formulation (velocities set). For instance, the BGK restores the same bulk and dynamic viscosities. The BGK model limits the porous media flow simulations, as they are viscosity dependent (ω parameter). Therefore, to be flexible with macroscopic parameters one should introduce richer velocities sets which are computationally costly or more complicated collision operators, such as two-relaxation time (TRT) or multi-relaxation time (MRT) collision operators. For instance, the minimal model to simulate Navier-Stokes equation in the two-dimensional case requires 6 velocities, but to simulate thermal flow one needs more velocites (Teixeira et al., 2000) or introduction of the coupled thermal lattices (Yuan and Schaefer, 2006b; Zhang and Chen, 2003).

In 1992, the Multi-Relaxation Time method based on the original matrix formulations of the Lattice Boltzmann method (Higuera and Jimenez, 1989; Higuera et al., 1989) was introduced by d'Humières (1992) bringing new advantages to the method, such as the Prandtl number different from unity, variable bulk and dynamic viscosity (d'Humières et al., 2002). The collision operator depends not on one parameter but on several parameters ω_0,...,ω_{n-1}, where n is the number of lattice velocities. Notice that taking all parameters equal each other is equivalent to the SRT collision operator formulation. The MRT model represents the collision operator in the matrix form. Hence, all moments of Navier-Stokes equation (density, current fluxes), bulk viscosity, local viscosity and Prandtl number can be controlled (d'Humières, 1992; d'Humières et al., 2002; Lallemand and Luo, 2000). The proper implementation of the MRT method is 15% to 20% slower

than the SRT method but it restores the proper hydrodynamics of the problem (Lallemand and Luo, 2000). For instance, the BGK model introduces ω-dependent solutions for the boundary conditions (Ginzburg, 2005a) for the velocity profile in the Poiseuille flow with Knudsen number close to unity (Luo, 2009b). The advantages also include low viscous multiphase flow (Premnath and Abraham, 2007), better symmetry for lid-driven cavity (Wu and Shao, 2004), improved boundary conditions (Ginzburg and d'Humières, 2003). Moreover, some models do not exist in the BGK variant as the D3Q13 which is the minimal model for three-dimensional case (Tölke and Krafczyk, 2008). Also, the MRT method has been applied to a few simulations of multiphase phenomena and it improved the available simulation range of viscosities (McCracken and Abraham, 2005), as well as obtaining better contact angle behaviour (Pooley et al., 2009).

The compromise between the simplicity of the BGK model and MRT model is the Two-Relaxation Time method (TRT) (Ginzburg, 2005b). The method is well developed for the advection-diffusion equation by Ginzburg. In comparison with the MRT, where a thorough analysis is not presented and the tuning of parameters is usually not well developed, except for some simple flows (Lallemand and Luo, 2000), the TRT gives comprehensive picture of tuning of parameters for stability (Ginzburg et al., 2009; Kuzmin et al., 2009), boundary conditions (Ginzburg, 2005a), and approximation errors for the advection-diffusion equation (Ginzburg, 2008). It was found that all the errors depend on the specific combination of the two relaxation times. This number equals:

$$\Lambda = \left(\frac{1}{\lambda^+} - \frac{1}{2}\right)\left(\frac{1}{\lambda^-} - \frac{1}{2}\right). \tag{2.1}$$

Taking $\Lambda = \frac{3}{16}$ eliminates the viscosity dependent boundary location for the bounce-back boundary conditions. The optimal stability is controlled by $\Lambda = \frac{1}{4}$. Taking $\Lambda = \{\frac{1}{12}, \frac{1}{6}\}$ eliminates the third-order and the fourth-order spatial errors. While λ^- is set by initial condition, λ^+ is a free parameter to be tuned to achieve accuracy, stability or the exact

boundary location.

There has been progress in understanding of the role of free parameters in the MRT and TRT models. However, many issues still need to be understood, especially the impact of parameters for the multiphase models. One of the topics which will be discussed in the present work is the MRT implementation for the multiphase model.

2.2 Multiphase models

One of the first models for mutliphase simulations implemented for the LBE was inherited from the lattice gas automata colour model (Gunstensen et al., 1991; Rothman and Keller, 1988). The model utilizes two distribution functions representing the red and blue fluids. Each of the distribution functions is run by the usual Lattice Boltzmann implementation. Then, at every time step the interface between two fluids is calculated. The surface tension is applied to the fluids as the external force. The original method allows one to obtain sharp interfaces but it is computationally demanding due to calculation of the surface location and surface tension terms at every time step. Also, the model is unstable for large fluid density ratios due to the different sound speeds in the media (Kehrwald, 2002) and spurious currents. However, a few modifications allow one to speed up the method, i.e. Ahrenholz et al. (2008), Ginzburg and Steiner (2002), and Kehrwald (2002) reformulated the Gunstensen scheme to obtain a better performance and introduce the MRT based color model.

Shan and Chen (1994) introduced the pseudopotential scheme, which mimics the multiphase behaviour. The authors used the shifting velocity to implement the force term (to be discussed later), which is the function utilizing the nearest node neigbours densities. The method is easy to implement, and is able to simulate different multiphase problems, such as the droplet formation (Kuzmin et al., 2008), breakup of a droplet

in a wind tunnel (Sehgal et al., 1999), micro-droplet formation in the T-shape channel (Yu et al., 2007), and thermal multiphase flow, such as boiling processes (Zhang and Chen, 2003). Though there are problems associated with Shan-Chen model, such as non-thermodynamic behaviour (Maxwell reconstruction involves pseudopotential but not densities, as required), additional spurious currents around the droplet, which eventually destroy the stability, gas-liquid ratio is up to $60 - 70$, the surface tension and the equation of state dependence on one parameter G. A few modifications appeared for the Shan-Chen model, such as elimination of spurious currents through better discretization introduced as multirange potential (Kuzmin and Mohamad, 2009; Sbragaglia et al., 2007; Shan, 2006), which allows one to also separately control the parameters in the equation of state and the surface tension term. The utilization of different equation of states, such as Peng-Robinson EOS, Carnahan-Sterling EOS, in the Shan-Chen pseudopotential allows one to decrease spurious currents, obtain a gas-liquid ratio up to a few thousand, and obtain better thermodynamically consistent behaviour (Yuan and Schaefer, 2006a).

Swift et al. (1995) introduced the free energy model. The model is based on the free-energy functional originating from the original idea of Landau and Lifshitz (1987). The model is able to simulate not only gas-liquid systems but binary liquids with different viscosities (Swift et al., 1996). The model can't simulate large gas-liquid density ratio problems and large viscosity ratio. Initially, there were problems with the Galilean invariance (Nourgaliev et al., 2003), which states that results should not depend on the velocity of the system as a whole. This was later solved by the introduction of additional terms to the equilibrium function (Pooley et al., 2008). The model is thermodynamically consistent though it introduces spurious currents around the droplet which can be solved by better discretization of the surface tension term (Pooley and Furtado, 2008). The model is able to simulate difficult phenomena, such as fingering between two fluids (Ledesma-Aguilar et al., 2007). Also, a few modifications of the model are introduced

allowing one to achieve large gas-liquid density ratios (Zheng et al., 2006).

Later on, He et al. (1998) used a series expansion of the intermolecular potential to obtain a proper force term accounting for multiphase behaviour. Two sets of distribution functions were used for tracking phase interface, pressure and velocity fields. The model is close to the original idea of the Shan-Chen model though the equation of state is separated from the surface tension term. The model can't simulate the large gas-liquid density ratio problems and experiences the numerical instabilities associated with the "stiffness" of the collision operator (Succi, 2001). Lee and Lin (2003) introduced a pressure-based multiphase model which allows one to obtain large gas-liquid ratios but is difficult due to the implicit implementation of the LBE. Luo (1998) introduced a finite density model based on the kinetic description of liquids or dense gases. However, the model is not well accepted.

2.3 MRT and Multiphase

Almost from the very beginning of the introduction of multiphase models, they were used in conjuction with the MRT collision operator. Almost every multiphase model was simulated using the MRT collision operator. These include the color model based simulation for the Poiseuille flow in inclined channels with different kinematic viscosities (Ginzbourg and Adler, 1995), the free-interface flow (Ginzburg and Steiner, 2002). Tölke et al. (2006) coupled the MRT model for multiphase flow simulations with adaptive grids. McCracken and Abraham (2005) used the Carnahan-Sterling EOS incorporated in the He multiphase model (He et al., 1998) together with the MRT model and obtained good comparison results with benchmark problems such as: capillary waves, the Laplace-Young test and the oscillation frequency of the liquid cylinder.

A few applications were published using the MRT model and multiphase models.

Premnath and Abraham (2005) simulated the drop collisions with the MRT model, and found that it is in excellent agreement with theoretical results. Wu and Shao (2004) simulated the lid-driven cavity obtaining consistent streamlines and the lower achievable viscosity limit. Authors report that the results showed significant improvement of the gas-liquid density ratio, i.e. up to 1000 (Mukherjee and Abraham, 2007), better low viscosity limit and stability.

Despite all the works on the application of the MRT collision operator to multiphase models many authors use the MRT collision operator as a tool to improve one-fluid hydrodynamics without rigorous analysis of the impact of the MRT collision operator on multiphase physics. Those include the absence of works on the application of the MRT collision operator to the Shan-Chen model, which is an objective of the present work.

2.4 Objectives

The present work concentrates on the Shan-Chen multiphase model which is the most popular approach because it is straightforward in its implementation. Here are a few contributions of the present work to the Shan-Chen model theory:

- The thorough analysis of the Shan-Chen model with the original formulation and the proper force incorporation (Guo et al., 2002) was performed. The results show the discrepancy between the theory and the numerical results with the original Shan-Chen formulation. However, the proper force incorporation allows one to avoid the viscosity dependent surface tension.

- The application of the MRT collision operator with the Shan-Chen model allows one to obtain a better stability and achievable gas-liquid density ratio than the original Shan-Chen model. However, with the proper force implementation the MRT model improvements are minor in terms of the gas-liquid ratio. Nevertheless,

they are extremely important if the proper physical behaviour is of concern.

- The introduction of a multirange model gives the ability to control the surface tension separately from the equation of state. The present work proposes improved multirange potentials with the isotropy in the fifth order term of the expansion.

- The general formulation of the Shan-Chen model allows one to simulate ferrofluidics problems and the anisotropic problems with different momentum fluxes.

The overall structure of the thesis is as follows:

A thorough analysis of the lattice Boltzmann equation and the force implementation will be given in Chapter Three. It includes the Chapman-Enskog analysis for the hydrodynamic equations with external force and mass terms. To the best of the authors knowledge, this is presented for the first time in the present work. The Chapman-Enskog analysis (Chapman and Cowling, 1995) allows the restoration of macroscopic equations from the microscopic formulation of the lattice Boltzmann method.

Chapter Four will discuss the original formulation of the Shan-Chen model. The mathematical formulation of the Shan-Chen force with the equation of state, surface tension restored and macroscopic equations restored through the Chapman-Enskog analysis will be introduced and discussed. The limitations of the Shan-Chen model will be indicated such as: non-thermodynamical behaviour, spurious currents around the droplet, etc. The multirange modification of the Shan-Chen model will be presented in Section 4.2. It allows to separately control the equation of state and the surface tension terms. Numerical results with a droplet between walls under different temperatures will be presented. The general formulation of the Shan-Chen model is presented in Section 4.3. The formulation allows one to introduce anisotropic phenomena equivalent to ferrohydrodynamics simulations.

Chapter Five introduces the MRT and the theory behind it. The extended equilibrium function which include the third and fourth order velocity polynomials are introduced through the consistent Hermite approximation of the Boltzmann equilibrium function. The restoration of the macroscopic equations with the mass and the force terms is mentioned. To the best of the author's knowledge this has not been yet presented in the literature. The simulation results with the proposed force implementation show that the Poiseuille flow velocity profile can be restored with the machine accuracy.

Chapter Six will provide the simulations of the Shan-Chen model with the MRT collision operator. The force incorporation strategy and macroscopic equations will be presented. The results show better stability limits and achievable gas-liquid density ratio, especially in the case of the original Shan-Chen formulation.

Finally, the main findings and suggestions for further work are summarized in Chapter Seven.

Chapter 3

Lattice Boltzmann Equation

Even though the lattice Boltzmann equation is inherited from lattice gas automata which is based on the original Boltzmann equation and operates with boolean numbers (Wolfram, 1986) and involves the LBE as one of the consequent steps to restore the Navier-Stokes equations (Succi, 2001). However, the LBE can be considered itself without connection to the lattice gas automata. Such an approach gives additional benefits which lattice gas automata don't have, i.e. the Galilean invariance violation and the narrow simulation stability region.

However, it was later recognized that the lattice Boltzmann equation can be obtained through the discretization of the Boltzmann equation with the help of Hermite polynomial series. Hereafter, we will consider the second approach to obtain the lattice Boltzmann equation as it gives a solid foundation to the theory and benefits in terms of the extended equilibrium function presented in the chapter five.

The LBE can be obtained from BE taking consecutive simplifications which will be the topic of the following section.

3.1 Boltzmann Equation

The motion of molecules is governed by the laws of classical mechanics. This involves the Hamiltonian of the system of N particles with $3N$ degrees of freedom for velocities and $3N$ degrees of freedom for coordinates. The Hamiltonian can be written through momenta $\boldsymbol{p_i}$ and coordinates $\boldsymbol{r_i}$ as follows:

$$H = \sum_i \left(\frac{\boldsymbol{p_i}^2}{2m_i} + U(\boldsymbol{r_i}) \right) + \sum_{i<j} \phi(|\boldsymbol{r_i} - \boldsymbol{r_j}|). \tag{3.1}$$

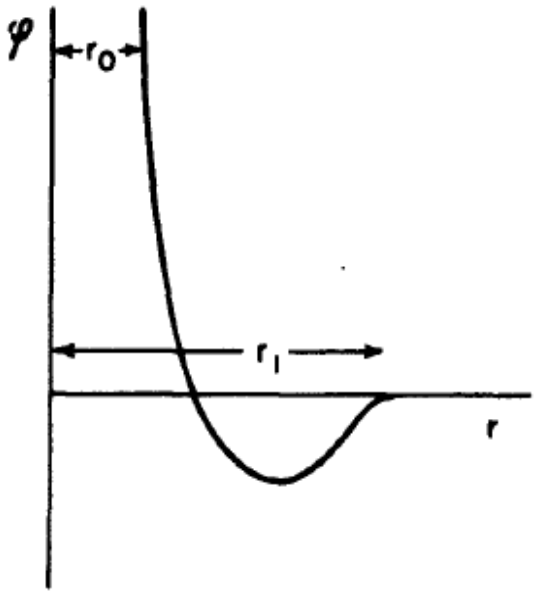

Figure 3.1: The interaction potential for molecules. Copyright from (Uhlenbeck et al., 1963).

The potential between molecules is a Lennard-Jones like potential, Fig. 3.1. The system can be represented in the Γ space by points with $6N$ coordinates. The motion is governed by the laws derived through the minimization procedure of the hamiltonian (3.1). As far as there are energy fluctuations in the system, and the Hamiltonian energy is not fixed (Uhlenbeck et al., 1963), one can follow the procedure of Gibbs and introduce the $6N$-dimensional probability distribution function in Γ-space. This step is not obvious, and it also introduces the irreversibility to reversible Hamiltonian equations. Then, by following the BBGKY procedure (Uhlenbeck et al., 1963) with the consecutive integration of the general $6N$-dimensional probability function to the one-dimensional probability distribution function, the Boltzmann equation (BE) can be obtained:

$$\partial_t f + v_\alpha \partial_\alpha f + F_\alpha \partial_{v_\alpha} f = \int \mathrm{d}\boldsymbol{v_1} \int g I(g,\theta)(f' f_1' - f f_1)\mathrm{d}\Omega. \tag{3.2}$$

The BE describes the behaviour of a number of particles in the representative infinitesimal volume $f(\boldsymbol{r},\boldsymbol{v},t)\mathrm{d}r\mathrm{d}\boldsymbol{v}$. The right hand side of BE (3.2) is the collision integral of two

particles. Notice that the collision integral is defined for rather dilute gas. Despite the external field and the complicated collision operator, the equation (3.2) has a steady-state solution, and this solution is the well-known Maxwell-Boltzmann distribution function:

$$f^{eq}(\boldsymbol{r}, \boldsymbol{v}, t) = \frac{\rho}{(2\pi m k_B T)^{3/2}} e^{-(\boldsymbol{v}-\boldsymbol{u})^2 / \frac{2k_B T}{m}}. \tag{3.3}$$

Note that the steady state approach to the equilibrium distribution function is achieved with different time scales - a short scale for a velocity then a longer one for coordinates (Uhlenbeck et al., 1963). The collision integral in the simplified case when the distribution function is close to the equilibrium distribution function can be represented by a series of Sonin polynomials with five zero eigenvalues related to the conservation laws. Those are the local density conservation, the three momentum conservation laws, and the energy conservation.

The next step was introduced by Bhatnagar et al. (1954), where they introduced the Single Relaxation Time collision operator (SRT) which states that the probability distribution function, f, is close to the Maxwell-Boltzmann equilibrium distribution function and it decays with the characteristic time between collisions τ:

$$\partial_t f + v_\alpha \partial_\alpha f + F_\alpha \partial_{v_\alpha} f = -\frac{f - f^{eq}}{\tau}. \tag{3.4}$$

Notice that equation (3.4) is more general than the initial BE (3.2). It allows one to simulate the fluid mechanics and particularly the Navier-Stokes equation. In contrast, the original BE is only valid for dilute gases. The integral BGK collision operator is able to simulate hydrodynamics because it conserves the five conservation laws:

$$\begin{aligned}
&\text{Density:} && \int f \mathrm{d}\boldsymbol{v} = \int f^{eq} \mathrm{d}\boldsymbol{v} = \rho \\
&\text{Momenta:} && \int f v_\alpha \mathrm{d}\boldsymbol{v} = \int f^{eq} v_\alpha \mathrm{d}\boldsymbol{v} = \rho u_\alpha \\
&\text{Energy:} && \int f \frac{(\boldsymbol{v}-\boldsymbol{u})^2}{2} \mathrm{d}\boldsymbol{v} = \int f^{eq} \frac{(\boldsymbol{v}-\boldsymbol{u})^2}{2} \mathrm{d}\boldsymbol{v} = \varepsilon,
\end{aligned} \tag{3.5}$$

where $\boldsymbol{u}$ is the average velocity.

The original BGK Boltzmann equation is continuous in the space and velocity variables. To be able to simulate this equation on the computer it needs to be discretized. The discretization needs to be done in a way to restore the Navier-Stokes equation. Two ways of the transition from the BE to the LBE are mentioned. The first one, which is briefly mentioned in the following section, is a series expansion of the equilibrium Boltzmann distribution in terms of Mach number with the Gauss quadrature rule applied to discretize it. The second approach uses a series expansion of the equilibrium distribution function with Hermite polynomials. The latter is adopted in the work and can bring some advantages (Chapter Five). Note that both approaches insure the abovementioned conservation laws (3.5). For generality, the equation will be rescaled in order to simplify calculations.

3.2 Dimensionless Boltzmann equation

The BGK Boltzmann equation can be rewritten in dimensionless form. The distribution function is scaled by the characteristic density ρ, velocity is scaled by the macroscopic velocity magnitude U_0, time is scaled by the macroscopic time L/U_0. After multiplying equation (3.4) by the parameter $L/(U_0\rho)$, the latter equation is rewritten in the non-dimensional form:

$$\frac{\partial \frac{f}{\rho}}{\partial \frac{t}{\frac{L}{U_0}}} + \frac{v_\alpha}{U_0}\frac{\partial \frac{f}{\rho}}{\partial \frac{x_\alpha}{L}} + F_\alpha U_0 L \frac{\partial \frac{f}{\rho}}{\partial \frac{v_\alpha}{U_0}} = -\frac{\frac{f}{\rho} - \frac{f^{eq}}{\rho}}{\frac{\tau}{\frac{L}{U_0}}}. \tag{3.6}$$

Parameter τ usually represents the average time between collisions. Therefore, the non-dimensional parameter $\hat{\tau} = \frac{\tau}{\frac{L}{U_0}}$ is a small parameter with magnitude close to the Knudsen number. The Knudsen number is defined as $Kn = \frac{l}{L} = \frac{\tau v/U_0}{L/U_0}$, where L is the characteristic length, l is the mean free path between collisions, v is the mean molecule speed. As it will be shown later through velocity abscissaes, the characteristic velocity v is close

to the macroscopic velocity U_0. Thus we state that the Knudsen number is proportional to $\hat{\tau}$. This fact will be utilized later on, when the LBE will be discretized in time. The non-dimensional Boltzmann equation can be rewritten as:

$$\frac{\partial \hat{f}}{\partial \hat{t}} + \hat{v}_\alpha \frac{\partial \hat{f}}{\partial \hat{x}_\alpha} + \hat{F} \frac{\partial \hat{f}}{\partial \hat{v}_\alpha} = -\frac{\hat{f} - \hat{f}^{eq}}{\hat{\tau}}, \tag{3.7}$$

where $\hat{f} = \frac{f}{\rho}$, $\hat{v}$, $\hat{t}$ are the non-dimensional distribution function, velocity, and time, respectively. Notice that the equilibrium distribution function is represented as:

$$\hat{f}^{eq} = \hat{f}^{(0)} = \frac{\hat{\rho}}{(2\pi\hat{\theta})^{D/2}} e^{-\frac{-(\hat{\boldsymbol{v}}-\hat{\boldsymbol{u}})^2}{2\hat{\theta}}}, \tag{3.8}$$

where $\hat{\theta} = \frac{k_B T}{m U_0^2}$. The consistency of the latter relationship can be checked by integration of the equation (3.8) in the non-dimensional velocity space:

$$\begin{aligned} &\int \hat{f}^{eq} \mathrm{d}\hat{\boldsymbol{v}} = \hat{\rho} \\ &\int \hat{f}^{eq} \hat{\boldsymbol{v}} \mathrm{d}\hat{\boldsymbol{v}} = \hat{\rho}\hat{\boldsymbol{v}}_\alpha \\ &\int \hat{f}^{eq} \frac{(\hat{\boldsymbol{v}} - \hat{\boldsymbol{u}})^2}{2} \mathrm{d}\hat{\boldsymbol{v}} = \hat{\rho}\hat{\theta}. \end{aligned} \tag{3.9}$$

Without loss of generality we hereafter omit the hat symbol and work only with the non-dimensional quantities.

3.3 From BE to LBE. Low Mach number approach

We refer to works of He and Luo (1997) and Shan et al. (2006). One can integrate the Boltzmann BGK equation without source terms with time Δt along the characteristic line as follows:

$$\begin{aligned} f(\boldsymbol{x} + \boldsymbol{\xi}\Delta t, \boldsymbol{\xi}, t + \Delta t) = \frac{1}{\tau} e^{-\Delta t/\tau} \int_0^{\Delta t} e^{t'/\tau} f^{eq}(\boldsymbol{x} + \boldsymbol{\xi} t', \boldsymbol{\xi}, t + t') \mathrm{d}t' + \\ e^{-\Delta t/\tau} f(\boldsymbol{x}, \boldsymbol{\xi}, t), \end{aligned} \tag{3.10}$$

where the velocity notation is changed to $\boldsymbol{v} \rightarrow \boldsymbol{\xi}$ to be consistent with the original work of He and Luo (1997). The equation (3.10), after the first order approximation of integral by using trapezoidal rule, becomes:

$$f(\boldsymbol{x}+\boldsymbol{\xi}\Delta t, \boldsymbol{\xi}, t+\Delta t) = \frac{e^{-\Delta t/\tau}}{\tau}\frac{f^{eq}(\boldsymbol{x},t)+f^{eq}(\boldsymbol{x}+\boldsymbol{\xi}\Delta t, \boldsymbol{\xi}, t+\Delta t)}{2}\Delta t + e^{-\Delta t/\tau} f(\boldsymbol{x},\boldsymbol{\xi},t). \tag{3.11}$$

Using the series expansion of $e^{\Delta t/\lambda}$ by Δt one can obtain the following expression up to the second order approximation, called BGK Boltzmann Equation:

$$f(\boldsymbol{x}+\boldsymbol{\xi}\Delta t, \boldsymbol{\xi}, t+\Delta t) = \left(1-\frac{\Delta t}{\tau}\right) f(\boldsymbol{x},\boldsymbol{\xi},t) + \frac{\Delta t}{\tau} f^{eq}(\boldsymbol{x},\boldsymbol{\xi}). \tag{3.12}$$

Notice that the velocity space is continuous. The next step is to discretize the velocity space. One can observe that the equilibrium function is a Gaussian-type function with the average velocity $\boldsymbol{u}$ in the exponent. One can expand the part with the velocity as follows:

$$f^{eq}(\boldsymbol{x},\boldsymbol{\xi}) = \frac{\rho}{(2\pi RT)^{D/2}} \exp(-\boldsymbol{\xi}^2/2RT)\left\{1+\frac{\boldsymbol{\xi u}}{RT}+\frac{(\boldsymbol{\xi u})^2}{2(RT)^2}-\frac{\boldsymbol{u}^2}{2RT}\right\}. \tag{3.13}$$

The aim is to have the equation (3.12) in the discretized version, as $f(\boldsymbol{x},\boldsymbol{\xi},t) \rightarrow f(\boldsymbol{x},\boldsymbol{\xi_i},t)$, with the conservation laws fulfilled. This is achieved by substitution of the expanded equilibrium in the conservation laws system (3.5). Then, the system will contain the terms of the following type:

$$\int \frac{\rho}{(2\pi RT)^{D/2}} \exp(-\boldsymbol{\xi}^2/2RT)\xi_\alpha^l \xi_\beta^m \xi_\gamma^n \mathrm{d}\boldsymbol{\xi}. \tag{3.14}$$

The feature of the Gaussian polynomial is that the integrals (3.14) can be taken exactly in certain velocity directions. It's called the Gauss quadrature rule. Therefore, all the macroscopic moments (3.5) are defined through the sum of certain populations with weights. He and Luo (1997) give a comprehensive review to obtain the following

conservation laws:

$$\begin{aligned}\rho &= \sum_i f_i = \sum_i f_i^{eq} \\ \rho \boldsymbol{u} &= \sum_i f_i \boldsymbol{\xi_i} = \sum_i f_i^{eq} \boldsymbol{\xi_i} \\ \rho\varepsilon &= \frac{1}{2}\sum_i f_i(\boldsymbol{\xi_i} - \boldsymbol{u})^2 = \sum_i f_i^{eq}(\boldsymbol{\xi_i} - \boldsymbol{u})^2,\end{aligned} \tag{3.15}$$

where the populations are defined as:

$$\begin{aligned}f_i &= f_i(\boldsymbol{x}, t) = w_i f(\boldsymbol{x}, \boldsymbol{\xi_i}, t) \\ f_i^{eq} &= f_i^{eq}(\boldsymbol{x}, t) = w_i f^{eq}(\boldsymbol{x}, \boldsymbol{\xi_i}, t).\end{aligned} \tag{3.16}$$

The LBE in this case is stated as:

$$f_i(\boldsymbol{x} + \boldsymbol{\xi_i}\Delta t, t + \Delta t) = \left(1 - \frac{\Delta t}{\tau}\right) f_i(\boldsymbol{x}, t) + \frac{\Delta t}{\tau} f_i^{eq}(\boldsymbol{x}, t). \tag{3.17}$$

3.4 From BE to LBE. Hermite polynomials approach

Another approach to obtain the LBE is to approximate the distribution probability function through Hermite polynomial series expansion. First, it is performed in the continuous space:

$$f(\boldsymbol{x}, \boldsymbol{\xi}, t) = \omega(\xi) \sum_{i=0}^{\infty} \frac{1}{n!} \boldsymbol{a}^{(n)}(\boldsymbol{x}, t) \boldsymbol{\mathcal{H}}^{(n)}(\boldsymbol{\xi}), \tag{3.18}$$

where $\boldsymbol{a}^{(n)}$ and $\boldsymbol{\mathcal{H}}^{(n)}$ are tensors of the n-th rank. The dimensionless coefficients, $\boldsymbol{a}^{(n)}(\boldsymbol{x}, t)$, are associated with hydrodynamic quantities as:

$$\boldsymbol{a^{(n)}(x, t)} = \int f(\boldsymbol{x}, \boldsymbol{\xi}, t) \boldsymbol{\mathcal{H}}^{(n)}(\boldsymbol{\xi}) \mathrm{d}\boldsymbol{\xi}, \tag{3.19}$$

where

$$\begin{aligned}&\text{Density:} && \boldsymbol{a}^{(0)} = \int f \mathrm{d}\boldsymbol{\xi} = \rho \\ &\text{Momentum:} && \boldsymbol{a}^{(1)} = \int f \boldsymbol{\xi} \mathrm{d}\boldsymbol{\xi} = \rho \boldsymbol{u} \\ &\text{Energy:} && \boldsymbol{a}^{(2)} = \int f(\boldsymbol{\xi}^2 - \boldsymbol{\delta}) \mathrm{d}\boldsymbol{\xi} = \boldsymbol{P} + \rho(\boldsymbol{u}^2 - \boldsymbol{\delta}) \\ &\text{Heat flux:} && \boldsymbol{a}^{(3)} = \int f(\boldsymbol{\xi}^3 - \boldsymbol{\xi}\boldsymbol{\delta}) \mathrm{d}\boldsymbol{\xi} = \boldsymbol{Q} + \boldsymbol{u}\boldsymbol{a}^{(2)} - (D-1)\rho \boldsymbol{u}^3.\end{aligned} \tag{3.20}$$

Here D is the space dimension and $\boldsymbol{\delta}$ is the Kronecker delta in n-dimensions, depending on the rank of the tensor $\boldsymbol{a}^{(n)}$. Following the work of Shan et al. (2006) with adoption of tensor shorthand notation, the product of two tensors (which is a scalar) means the sum of all possible permutations of the tensor product, i.e. $\boldsymbol{a}^{(2)}\boldsymbol{b}$ stands for $b_i a^{(2)}_{jk} + b_j a^{(2)}_{ik} + b_k a^{(2)}_{ij}$, where $\{i, j, k\} = \{x, y\}$. Therefore, in a two-dimensional case the tensor product is a scalar $\boldsymbol{a}^{(2)}\boldsymbol{b} = a_{xx}(b_x + b_y) + 2a_{xy}(b_x + b_y) + a_{yy}(b_x + b_y)$. Note that the same stands for the terms $\boldsymbol{\xi}^2$ and $\boldsymbol{\xi}^3$ in the definition of coefficients $\boldsymbol{a}^{(n)}$ (3.20).

The next step is to take a finite number of harmonics in the Hermite polynomials series expansion of the probability distribution function instead of an infinite number of Hermite polynomials:

$$f(\boldsymbol{x}, \boldsymbol{\xi}, t) \approx f^N(\boldsymbol{x}, \boldsymbol{\xi}, t) = \omega(\xi) \sum_{i=0}^{N} \frac{1}{n!} \boldsymbol{a}^{(n)}(\boldsymbol{x}, t) \boldsymbol{\mathcal{H}}^{(n)}(\boldsymbol{\xi}). \tag{3.21}$$

Note that the approximation by N Hermite polynomials guarantees that the approximation restores the first N hydrodynamic moments. Therefore, in terms of hydrodynamic quantities, the approximation is the same as the original probability distribution function:

$$\begin{aligned} &\boldsymbol{a}^{(n)}(\boldsymbol{x}, t) = \int f(\boldsymbol{x}, \boldsymbol{\xi}, t) \boldsymbol{\mathcal{H}}^{(n)}(\boldsymbol{\xi}) \mathrm{d}\boldsymbol{\xi} = \\ &\int f^N(\boldsymbol{x}, \boldsymbol{\xi}, t) \boldsymbol{\mathcal{H}}^{(n)}(\boldsymbol{\xi}) \mathrm{d}\boldsymbol{\xi} = \int \omega(\xi) \sum_{m=0}^{N} \frac{1}{m!} \boldsymbol{a}^{(m)}(\boldsymbol{x}, t) \boldsymbol{\mathcal{H}}^{(m)}(\boldsymbol{\xi}) \boldsymbol{\mathcal{H}}^{(n)}(\boldsymbol{\xi}) \mathrm{d}\boldsymbol{\xi} = \\ &\int \omega(\xi) p(\boldsymbol{x}, \boldsymbol{\xi}, t) \mathrm{d}\boldsymbol{\xi}, \end{aligned} \tag{3.22}$$

where $p(\boldsymbol{x}, \boldsymbol{\xi}, t)$ is the polynomial of degree $N + n$ in terms of the variable $\boldsymbol{\xi}$. It should be mentioned that any Hermite polynomial integral can be taken exactly on certain velocity abscissas $\{\boldsymbol{\xi_i}\}$. Moreover, the multiplication of two Hermite polynomials of different degrees in the equation (3.22) can be expressed through the sum of Hermite polynomials, where the integral of each of them can be taken exactly in a discrete velocity space. The interested reader can refer to the work of Shan et al. (2006) which presents a thorough explanation of Hermite polynomials and their properties. Therefore, the coefficients $\boldsymbol{a}^{(n)}$

can be expressed as follows,

$$\boldsymbol{a}^{(n)} = \int \omega(\xi) p(\boldsymbol{x}, \boldsymbol{\xi}, t) \mathrm{d}\boldsymbol{\xi} = \sum_{i=1}^{d} w_i p(\boldsymbol{x}, \boldsymbol{\xi_i}, t) = \sum_{i=1}^{d} \frac{w_i}{\omega(\xi_i)} f^N(\boldsymbol{x}, \boldsymbol{\xi_i}, t) \boldsymbol{\mathcal{H}}^{(n)}(\boldsymbol{\xi_i}), \quad (3.23)$$

where w_i and $\boldsymbol{\xi_i}$ are the weights and abscissae of a Gauss-Hermite quadrature. The same can be done with the equilibrium distribution function which has Gauss-bell shape. The substitution of the equilibrium distribution function into the expansion coefficients allows to obtain them exactly, because the equilibrium distribution function is a particular case of a Hermite polynomial:

$$\begin{aligned}
\boldsymbol{a}_0^{(0)} &= \rho \\
\boldsymbol{a}_0^{(1)} &= \rho \boldsymbol{u} \\
\boldsymbol{a}_0^{(2)} &= \rho(\boldsymbol{u}^2 + (\theta - 1)\boldsymbol{\delta}) \\
\boldsymbol{a}_0^{(3)} &= \rho(\boldsymbol{u}^3 + (\theta - 1)\boldsymbol{\delta u}) \\
\boldsymbol{a}_0^{(4)} &= \rho(\boldsymbol{u}^4 + (\theta - 1)\boldsymbol{\delta u}^2 + (\theta - 1)^2 \boldsymbol{\delta}^2),
\end{aligned} \quad (3.24)$$

where θ is the temperature-like parameter, which was introduced in the rescaling procedure, Section 3.2. Therefore, the Hermite expansion of the equilibrium distribution function up to fourth order terms yields:

$$\begin{aligned}
f^{(0)}(\boldsymbol{\xi}) = \omega(\xi)\rho\Bigg(& 1 + \boldsymbol{\xi} \cdot \boldsymbol{u} + \frac{1}{2}[(\boldsymbol{\xi} \cdot \boldsymbol{u})^2 - u^2 + (\theta - 1)(\xi^2 - D)] + \\
& \frac{\boldsymbol{\xi} \cdot \boldsymbol{u}}{6}[(\boldsymbol{\xi} \cdot \boldsymbol{u})^2 - 3u^2 + 3(\theta - 1)(\xi^2 - D - 2)] + \\
& \frac{1}{24}[(\boldsymbol{\xi} \cdot \boldsymbol{u})^4 - 6\boldsymbol{u}^2(\boldsymbol{\xi} \cdot \boldsymbol{u})^2 + 3\boldsymbol{u}^4 + \\
& 6(\theta - 1)\big((\boldsymbol{\xi} \cdot \boldsymbol{u})^2(\boldsymbol{\xi}^2 - D - 4) + \boldsymbol{u}^2(D + 2 - \boldsymbol{\xi}^2)\big) + \\
& 3(\theta - 1)^2(\boldsymbol{\xi}^4 - (D + 2)\boldsymbol{\xi}^2 + D(D + 2))]\Bigg).
\end{aligned} \quad (3.25)$$

For an isothermal system $\theta = 1$ many terms will be eliminated. If one eliminates also the third and the fourth order polynomials in the equilibrium function (3.25), then the discretized version of the most popular in applications equilibrium distribution function

can be obtained (Qian et al., 1992):

$$f^{(0)}(\boldsymbol{\xi}) = \omega(\xi)\rho\big(1 + \boldsymbol{\xi}\cdot\boldsymbol{u} + \frac{1}{2}[(\boldsymbol{\xi}\cdot\boldsymbol{u})^2 - u^2]\big). \tag{3.26}$$

However, the role of the third and the fourth order velocity polynomials is significant for the MRT model and the stability expansion. It will be discussed later.

3.5 Chapman-Enskog derivation of hydrodynamics equations

The Chapman-Enskog procedure (Chapman and Cowling, 1995) allows the restoration of hydrodynamics equations from the Boltzmann equation in the low Knudsen number limit. The procedure starts from the continuous BGK BE. Then, it is applied to the discretized LBE. The Chapman-Enskog expansion is one of the two tools available for analysis of LBE macro limits and will be thoroughly analyzed in this work.

3.5.1 Chapman-Enskog ansatz

Let us introduce the series expansion for the distribution function in terms of the Knudsen number around the equilibrium distribution function:

$$f_i = \sum_{n=0}^{\infty} \epsilon^n f_i^{(n)} \quad , \tag{3.27}$$

where $f_i^{(0)} = f_i^{eq}$ is the equilibrium distribution function. As far as the collision operator conserves density, momentum flux and energy (we do not consider energy for the isothermal case), the following conditions should be implied in a discrete velocity set. For the sake of simplicity, we consider the equation without any mass and force terms:

$$\begin{aligned} \sum_i f_i &= \rho \\ \sum_i f_i \xi_{i\alpha} &= \rho u_\alpha. \end{aligned} \tag{3.28}$$

However, the equilibrium distribution function gives the same moments:

$$\begin{aligned} \sum_i f_i^{(0)} &= \rho \\ \sum_i f_i^{(0)} \xi_{i\alpha} &= \rho u_\alpha. \end{aligned} \tag{3.29}$$

Therefore, the higher order expansions by Knudsen number should be set zero:

$$\begin{aligned} \sum_i f_i^{(n)} &= 0, \qquad \text{for } n > 0 \\ \sum_i f_i^{(n)} \xi_{i\alpha} &= 0, \quad \text{for } n > 0. \end{aligned} \tag{3.30}$$

Notice that we do not restrict at this particular moment any Mach number expansion to the equilibrium distribution function. Substituting the Knudsen expansion (3.27) in the Boltzmann equation (3.7) and summing it with velocity set moments $1, \xi_{i\alpha}$ yields

$$\begin{aligned} &\partial_t (f_i^{(0)} + \epsilon f_i^{(1)} + ...) + \partial_\alpha \xi_{i\alpha} (f_i^{(0)} + \epsilon f_i^{(1)}) = -\frac{1}{\tau} \sum_{n=1}^{\infty} \epsilon^n f^{(n)} \\ &\partial_t \rho + \partial_\alpha \rho u_\alpha = 0 \\ &\partial_t \rho u_\alpha + \partial_\beta \alpha\beta \Pi^{(0)} + \epsilon \partial_\beta \Pi_{\alpha\beta}^{(1)} + \epsilon^2 \partial_\beta \Pi_{\alpha\beta}^{(2)} + ... = 0, \end{aligned} \tag{3.31}$$

where $\Pi_{\alpha\beta}^{(n)} = \sum_i f_i^{(n)} \xi_{i\alpha} \xi_{i\beta}$.

Let us introduce a series of consecutive approximations due to the Knudsen number of the equation above and consecutive time scale.

Mass conservation:

$$\begin{aligned} \epsilon^0 : &\quad \partial_{t_0} \rho = -\partial_\alpha \rho u_\alpha \\ \epsilon^n : &\quad \partial_{t_n} \rho = 0. \end{aligned} \tag{3.32}$$

Momentum flux conservation:

$$\begin{aligned} \epsilon^0 : &\quad \partial_{t_0} \rho u_\alpha = -\partial_\beta \Pi_{\alpha\beta}^{(n)} \\ \epsilon^n : &\quad \partial_{t_n} \rho u_\alpha = -\partial_\beta \Pi_{\alpha\beta}^{(n)}. \end{aligned} \tag{3.33}$$

Therefore, one can use the Chapman-Enskog ansatz (Chapman and Cowling, 1995) relation stating that the distribution function implicitly depends on the conservative variables

ρ, ρu_α and $\rho\varepsilon$. Thus, the time partial derivative of the equilibrium distribution function can be estimated by the chain rule:

$$\frac{\partial f_i}{\partial t} = \frac{\partial f_i}{\partial \rho}\frac{\partial \rho}{\partial t} + \frac{\partial f_i}{\partial \rho u_\alpha}\frac{\partial \rho u_\alpha}{\partial t} + \frac{\partial f_i}{\partial \rho\varepsilon}\frac{\partial \rho\varepsilon}{\partial t}, \tag{3.34}$$

where all the derivatives can be represented as follows:

$$\begin{aligned} \partial_t \rho &= \partial_{t_0}\rho + \varepsilon\partial_{t_1}\rho + \epsilon^2\partial_{t_2}\rho + ... \\ \partial_t \rho u_\alpha &= \partial_{t_0}\rho u_\alpha + \epsilon\partial_{t_1}\rho u_\alpha + \epsilon^2\partial_{t_2}\rho u_\alpha + ... \end{aligned} \tag{3.35}$$

There is no explicit time inclusion in the equation (3.34) but through local conserved quantities with consecutive time approximations. Therefore, the expansion $\partial_t = \partial_{t_0} + \epsilon\partial_{t_1} + \epsilon^2\partial_{t_2} + ...$ is proved and valid.

3.5.2 Finite difference BE

Let us recall the BGK Boltzmann equation after the integration along the characteristic line 3.12:

$$f_i(\boldsymbol{x} + \boldsymbol{\xi_i}\Delta t, t + \Delta t) - f_i(\boldsymbol{x}, t) = -\frac{f_i - f_i^{eq}}{\tau}\Delta t, \tag{3.36}$$

where $f_i(\boldsymbol{x}, t) = f_i(\boldsymbol{x}, \boldsymbol{\xi_i}, t)$.

It is necessary to simulate equation (3.36) on a computer. However, a thorough examination of the Hermite polynomial abscissae reveals irrational numbers (Shan et al., 2006), i.e. $\|\xi_i\| = \sqrt{3}$ for the two-dimensional nine-speed D2Q9 model. Therefore, a mapping is needed in order to avoid irrational numbers for the velocity set. Therefore, a new velocity set is introduced with magnitudes of order one:

$$c_i = c_s\xi_i, \tag{3.37}$$

where c_s is often named the sound speed in many LBM papers, but it is simply a scaling factor. The equation (3.36) stays the same. However, one needs to redefine the macroscopic non-dimensional velocity and the equilibrium distribution function (to be defined

later):

$$\sum_i f_i \xi_{i\alpha} = c_s \sum_i f_i c_{i\alpha} = \rho u_\alpha$$
$$\sum f_i c_{i\alpha} = \rho \frac{u_\alpha}{c_s} = \rho \tilde{u}_\alpha \tag{3.38}$$

Without loss of generality one can omit the tilde for the velocity.

As was previously discussed, the parameter τ is of order of the Knudsen number. To capture the physics, we need to introduce the same time step in the order of the Knudsen number. Thus, $\Delta t = Kn = \epsilon$. Therefore, the new time step is introduced as $\hat{\tau} = \frac{\tau}{\Delta t} = \frac{\tau}{\epsilon}$, which itself is a quantity of unity. Therefore we reformulate equation (3.36) as

$$f(\boldsymbol{x} + \boldsymbol{c_i}\epsilon, t + \epsilon) - f(\boldsymbol{x}, t) = -\frac{f_i - f_i^{eq}}{\hat{\tau}}, \tag{3.39}$$

where $\hat{\tau} = \frac{\tau}{\Delta t}$ is the quantity of unity. Without loss of generality, we hereafter omit the hat symbol.

For general problems the force population is introduced to the LBE equation to properly capture the physics of a mass term and/or a source term. To the best of the author's knowledge, this has not been done to date. The LBE to be analyzed is the following:

$$f(\boldsymbol{x} + \boldsymbol{c_i}\epsilon, t + \epsilon) - f(\boldsymbol{x}, t) = -\frac{f_i - f_i^{eq}}{\tau} + \epsilon F_i. \tag{3.40}$$

3.5.3 Chapman-Enskog expansion

The Taylor expansion of equation (3.40) yields the following:

$$\sum_{n=1}^{\infty} \frac{D^n}{n!} \epsilon^n (f_i^{(0)} + \epsilon f_i^{(1)} + \epsilon^2 f_i^{(2)} + ...) = -\frac{\sum_{n=1}^{\infty} \epsilon^n f_i^{(n)}}{\tau} + \epsilon F_i \quad , \tag{3.41}$$

where $D = \partial_t + c_{i\alpha}\partial_\alpha = \sum_{n=0}^{\infty} \epsilon^n \partial_{t_n} + c_{i\alpha}\partial_\alpha$. It's easy to check that consecutive approximations in powers of ϵ are as follows:

$$\begin{aligned}
&\epsilon^0 : f_i^{(0)} = f_i^{eq} \\
&\epsilon^1 : (\partial_{t_0} + c_{i\alpha}\partial_\alpha) f_i^{(0)} = -\frac{f_i^{(1)}}{\tau} + F_i \\
&\epsilon^2 : \partial_{t_1} f_i^{(0)} + (\partial_{t_0} + c_{i\alpha}\partial_\alpha) f_i^{(1)} + \frac{(\partial_{t_0} + c_{i\alpha}\partial_\alpha)^2 f_i^{(0)}}{2} = -\frac{f_i^{(2)}}{\tau},
\end{aligned} \tag{3.42}$$

where ϵ^0 terms are taken from the fact that the expansion is performed around the equilibrium distribution function.

3.5.4 Macroscopic equations

Once the Chapman-Enskog system is written, Equation (3.42), the macroscopic equations to be obtained, is necessary to control the quality of the restoration through the Chapman-Enskog procedure. With the force and mass term introduced one needs to restore the following system:

$$\begin{aligned}
&\partial_t \rho + \partial_\alpha \rho u_\alpha = M \\
&\rho(\partial_t + (\boldsymbol{u} \cdot \boldsymbol{\nabla}))u_\alpha = \partial_\alpha p + \eta \partial_{\beta\beta} u_\alpha + \left(\frac{\eta}{3} + \zeta\right) \partial_{\alpha\beta} u_\beta + F_\alpha.
\end{aligned} \tag{3.43}$$

In terms of microscopic equations we adapt the LBE formulation of Ginzburg et al. (2008):

$$\begin{aligned}
&\tilde{f}_i(\boldsymbol{x}, t) = f_i(\boldsymbol{x}, t) - \frac{f_i(\boldsymbol{x}, t) - f_i^{eq}(\boldsymbol{x}, t)}{\tau} + \epsilon F_i \\
&f(\boldsymbol{x} + \boldsymbol{c_i}\epsilon, t + \epsilon) = \tilde{f}_i(\boldsymbol{x}, t),
\end{aligned} \tag{3.44}$$

where F_i is the force population introduced to capture the effects of the source and the mass terms. If the mass and the source terms are present, then the density and the momentum should be corrected after the collision. Therefore, the conservation laws as for the system without the mass and the force term (3.15) will be changed. The goal is to find the force populations F_i such that the system (3.43) can be restored. In terms of

the populations it can be represented as:

$$\begin{aligned}\sum_i \tilde{f}_i(\boldsymbol{x},t) &= \sum_i f_i(\boldsymbol{x},t) + \epsilon M \\ \sum_i \tilde{f}_i(\boldsymbol{x},t)c_{i\alpha} &= \sum_i f_i(\boldsymbol{x},t)c_{i\alpha} + \epsilon F_\alpha,\end{aligned} \tag{3.45}$$

where F and M are the source and the mass terms, respectively.

Thus, as was mentioned before (Ginzburg et al., 2008), one can distribute the mass and the source term between the moments of the equilibrium distribution function and the force distribution population F_α:

$$\begin{aligned}\epsilon M &= \epsilon\mathcal{M} - \sum_i \frac{f_i}{\tau} + \sum_i \frac{f_i^{eq}}{\tau} \\ \epsilon F_\alpha &= \epsilon\mathcal{F}_\alpha - \sum_i \frac{f_i c_{i\alpha}}{\tau} + \sum_i \frac{f_i^{eq} c_{i\alpha}}{\tau},\end{aligned} \tag{3.46}$$

where the $\mathcal{M} = \sum_i F_i$ and $\mathcal{F}_\alpha = \sum_i F_i c_{i\alpha}$ are the moments of force populations F_i. By recognizing the microscopic density $\rho = \sum_i f_i$ and the momentum $\rho u_\alpha = \sum_i f_i c_{i\alpha}$, and introducing the moments of the equilibrium distribution function $\sum_i f_i^{eq} = \rho^{eq}$ and $\sum_i f_i^{eq} c_{i\alpha} = \rho^{eq} u_\alpha^{eq}$, one can rewrite system (3.46) as follows,

$$\begin{aligned}\epsilon M &= \epsilon\mathcal{M} - \frac{\rho}{\tau} + \frac{\rho^{eq}}{\tau} \\ \epsilon F_\alpha &= \epsilon\mathcal{F}_\alpha - \frac{\rho u_\alpha}{\tau} + \frac{\rho^{eq} u_\alpha^{eq}}{\tau}.\end{aligned} \tag{3.47}$$

Therefore, the mass and the source terms can be distributed between the equilibrium distribution function and the moments of force populations. The most distinguishable situations (Ginzburg et al., 2008) are when the force population moments equal the mass and the force term moments, when the mass and the force terms are distributed between the equilibrium distribution function and the moment of force populations, and when the mass and the force terms are included to the equilibrium distribution function, respectively:

1.

$$\begin{aligned}
&\rho^{eq} = \rho = \rho^m - \epsilon\frac{M}{2} \qquad\qquad , \mathcal{M} = M \quad , -\frac{\sum_i (f_i - f_i^{eq})}{\tau} = 0 \\
&\rho^{eq} u_\alpha^{eq} = \rho u_\alpha = \rho^m u_\alpha^m - \epsilon\frac{F_\alpha}{2} \quad , \mathcal{F}_\alpha = F_\alpha \quad , -\frac{\sum_i (f_i - f_i^{eq}) c_{i\alpha}}{\tau} = 0
\end{aligned} \tag{3.48}$$

2.

$$\begin{aligned}
&\rho^{eq} = \rho^m \qquad\qquad , \mathcal{M} = \left(1 - \frac{1}{2\tau}\right) M \quad , -\frac{\sum_i (f_i - f_i^{eq})}{\tau} = \epsilon\frac{M}{2\tau} \\
&\rho^{eq} u_\alpha^{eq} = \rho^m u_\alpha^m \quad , \mathcal{F}_\alpha = \left(1 - \frac{1}{2\tau}\right) F_\alpha \quad , -\frac{\sum_i (f_i - f_i^{eq}) c_{i\alpha}}{\tau} = \epsilon\frac{F_\alpha}{2\tau}
\end{aligned} \tag{3.49}$$

3.

$$\begin{aligned}
&\rho^{eq} = \rho + \epsilon M\tau = \rho^m + \epsilon\left(\tau - \frac{1}{2}\right) M \qquad\qquad , \mathcal{M} = 0 \\
&-\frac{\sum_i (f_i - f_i^{eq})}{\tau} = \epsilon M
\end{aligned} \tag{3.50}$$

$$\begin{aligned}
&\rho^{eq} u_\alpha^{eq} = \rho u_\alpha + \epsilon F_\alpha\tau = \rho^m u_\alpha^m + \epsilon\left(\tau - \frac{1}{2}\right) F_\alpha \quad , \mathcal{F}_\alpha = 0 \\
&-\frac{\sum_i (f_i - f_i^{eq}) c_{i\alpha}}{\tau} = \epsilon F_\alpha,
\end{aligned}$$

where $\rho^m = \rho + \epsilon\frac{M}{2}$, $\rho^m u_\alpha^m = \rho u_\alpha + \epsilon\frac{F_\alpha}{2}$ are the macroscopic density and momentum flux which participate in the restored equations (Guo et al., 2002; Luo, 2000). Note that the macroscopic equations (3.43) define their own density and momentum flux different from the microscopic density, $\rho = \sum_i f_i$, and the microscopic momentum flux, $\rho u_\alpha = \sum_i f_i c_{i\alpha}$. Therefore, there are three different notations for the density and the momentum. One is the microscopic definition, ρ and ρu_α; another one is the equilibrium moments, ρ^{eq} and $\rho^{eq} u_\alpha^{eq}$ and the third one is the macroscopic, ρ^m and $\rho^m u_\alpha^m$. The second method (3.49) is adopted here, where $\rho^{eq} = \rho^m$ and $\rho^{eq} u_\alpha^{eq} = \rho^m u_\alpha^m$.

3.5.5 Restoration of macroscopic equations

Recalling the Chapman-Enskog expansion (3.27) one can substitute it in the adapted method:

$$\begin{aligned}
\rho^{eq} &= \sum_i f_i^{eq} = \rho + \epsilon\frac{M}{2} = \sum_i f_i + \epsilon\frac{M}{2} \\
\rho^{eq} &= \sum_i \sum_{n=0}^{\infty} \epsilon^n f_i^{(n)} = \sum_i f_i^{eq} + \epsilon \sum_i f_i^{(1)} + \epsilon\frac{M}{2} \\
\rho^{eq} &= \rho^{eq} + \epsilon \sum_i f_i^{(1)} + \epsilon\frac{M}{2}
\end{aligned} \tag{3.51}$$

$$\begin{aligned}
\rho^{eq} u_\alpha^{eq} &= \rho u_\alpha + \epsilon\frac{F_\alpha}{2} = \sum_i f_i c_{i\alpha} + \epsilon\frac{F_\alpha}{2} \\
\rho^{eq} u_\alpha^{eq} &= \sum_i \sum_{n=0}^{\infty} \epsilon^n f_i^{(n)} c_{i\alpha} = \sum_i f_i^{eq} c_{i\alpha} + \epsilon \sum_i f_i^{(1)} c_{i\alpha} + \epsilon\frac{F_\alpha}{2} \\
\rho^{eq} u_\alpha^{eq} &= \sum_i f_i^{eq} c_{i\alpha} + \epsilon \sum_i f_i^{(1)} c_{i\alpha} + \epsilon\frac{F_\alpha}{2}.
\end{aligned}$$

Notice that all the moments $\sum_i f_i^{(n)} = 0$ and $\sum_i f_i^{(n)} c_{i\alpha} = 0$ for $n > 1$. The presence of the mass and the force terms is included in the first approximation $f_i^{(1)}$. Therefore, the moments of $f_i^{(1)}$ can be obtained from (3.51) as:

$$\begin{aligned}
\sum_i f_i^{(1)} &= -\frac{M}{2} \\
\sum_i f_i^{(1)} c_{i\alpha} &= -\frac{F_\alpha}{2}.
\end{aligned} \tag{3.52}$$

By summation of the second and third equations from system (3.42) over i and using the local conservation conditions (3.28), the following equations can be obtained:

$$\begin{aligned}
&\partial_{t_0} \rho^m + \partial_\alpha \rho^m u_\alpha^m = 0 \\
&\partial_{t_1} \rho^m + \partial_{t_0} \sum_i f_i^{(1)} + \partial_\alpha \sum_i f_i^{(1)} c_{i\alpha} + \\
&\sum_i \frac{(\partial_{t_0} + c_{i\alpha}\partial_\alpha)}{2} \left(-\frac{f_i^{(1)}}{\tau} + F_i \right) = 0.
\end{aligned} \tag{3.53}$$

By substitution of the known first and second moments from (3.52) the system of equations is rewritten as follows:

$$\begin{aligned}
&\epsilon^1 : \partial_{t_0}\rho^m + \partial_\alpha \rho^m u_\alpha^m = \frac{M}{2\tau} + \sum_i F_i \\
&\epsilon^2 : \partial_{t_1}\rho^m - \partial_{t_0}\frac{M}{2} - \partial_\alpha \frac{F_\alpha}{2} + \partial_{t_0}\frac{M}{2\tau} + \partial_\alpha \frac{F_\alpha}{2\tau} + \frac{(\partial_{t_0} + c_{i\alpha}\partial_\alpha)}{2} F_i = 0.
\end{aligned} \tag{3.54}$$

Equivalently the second equation of the system (3.54) is grouped as follows,

$$\epsilon^2 : \partial_{t_1}\rho^m - \partial_{t_0}\frac{M}{2}\left(1 - \frac{1}{2\tau}\right) - \partial_\alpha \frac{F_\alpha}{2}\left(1 - \frac{1}{2\tau}\right) + \frac{(\partial_{t_0} + c_{i\alpha}\partial_\alpha)}{2} F_i = 0. \tag{3.55}$$

Thus, if we take the force distribution as follows, one can eliminate terms with partial derivatives by taking appropriate force population moments:

$$\begin{aligned}
\sum_i F_i &= M\left(1 - \frac{1}{2\tau}\right) \\
\sum_i F_i c_{i\alpha} &= F_\alpha \left(1 - \frac{1}{2\tau}\right).
\end{aligned} \tag{3.56}$$

Then, the system of equations (3.54) can be simplified to:

$$\begin{aligned}
&\epsilon^1 : \partial_{t_0}\rho^m + \partial_\alpha \rho^m u_\alpha^m = M \\
&\epsilon^2 : \partial_{t_1}\rho^m = 0.
\end{aligned} \tag{3.57}$$

By multiplying the second equation of system (3.54) by ϵ and summing it up with the first equation the continuity equation can be restored:

$$\begin{aligned}
&\partial_{t_0}\rho^m + \partial_\alpha \rho^m u_\alpha^m + \epsilon \partial_{t_1}\rho^m = M \\
&\partial_t \rho^m + \partial_\alpha \rho^m u_\alpha^m = M.
\end{aligned} \tag{3.58}$$

The multiplication of the Chapman-Enskog system (3.42) by $c_{i\alpha}$ and summing it over the index i allows one to obtain the Navier-Stokes equation:

$$\begin{aligned}
\epsilon^1 :&\quad \partial_{t_0}\sum_i f_i^{(0)} c_{i\alpha} + \partial_\beta \sum_i c_{i\alpha}c_{i\beta} f_i^{(0)} = -\frac{\sum_i f_i^{(1)} c_{i\alpha}}{\tau} + \sum_i F_i c_{i\alpha} \\
\epsilon^2 :&\quad \partial_{t_1}\sum_i f_i^{(0)} c_{i\alpha} + \partial_{t_0}\sum_i f_i^{(1)} c_{i\alpha} + \partial_\beta \sum_i f_i^{(1)} c_{i\alpha}c_{i\beta} - \\
&- \frac{1}{2\tau}\partial_{t_0}\sum_i f_i^{(1)} c_{i\alpha} - \frac{1}{2\tau}\partial_\beta c_{i\alpha}c_{i\beta} f_i^{(1)} + \frac{1}{2}\partial_{t_0}\sum_i F_i c_{i\alpha} + \frac{1}{2}\partial_\beta \sum_i F_i c_{i\alpha}c_{i\beta} = 0.
\end{aligned} \tag{3.59}$$

After substitution of the known moments, $\sum_i f_i^{(1)} c_{i\alpha} = -\frac{F_\alpha}{2}$ and $\sum_i F_i c_{i\alpha} = F_\alpha \left(1 - \frac{1}{2\tau}\right)$, system (3.59) becomes:

$$\begin{aligned}
&\epsilon^1: \quad \partial_{t_0} \rho^m u_\alpha^m + \partial_\beta \sum_i c_{i\alpha} c_{i\beta} f_i^{(0)} = F_\alpha \\
&\epsilon^2: \quad \partial_{t_1} \rho^m u_\alpha^m + \left(1 - \frac{1}{2\tau}\right) \partial_{t_0} \sum_i f_i^{(1)} c_{i\alpha} + \frac{1}{2} \partial_{t_0} \sum_i F_i c_{i\alpha} + \\
&\qquad \left(1 - \frac{1}{2\tau}\right) \partial_\beta \sum_i f_i^{(1)} c_{i\alpha} c_{i\beta} + \frac{1}{2} \partial_\beta \sum_i F_i c_{i\alpha} c_{i\beta} = 0.
\end{aligned} \tag{3.60}$$

Notice that some terms are eliminated:

$$\begin{aligned}
&\epsilon^1: \quad \partial_{t_0} \rho^m u_\alpha^m + \partial_\beta \sum_i c_{i\alpha} c_{i\beta} f_i^{(0)} = F_\alpha \\
&\epsilon^2: \quad \partial_{t_1} \rho^m u_\alpha^m + \left(1 - \frac{1}{2\tau}\right) \partial_\beta \sum_i f_i^{(1)} c_{i\alpha} c_{i\beta} + \frac{1}{2} \partial_\beta \sum_i F_i c_{i\alpha} c_{i\beta} = 0.
\end{aligned} \tag{3.61}$$

One needs to calculate the term $\left(1 - \frac{1}{2\tau}\right) \partial_\beta \sum_i f_i^{(1)} c_{i\alpha} c_{i\beta}$ and substitute it back into the system. From the initial Chapman-Enskog system one can represent $f_i^{(1)}$ through the force populations and derivatives of the equilibrium distribution function:

$$f_i^{(1)} = \tau \left(F_i - (\partial_{t_0} + c_{i\gamma} \partial_\gamma) f_i^{(0)}\right). \tag{3.62}$$

Therefore one can calculate the second order moment of $f_i^{(1)}$ as follows:

$$\sum_i f_i^{(1)} c_{i\alpha} c_{i\beta} = \tau \left(\sum_i F_i c_{i\alpha} c_{i\beta} - \partial_{t_0} \sum_i f_i^{(0)} c_{i\alpha} c_{i\beta} - \partial_\gamma \sum_i f_i^{(0)} c_{i\alpha} c_{i\beta} c_{i\gamma}\right). \tag{3.63}$$

Therefore, the term to be substituted into the system (3.61) is expanded through the force populations and the derivatives of the equilibrium function as:

$$\begin{aligned}
&\left(1 - \frac{1}{2\tau}\right) \partial_\beta \sum_i f_i^{(1)} c_{i\alpha} c_{i\beta} = \left(\tau - \frac{1}{2}\right) \partial_\beta \sum_i F_i c_{i\alpha} c_{i\beta} - \\
&\left(\tau - \frac{1}{2}\right) \partial_\beta \partial_{t_0} \sum_i f_i^{(0)} c_{i\alpha} c_{i\beta} - \left(\tau - \frac{1}{2}\right) \partial_\beta \partial_\gamma \sum_i f_i^{(0)} c_{i\alpha} c_{i\beta} c_{i\gamma}.
\end{aligned} \tag{3.64}$$

3.5.6 Discretized equilibrium distribution function

To find the moment $f_i^{(0)} c_{i\alpha} c_{i\beta}$ one needs to know the form of the equilibrium distribution function. Let us recall that we performed the Hermite polynomial expansion in the

velocity space (Section 3.4) and mentioned how to discretize the distribution function (Section 3.3) with the renormalization of the velocities to match it to the rectangular grid (Section 3.5.2). This section gives the full representation of the equilibrium distribution function discretized for the rectangular grid usage.

Let us recall the equilibrium distribution function in the continuous space for the isothermal case:

$$\begin{aligned} f^{(0)}(\boldsymbol{\xi}) =& \omega(\xi)\rho\Bigg(1 + \boldsymbol{\xi}\cdot\boldsymbol{u} + \frac{1}{2}[(\boldsymbol{\xi}\cdot\boldsymbol{u})^2 - u^2] + \\ & \frac{\boldsymbol{\xi}\cdot\boldsymbol{u}}{6}[(\boldsymbol{\xi}\cdot\boldsymbol{u})^2 - 3u^2] + \frac{1}{24}[(\boldsymbol{\xi}\cdot\boldsymbol{u})^4 - 6\boldsymbol{u}^2(\boldsymbol{\xi}\cdot\boldsymbol{u})^2 + 3\boldsymbol{u}^4]\Bigg). \end{aligned} \tag{3.65}$$

The equilibrium function can be also written in terms of Hermite polynomials:

$$f^{(0)}(\boldsymbol{\xi}) = \omega(\xi)\sum_{n=0}^{N}\frac{\boldsymbol{a}_0^{(n)}}{n!}\boldsymbol{\mathcal{H}}^{(n)}(\boldsymbol{\xi}). \tag{3.66}$$

The tensorial structure of the coefficients and Hermite polynomials needs to be accounted for. Here is a sample list of Hermite polynomials:

$$\begin{aligned} \mathcal{H}^{(0)}(\boldsymbol{\xi}) &= 1 \\ \mathcal{H}^{(1)}_{\alpha}(\boldsymbol{\xi}) &= \xi_\alpha \\ \mathcal{H}^{(2)}_{\alpha\beta}(\boldsymbol{\xi}) &= \xi_\alpha\xi_\beta - \delta_{\alpha\beta}, \end{aligned} \tag{3.67}$$

and the recurrence relation is:

$$\xi_\alpha\mathcal{H}^{(n)}_{\beta\gamma..\omega}(\boldsymbol{\xi}) = \mathcal{H}^{(n+1)}_{\alpha\beta\gamma..\omega}(\xi) + \sum_{k=\alpha}^{\omega}\delta_{\alpha k}\mathcal{H}_{\alpha\beta..(k-1)(k+1)..\omega}(\boldsymbol{\xi}), \tag{3.68}$$

where the greek notation is related to coordinates notation, i.e. x, y and z. But any Hermite polynomial is a symmetric function in terms of the coordinate permutations (greek notation). Therefore, coefficients to account for the permutations need to be

introduced:

$$
\begin{aligned}
f^{(0)}(\boldsymbol{\xi}) =&\omega(\xi)\rho\Bigg(\mathcal{H}^{(0)}+\mathcal{H}^{(1)}_{\alpha}u_{\alpha}+\frac{1}{2}[\mathcal{H}^{(2)}_{xx}u_x^2+C_2^1\mathcal{H}^{(2)}_{xy}u_xu_y+\mathcal{H}^{(2)}_{yy}u_y^2]+\\
&\frac{1}{6}[\mathcal{H}^{(3)}_{xxx}u_x^3+C_3^1\mathcal{H}^{(3)}_{xxy}u_x^2u_y+C_3^1\mathcal{H}^{(3)}_{yyx}u_y^2u_x+\mathcal{H}^{(3)}_{yyy}u_y^3]+\\
&\frac{1}{24}[\mathcal{H}^{(4)}_{xxxx}u_x^4+C_4^1\mathcal{H}^{(4)}_{xxxy}u_x^3u_y+C_4^2\mathcal{H}^{(4)}_{xxyy}u_x^2u_y^2+C_4^1\mathcal{H}^{(4)}_{xyyy}u_xu_y^3+\mathcal{H}^{(4)}_{yyyy}u_y^4]\Bigg),
\end{aligned}
\tag{3.69}
$$

where $C_n^m=\frac{n!}{m!(n-m)!}$ counts the number of permutations with the same indices.

In the discretized world the situation is different. It was mentioned that the discretization for the equilibrium distribution function is performed as:

$$
f_i^{(0)}=\frac{w_i}{\omega(\xi_i)}f^{(0)}(\boldsymbol{\xi_i}). \tag{3.70}
$$

For the two-dimensional nine velocity components case, as was mentioned before, the velocity magnitude is proportional to $\frac{1}{c_s}=\sqrt{3}$. Also, the velocity set contains deficiency in terms of the construction of higher order Hermite polynomials, for instance:

$$
\begin{aligned}
c_xc_xc_x &= c_x\\
c_yc_yc_y &= c_y\\
c_xc_xc_xc_x &= c_x^2\\
c_yc_yc_yc_y &= c_y^2.
\end{aligned}
\tag{3.71}
$$

Therefore, for the $D2Q9$ model, the most popular two-dimensional model, the equilibrium after adjusting it to the rectangular grid has the following form:

$$
\begin{aligned}
f_i^{(0)} =&w_i\rho\Bigg(1+\frac{\hat{u}_{\alpha}c_{i\alpha}}{c_s^2}+\frac{1}{2c_s^4}\Big[\Big(c_{ix}c_{ix}-\frac{1}{3}\Big)\hat{u}_x^2+2c_{ix}c_{iy}\hat{u}_x\hat{u}_y+\Big(c_{iy}c_{iy}-\frac{1}{3}\Big)u_y^2\Big]+\\
&\frac{1}{2c_s^6}\Big[\Big(c_{ix}c_{ix}c_{iy}-\frac{c_{iy}}{3}\Big)\hat{u}_x^2\hat{u}_y+\Big(c_{ix}c_{iy}c_{iy}-\frac{c_{ix}}{3}\Big)\hat{u}_x\hat{u}_y^2\Big]+\\
&\frac{1}{4c_s^8}\Big(c_{ix}^2c_{iy}^2-\frac{c_{ix}^2}{3}-\frac{c_{iy}^2}{3}+\frac{1}{9}\Big)\hat{u}_x^2\hat{u}_y^2\Bigg),
\end{aligned}
\tag{3.72}
$$

where the hat symbol stands for $\hat{\boldsymbol{u}}=\frac{\boldsymbol{u}}{c_s}$ and is omitted from herein. Basically, for the restoration of the Navier-Stokes equation, it is sufficient to omit the third and fourth

order velocity polynomials in the equilibrium distribution function:

$$f_i^{(0)} = w_i \rho \left(1 + \frac{u_\alpha c_{i\alpha}}{c_s^2} + \frac{1}{2c_s^4} \left[\left(c_{ix} c_{ix} - \frac{1}{3} \right) u_x^2 + 2 c_{ix} c_{iy} u_x u_y + \left(c_{iy} c_{iy} - \frac{1}{3} \right) u_y^2 \right] \right). \tag{3.73}$$

Therefore, all the necessary moments of the equilibrium distribution function can be rewritten as:

$$\begin{aligned} \sum_i f_i^{(0)} &= \rho^m \\ \sum_i f_i^{(0)} c_{i\alpha} &= \rho^m u_\alpha^m \\ \sum_i f_i^{(0)} c_{i\alpha} c_{i\beta} &= c_s^2 \rho \delta_{\alpha\beta} + \rho u_\alpha u_\beta \\ \sum_i f_i^{(0)} c_{i\alpha} c_{i\beta} c_{i\gamma} &= \rho^m (u_\alpha^m \delta_{\beta\gamma} + u_\beta^m \delta_{\alpha\gamma} + u_\gamma^m \delta_{\alpha\beta}), \end{aligned} \tag{3.74}$$

where c_s^2 is the convention for the abscissae amplitude for the set of velocities $\{\boldsymbol{c_i}\}$. One of the most utilized in the LBM community the two-dimensional model uses nine directions and is called as D2Q9. The velocity directions are shown in Fig. 4.11 (0 to 8). Through the Hermite polynomial expansion the weights can be obtained as: The weights w_i for D2Q9 model are:

$$\begin{aligned} &\frac{4}{9}, && \text{for } i = 0 \\ &\frac{1}{9}, && \text{for } i = 1 \ldots 4 \\ &\frac{1}{36}, && \text{for } i = 5 \ldots 8. \end{aligned} \tag{3.75}$$

3.5.7 D2Q9 Chapman-Enskog procedure

Let us recall the Chapman-Enskog procedure. After knowing the moments of the equilibrium distribution function, one can estimate the second order of the first harmonic

$f_i^{(1)}$ and substitute it into the Navier-Stokes equation:

$$\left(1-\frac{1}{2\tau}\right)\partial_\beta\sum_i f_i^{(1)}c_{i\alpha}c_{i\beta}=\left(\tau-\frac{1}{2}\right)\partial_\beta\sum_i F_i c_{i\alpha}c_{i\beta}-$$
$$\left(\tau-\frac{1}{2}\right)\partial_\beta\partial_{t_0}(c_s^2\rho^m\delta_{\alpha\beta}+\rho^m u_\alpha^m u_\beta^m)-c_s^2\left(\tau-\frac{1}{2}\right)\partial_\beta\partial_\gamma\rho^m(u_\alpha^m\delta_{\beta\gamma}+u_\beta^m\delta_{\alpha\gamma}+u_\gamma^m\delta_{\alpha\beta})=$$
$$\left(\tau-\frac{1}{2}\right)\partial_\beta\sum_i F_i c_{i\alpha}c_{i\beta}-\left(\tau-\frac{1}{2}\right)\partial_\alpha\partial_{t_0}c_s^2\rho^m+\left(\tau-\frac{1}{2}\right)\partial_\beta\partial_{t_0}\rho^m u_\alpha u_\beta-$$
$$c_s^2\left(\tau-\frac{1}{2}\right)\partial_\beta\partial_\gamma\rho^m(u_\alpha^m\delta_{\beta\gamma}+u_\beta^m\delta_{\alpha\gamma}+u_\gamma^m\delta_{\alpha\beta}). \tag{3.76}$$

Let us examine the terms of (3.76) separately, assuming the low Mach expansion (only velocity terms of no more than the second order are kept):

$$\left(\tau-\frac{1}{2}\right)\partial_\alpha\partial_{t_0}c_s^2\rho^m=c_s^2\left(\tau-\frac{1}{2}\right)\partial_\alpha(M-\partial_\gamma\rho^m u_\gamma^m) \tag{3.77}$$

$$\left(\tau-\frac{1}{2}\right)\partial_\beta\partial_{t_0}\rho^m u_\alpha^m u_\beta^m=\left(\tau-\frac{1}{2}\right)\partial_\beta(-u_\alpha^m u_\beta^m\partial_{t_0}\rho+u_\alpha^m\partial_{t_0}\rho u_\beta^m+u_\beta^m\partial_{t_0}\rho u_\alpha)=$$
$$\left(\tau-\frac{1}{2}\right)\partial_\beta\Big(-u_\alpha^m u_\beta^m(M-\partial_\gamma\rho^m u_\gamma^m)+u_\alpha^m(F_\beta-\partial_\beta c_s^2\rho^m-\partial_\gamma\rho^m u_\beta^m u_\gamma^m)+$$
$$u_\beta^m(F_\alpha-\partial_\alpha c_s^2\rho^m-\partial_\gamma\rho^m u_\alpha^m u_\gamma^m)\Big)\approx \tag{3.78}$$
$$\left(\tau-\frac{1}{2}\right)\partial_\beta(u_\alpha^m F_\beta+u_\beta^m F_\alpha)-c_s^2\left(\tau-\frac{1}{2}\right)\partial_\beta(u_\alpha^m\partial_\beta\rho+u_\beta^m\partial_\alpha\rho)$$

$$c_s^2\left(\tau-\frac{1}{2}\right)\partial_\beta\partial_\gamma\rho^m(u_\alpha^m\delta_{\beta\gamma}+u_\beta^m\delta_{\alpha\gamma}+u_\gamma^m\delta_{\alpha\beta})=$$
$$c_s^2\left(\tau-\frac{1}{2}\right)\partial_\beta\partial_\beta\rho^m u_\alpha^m+c_s^2\left(\tau-\frac{1}{2}\right)\partial_\beta\partial_\alpha\rho^m u_\beta^m+c_s^2\left(\tau-\frac{1}{2}\right)\partial_\alpha\partial_\gamma\rho^m u_\gamma^m=$$
$$c_s^2\left(\tau-\frac{1}{2}\right)\partial_\beta(\rho^m\partial_\beta u_\alpha^m+u_\alpha^m\partial_\beta\rho^m)+c_s^2\left(\tau-\frac{1}{2}\right)\partial_\beta(\rho^m\partial_\alpha u_\beta^m+u_\beta^m\partial_\alpha\rho^m)+ \tag{3.79}$$
$$c_s^2\left(\tau-\frac{1}{2}\right)\partial_\alpha\partial_\gamma\rho^m u_\gamma^m,$$

where the term $-u_\alpha u_\beta M$ was neglected as it is of the second order in the velocity magnitude and first order in the Knudsen number ϵ.

Then, the second moment $\sum_i f_i^{(1)} c_{i\alpha} c_{i\beta}$ can be restored:

$$\left(1-\frac{1}{2\tau}\right)\sum_i f_i^{(1)} c_{i\alpha}c_{i\beta} = \left(\tau-\frac{1}{2}\right)\partial_\beta \sum_i F_i c_{i\alpha}c_{i\beta} - c_s^2\left(\tau-\frac{1}{2}\right)\partial_\alpha(M-\partial_\gamma \rho^m u_\gamma^m) -$$
$$\left(\tau-\frac{1}{2}\right)\partial_\beta(u_\alpha^m(F_\beta-\partial_\beta c_s^2\rho^m)+u_\beta^m(F_\alpha-\partial_\alpha c_s^2\rho^m)) -$$
$$c_s^2\left(\tau-\frac{1}{2}\right)\partial_\beta\partial_\beta\rho^m u_\alpha^m - c_s^2\left(\tau-\frac{1}{2}\right)\partial_\beta\partial_\alpha\rho^m u_\beta^m - c_s^2\left(\tau-\frac{1}{2}\right)\partial_\alpha\partial_\gamma\rho^m u_\gamma^m =$$
$$\left(\tau-\frac{1}{2}\right)\partial_\beta\sum_i F_i c_{i\alpha}c_{i\beta} - c_s^2\left(\tau-\frac{1}{2}\right)\partial_\alpha M -$$
$$\left(\tau-\frac{1}{2}\right)\partial_\beta(u_\alpha^m F_\beta + u_\beta^m F_\alpha) - c_s^2\left(\tau-\frac{1}{2}\right)\partial_\beta\rho^m\partial_\beta u_\alpha^m - c_s^2\left(\tau-\frac{1}{2}\right)\partial_\beta\rho^m\partial_\alpha u_\beta^m. \tag{3.80}$$

Overall, the system (3.61) can be written as follows:

$$\begin{aligned}
\epsilon^1:\ & \partial_{t_0}\rho^m u_\alpha^m + \partial_\beta\sum_i c_{i\alpha}c_{i\beta}f_i^{(0)} = F_\alpha \\
\epsilon^2:\ & \partial_{t_1}\rho^m u_\alpha^m + \frac{1}{2}\partial_\beta\sum_i F_i c_{i\alpha}c_{i\beta} + \left(\tau-\frac{1}{2}\right)\partial_\beta\sum_i F_i c_{i\alpha}c_{i\beta} - c_s^2\left(\tau-\frac{1}{2}\right)\partial_\alpha M - \\
& \left(\tau-\frac{1}{2}\right)\partial_\beta(u_\alpha^m F_\beta + u_\beta^m F_\alpha) - c_s^2\left(\tau-\frac{1}{2}\right)\partial_\beta\rho^m\partial_\beta u_\alpha^m - \\
& c_s^2\left(\tau-\frac{1}{2}\right)\partial_\beta\rho^m\partial_\alpha u_\beta^m = 0 \\
\epsilon^2:\ & \partial_{t_1}\rho^m u_\alpha^m + \tau\partial_\beta\sum_i F_i c_{i\alpha}c_{i\beta} - c_s^2\left(\tau-\frac{1}{2}\right)\partial_\alpha M - \left(\tau-\frac{1}{2}\right)\partial_\beta(u_\alpha^m F_\beta + u_\beta^m F_\alpha) = \\
& c_s^2\left(\tau-\frac{1}{2}\right)\partial_\beta\rho^m\partial_\beta u_\alpha^m + c_s^2\left(\tau-\frac{1}{2}\right)\partial_\beta\rho^m\partial_\alpha u_\beta^m.
\end{aligned} \tag{3.81}$$

At this stage, we force the second order moment of the force populations $F_i c_{i\alpha} c_{i\beta}$ to equal the following terms:

$$\tau\partial_\beta\sum_i F_i c_{i\alpha}c_{i\beta} = c_s^2\left(\tau-\frac{1}{2}\right)\partial_\alpha M + \left(\tau-\frac{1}{2}\right)\partial_\beta(u_\alpha^m F_\beta + u_\beta^m F_\alpha). \tag{3.82}$$

This can be accomplished with the following force population representation, which is the main result for simulation of the hydrodynamic system with the mass and the source

terms:

$$F_i = w_i \left(1 - \frac{1}{2\tau}\right) \left(M + \frac{\boldsymbol{F}\boldsymbol{c_i}}{c_s^2} + \frac{c_{i\alpha}c_{i\beta} - c_s^2\delta_{\alpha\beta}}{2c_s^4} F_\alpha u_\beta\right). \tag{3.83}$$

The Chapman-Enskog system with the force populations defined for the Navier-Stokes equation becomes:

$$\begin{aligned}
&\epsilon^1: \quad \partial_{t_0}\rho^m u_\alpha^m + \partial_\beta \sum_i c_{i\alpha}c_{i\beta}f_i^{(0)} = F_\alpha \\
&\epsilon^1: \quad \partial_{t_0}\rho^m u_\alpha^m + c_s^2\partial_\alpha\rho + \partial_\beta\rho u_\alpha u_\beta = F_\alpha \\
&\epsilon^2: \quad \partial_{t_1}\rho^m u_\alpha^m = c_s^2\left(\tau - \frac{1}{2}\right)\partial_\beta\rho^m\partial_\beta u_\alpha^m + c_s^2\left(\tau - \frac{1}{2}\right)\partial_\beta\rho^m\partial_\alpha u_\beta^m
\end{aligned} \tag{3.84}$$

Multiplying the second equation of system (3.84) by ϵ and summing it with the first equation, the Navier-Stokes equation is obtained:

$$\begin{aligned}
&\partial_{t_0}\rho^m u_\alpha^m + \varepsilon\partial_{t_1}\rho^m u_\alpha^m + \partial_\beta\rho u_\alpha^m u_\beta^m = -\partial_\alpha c_s^2\rho + F_\alpha + \\
&c_s^2\varepsilon\left(\tau - \frac{1}{2}\right)\partial_\beta\rho^m\partial_\beta u_\alpha^m + c_s^2\varepsilon\left(\tau - \frac{1}{2}\right)\partial_\beta\rho^m\partial_\alpha u_\beta^m = \\
&-\partial_\alpha c_s^2\rho + F_\alpha + \nu\partial_\beta(\rho^m\partial_\beta u_\alpha^m + \rho^m\partial_\alpha u_\beta^m)
\end{aligned} \tag{3.85}$$

$$\partial_t\rho^m u_\alpha^m + \partial_\beta\rho^m u_\alpha^m u_\beta^m = -\partial_\alpha c_s^2\rho + F_\alpha + \nu\partial_\beta\rho^m\partial_\beta u_\alpha^m + \rho^m\partial_\alpha u_\beta^m.$$

The dynamic and kinematic viscosities are the same and equal to $\mu = \nu = c_s^2\epsilon\left(\tau - \frac{1}{2}\right)$. Note, from the numerical point of view it is convenient to take the time step equals unity. Therefore, the viscosities equal $\mu = \nu = c_s^2\left(\tau - \frac{1}{2}\right)$

This analysis is complete and allows one to incorporate the mass and the force terms to the LBE. One of the possible incorporations is to add a force responsible for the multiphase phenomena, which is the topic of the next chapter.

Chapter 4

Shan-Chen multiphase model

As mentioned previously, one of the most popular multiphase models is the Shan-Chen model. Originally introduced in 1993 (Shan and Chen, 1994) the model attracted a multitude of researchers by its simplicity. The results of the model were applied in simulation of two-phase blood flow (Dupin et al., 2003), flow in microchannels (Yu et al., 2007), thermal flow (Zhang and Chen, 2003), and studies of break-up of the liquid droplet (Sehgal et al., 1999). Many researchers use the model in its original formulation, which has many discrepancies with physics, such as the viscosity dependance of steady-state droplet condition. Thus, the aim of this thesis is to explore the basics of the Shan-Chen model and to resolve the problems associated with it. In this chapter the theory behind the original Shan-Chen model will be presented. The problems coming from the formulation will be enumerated, i.e. the achieved gas-liquid ratio limit, the non-thermodynamical behaviour, the dependence of the surface tension on the same parameter as the equation of state. All of the limitations will be thoroughly examined and supported simulations. Some limitations of the Shan-Chen model will be overcome. For instance, the stability limit can be expanded by applying the extended equilibrium distribution function. The dependence of the surface tension and the equation of state on one parameter is solved with the multirange potential. Also, the extension of the Shan-Chen model, the so-called generalized Shan-Chen model, is presented in order to simulate ferro-fluidics.

For simplicity, the two-dimensional implementation of the Shan-Chen model with 9 velocities, the D2Q9 model, is used in this chapter. However, the results are general in nature and can be applied to three-dimensional problems.

4.1 Shan-Chen model

In the Shan-Chen model (Shan and Chen, 1994) the force at a given node depends on all local neighbours characteristics:

$$\boldsymbol{F} = G\psi_0 \sum_i w_i \psi_i \boldsymbol{c_i}, \tag{4.1}$$

where ψ is the function of local characteristics of node, i.e. density. The function ψ is usually in the literature noted as the pseudopotential. In the above, ψ_0 denotes the local value at a given lattice site, and the summation, i, is taken over neighbours of the node defined by the discrete velocity set $\{\boldsymbol{c_i}\}$. Coefficient G is responsible for the attraction force between the molecules. Overall, the Shan-Chen force is the approximation of the force between molecules (Zhang and Kwok, 2004; Zhang et al., 2004).

4.1.1 Force inclusion

The original inclusion of the Shan-Chen force, as stated in (Shan and Chen, 1994), is by the shifting velocity method:

$$\rho \boldsymbol{u^{eq}} = \rho \boldsymbol{u} + \boldsymbol{F}\tau, \tag{4.2}$$

where $\rho \boldsymbol{u} = \sum_i f_i \boldsymbol{c_i}$ and $\boldsymbol{u^{eq}}$ is used for the calculation of the equilibrium distribution function. One can go through the lengthy algebra and determine that the following system of equations is restored on the macroscopic level:

$$\begin{aligned} &\partial_t \rho^{eq} + \partial_\alpha \rho^{eq} u_\alpha^{eq} = \left(\tau - \frac{1}{2}\right) \partial_\alpha F_\alpha \\ &\partial_t \rho^{eq} u_\alpha^{eq} + \partial_\beta \rho^{eq} u_\alpha^{eq} u_\beta^{eq} = F_\alpha + c_s^2(\tau - \frac{1}{2})\partial_\beta(\partial_\beta \rho^{eq} u_\alpha^{eq} + \partial_\alpha u_\beta^{eq}), \end{aligned} \tag{4.3}$$

where $\rho^{eq} u_\alpha^{eq} = \sum_i F_i c_{i\alpha} + F_\alpha \tau$. This equation in terms of $\rho^m u_\alpha^m = \sum_i f_i c_{i\alpha} + F_\alpha/2$ contains a number of additional viscosity terms. Calculations show that the inclusion of the force through the shifting velocity procedure can certainly increase the gas-liquid ratios for the droplet. This can be explained as follows, while the droplet considered

in the steady-state, there is no any difference between the shifting velocity method and the proper method (presented before) for the bulk. However, on the interface where the spurious currents exist one can see that they are influenced by additional force terms in the system of equations, which artificially increase the viscosity. Therefore, the scheme is more stable.

4.1.2 Equation of state

The equation of state for the LBE (Succi, 2001) is $P = c_s^2\rho$, as it was shown in equation (3.85), where c_s is the scaling parameter which for the D2Q9 model equals $c_s = 1/\sqrt{3}$. However, the inclusion of a density-dependent force term brings about a non-ideal contribution. Using the Taylor expansion, the Shan-Chen force (4.1) for the D2Q9 model can be expressed as follows:

$$\begin{aligned}\boldsymbol{F} =& G\psi(x,y)(w_1\psi(x+c\Delta t,y)\boldsymbol{c_1} + w_2\psi(x,y+c\Delta t)\boldsymbol{c_2} + w_3\psi(x-c\Delta t,y)\boldsymbol{c_3}+\\ & w_4\psi(x,y-c\Delta t)\boldsymbol{c_4} + w_5\psi(x+c\Delta t,y+c\Delta t)\boldsymbol{c_5}+\\ & w_6\psi(x-c\Delta t,y+c\Delta t)\boldsymbol{c_6} + w_7\psi(x-c\Delta t,y-c\Delta t)\boldsymbol{c_7}+\\ & w_8\psi(x+c\Delta t,y-c\Delta t)\boldsymbol{c_8}) = G\psi(\frac{1}{3}\boldsymbol{\nabla}\psi + \frac{1}{18}\boldsymbol{\nabla}\Delta\psi).\end{aligned} \tag{4.4}$$

The following formulation is derived algebraically:

$$\begin{aligned}F_\alpha &= G\psi\left(\frac{1}{3}\partial_\alpha\psi + \frac{1}{18}\partial_\alpha\Delta\psi\right) = G\left(\frac{1}{6}\partial_\alpha\psi^2 + \frac{1}{18}\Big(\partial_\alpha(\psi\Delta\psi) - \Delta\psi\partial_\alpha\psi\Big)\right)\\ &= G\left(\frac{1}{6}\partial_\alpha\psi^2 + \frac{1}{18}\Big(\partial_\alpha(\psi\Delta\psi) + \frac{1}{2}\partial_\alpha|\boldsymbol{\nabla}\psi|^2 - \partial_\beta\partial_\alpha\psi\partial_\beta\psi\Big)\right).\end{aligned} \tag{4.5}$$

The force influence can be included to the momentum-flux tensor (Sbragaglia et al., 2007):

$$\partial_\beta P_{\alpha\beta} = -F_\alpha + \partial_\alpha p = -F_\alpha + \partial_\alpha(c_s^2\rho).$$

Thus, the flux tensor $P_{\alpha\beta}$ is modified as follows:

$$P_{\alpha\beta} = \left(c_s^2\rho + \frac{G}{6}\psi^2 + \frac{G}{36}|\boldsymbol{\nabla}\psi|^2 + \frac{G}{18}\psi\Delta\psi\right)\delta_{\alpha\beta} - \frac{G}{18}\partial_\alpha\psi\partial_\beta\psi.$$

By analogy with classical mechanics, the potential of the force can be introduced as:

$$U = \frac{G}{6}\psi^2 + \frac{G}{36}|\boldsymbol{\nabla}\psi|^2 + \frac{G}{18}\psi\Delta\psi. \tag{4.6}$$

Since the gradient terms in equation (4.6) are small compared with the leading terms (the characteristic length of the interface is longer than the lattice spacing, as in all diffuse-interface methods), the equation (4.6) can be approximated as

$$p = \rho c_s^2 + \frac{G}{6}\psi^2. \tag{4.7}$$

By a suitable choice of the pseudo-potential $\psi(\rho)$, this equation can describe phase-separation. Let assume that the function ψ depends on ρ only. We can determine G_{crit} and ρ_{crit} from the following equations:

$$\begin{aligned} \frac{\mathrm{d}p}{\mathrm{d}\rho} &= c_s^2 + \frac{G}{3}\psi\dot{\psi} = 0 \\ \frac{\mathrm{d}^2p}{\mathrm{d}\rho^2} &= \frac{G}{3}(\psi\ddot{\psi} + (\dot{\psi})^2) = 0. \end{aligned} \tag{4.8}$$

For the typical choice $\psi(\rho) = 1 - e^{-\rho}$ (see later), this delivers the critical conditions for G and ρ:

$$G < G_{crit} = -4$$

and $\rho_{crit} = \ln 2$. Note that negative G corresponds to attractive interactions, the typical case of Shan-Chen applications.

4.1.3 Two-dimensional phase separation

Let us examine a phase transition in a planar case for steady-state conditions with the y coordinate normal to the interface. The gas/vapor phase occupies the upper domain, while a liquid occupies the lower domain. There are two far-field conditions: $\rho(\infty) = \rho_g$ and $\rho(-\infty) = \rho_l$. The normal component P_{yy} to the phase interface should be constant as one of the boundary conditions on the interface. As the pressure is the same in both

domains $P_{yy}(\infty) = P_{yy}(-\infty)$, then

$$p_0 = c_s^2\rho + \frac{G}{6}\psi(\rho_g)^2 = c_s^2\rho + \frac{G}{6}\psi(\rho_l)^2. \tag{4.9}$$

The condition of constant flux P_{yy}, which we note as p_0, reads as:

$$p_0 = c_s^2\rho + \frac{G}{6}\psi^2 - \frac{G}{36}(\dot{\psi}\rho')^2 + \frac{G}{18}\psi(\ddot{\psi}\rho'^2 + \dot{\psi}\rho''), \tag{4.10}$$

where prime symbol for the derivative with respect to y, $\dfrac{\mathrm{d}}{\mathrm{d}y}$. In the equation above, there is no independent variable. In such a situation the substitution $(\rho')^2 = z$ simplifies it; note that $\rho'' = \frac{\mathrm{d}\rho'}{\mathrm{d}\rho}\frac{\mathrm{d}\rho}{\mathrm{d}y} = \frac{\mathrm{d}\sqrt{z}}{\mathrm{d}\rho}\sqrt{z} = \frac{\dot{z}}{2}$, where the dot symbol is for the derivative by ρ, $\dfrac{\mathrm{d}}{\mathrm{d}\rho}$. The following first-order equation is obtained algebraically:

$$\frac{G}{36}\psi\dot{\psi}\dot{z} + \frac{G}{36}(2\psi\ddot{\psi}'' - \psi'^2)z = p_0 - c_s^2\rho - \frac{G}{6}\psi^2$$

The equation presented in the linear first order form, $\dot{y} + p(x)y = q(x)$, has the following solution $y = e^{-\int p(x)\mathrm{d}x}\big(\int q(x)e^{\int p(x')\mathrm{d}x'}\mathrm{d}x + C\big)$. Therefore,

$$z = \frac{\psi}{\dot{\psi}^2}\left(\frac{36}{G}\int \big(p_0 - c_s^2\rho - \frac{G}{6}\psi^2\big)\frac{\dot{\psi}}{\psi^2}\mathrm{d}\rho + C\right) \tag{4.11}$$

For equation (4.11) to be consistent with boundary conditions and to define constant C, we need to impose:

$$\int_{\rho_g}^{\rho_l} \big(p_0 - c_s^2\rho - \frac{G}{6}\psi^2\big)\frac{\dot{\psi}}{\psi^2}\mathrm{d}\rho = 0 \tag{4.12}$$

Substituting the expression for z into $z = (\rho')^2$ one can restore the theoretical profiles for different G parameters:

$$\begin{aligned} \rho' &= \sqrt{z(\rho)} \\ \int_{\rho_g}^{\rho} \frac{\mathrm{d}\rho}{\sqrt{z(\rho)}} &= y \end{aligned} \tag{4.13}$$

Note that the function $z(\rho)$ has singularities in $\rho = \rho_{g,l}$, and these singularities are non-integratable. However, in the published literature the authors do not specify it and use approximate equations to restore profiles. But profiles can be restored through the streamlines which can still provide the analytical solution but without analytical expression.

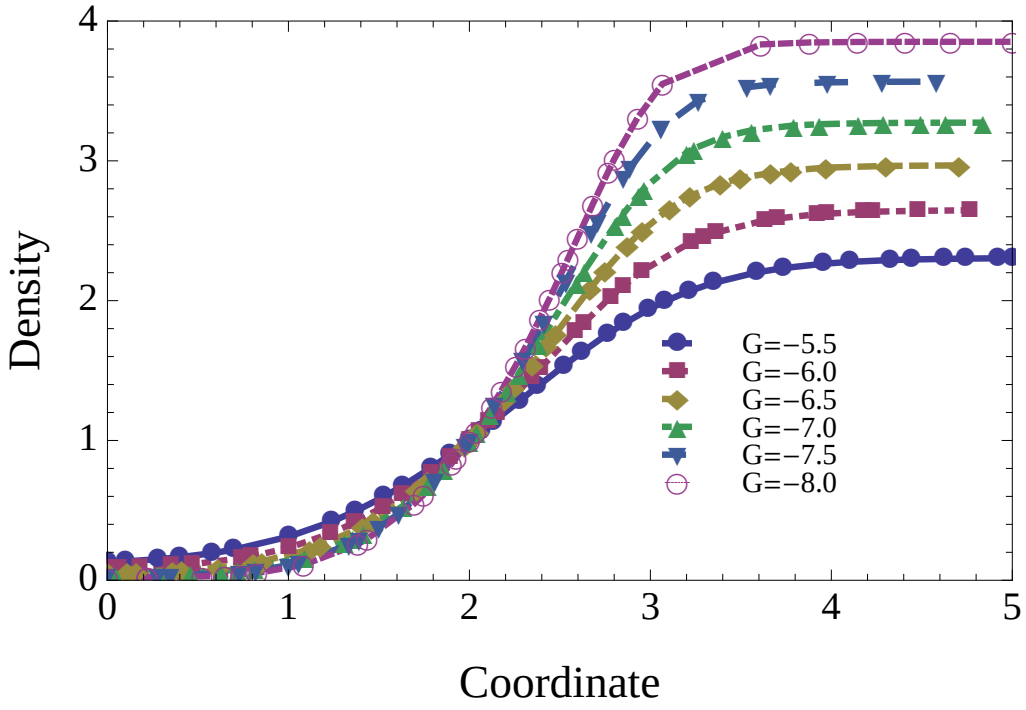

Figure 4.1: Theoretical plane density profiles after 10000 steps for different G parameters.

4.1.4 The original form of the pseudopotential

The exact form of the function ψ being available, we can derive all unknown values ρ_g,ρ_l from (4.9, 4.12). Once the values are known, the density profile (4.13) can be restored.

For the standard form of the function $\psi(\rho) = 1 - e^{-\rho}$, one can perform simulation and obtain ρ_g and ρ_l dependency on G (Fig. 4.4). Fig. 4.1 shows the plane density profiles depending on G parameter for the original Shan-Chen choice of the pseudopotential. The profiles are restored through the streamlines.

For comparison, the simulation profiles for the plane interface are given in Fig. 4.2. The half domain was initialized with ρ_g and another half with ρ_l taken from the equation of state and the Maxwell area rule (4.12). The system is thereby allowed to approach the equilibrium condition.

The comparison between the theoretical and simulation profiles is presented in Fig.

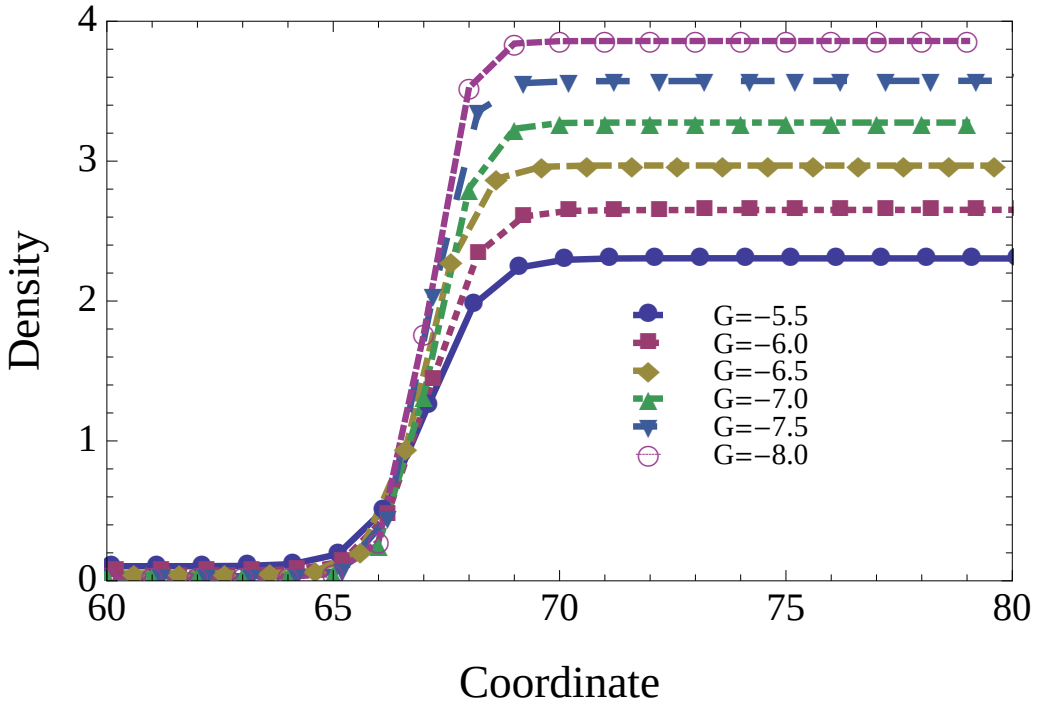

Figure 4.2: Simulation plane density profiles after 10000 steps for different G parameters.

4.3 for $G = -5.5$, $G = -6.5$ and $G = -7.5$. Even though the calculated ρ_g and ρ_l coincide with simulated results, the theoretical profile is steeper. The steepness can be caused by the force inclusion (velocity shift) of the Shan-Chen model, which can introduce numerical diffusion.

Equation (4.12) is analogous to the Maxwell reconstruction law, stating the following $\int_{\upsilon_l}^{\upsilon_g}(p_0 - p)d\upsilon = 0$ (Shan and Chen, 1994), where $\upsilon \approx 1/\rho$. Hence, to be consistent with physics the equation (4.12) should have the same form as follows:

$$\int_{\rho_g}^{\rho_l} \left(p_0 - c_s^2\rho - \frac{Gc_s^2}{2}\psi^2\right)\frac{1}{\rho^2}\mathrm{d}\rho = 0.$$

That is fulfilled if $\frac{\psi'}{\psi^2} = \frac{1}{\rho^2}$. Therefore, the function $\psi(\rho) = \frac{1}{C+\frac{1}{\rho}}$. If constant $C = 0$, then $\psi(\rho) = \rho$. However, for large ρ the term $\psi(\rho) = \rho$ becomes large which provoke the instabilities associated with large density gradients. That is why in order to correct

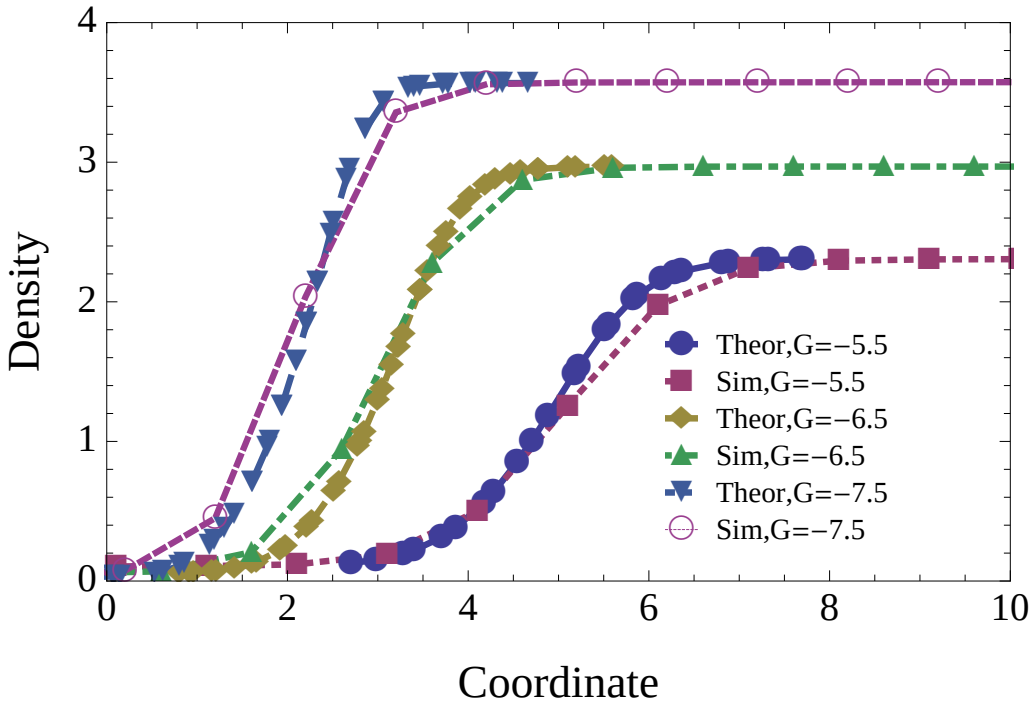

Figure 4.3: Comparison between theoretical ("Theor") and simulated ("Sim") plane density profiles for different G parameters.

these instabilities the function is taken in the original Shan-Chen form:

$$\psi(\rho) = 1 - e^{-\rho} \tag{4.14}$$

Note that at high densities $\rho > 0$, the potential goes to a constant, and consequently the associated force vanishes, thereby saturating the attractive instability.

4.1.5 The Navier-Stokes surface tension

As mentioned before, the Maxwell reconstruction for the Navier-Stokes diffusive interface models is different. Also, the momentum flux tensor is changed and should have the form as follows:

$$P_{\alpha\beta} = \left(c_s^2 \rho + \frac{G}{6}\psi^2 - \frac{k(\nabla\rho)^2}{2} - k\rho\Delta\rho \right) \delta_{\alpha\beta} + k\delta_\alpha\rho\delta_\beta\rho. \tag{4.15}$$

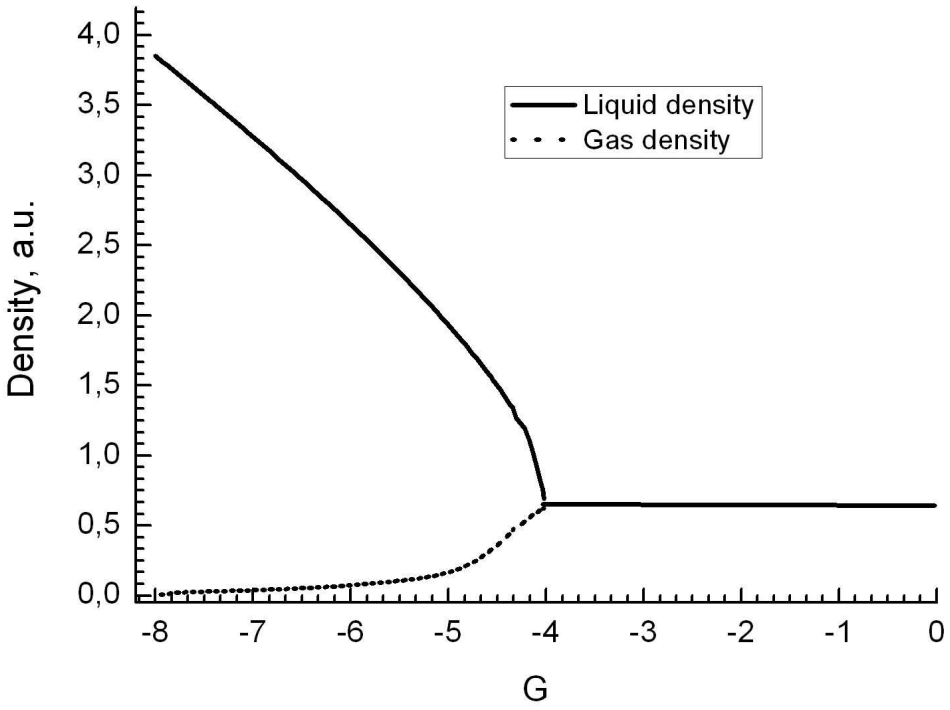

Figure 4.4: High and low density dependence on G. Curve obtained from equations (4.9,4.12). There is no separation until G equals $G_{crit} = -4$. The initial density was taken as the critical density, $\rho_{crit} = \ln 2$.

Thus, the simulation profiles are changed due to change in the function z:

$$\begin{aligned} z' - \frac{z}{\rho} &= -\frac{2}{\rho k}\left(p_0 - c_s^2\rho - \frac{G}{6}\psi^2\right) \\ z &= -\frac{2\rho}{k}\int\left(p_0 - c_s^2\rho - \frac{G}{6}\psi^2\right)\frac{\mathrm{d}\rho}{\rho^2}. \end{aligned} \tag{4.16}$$

The comparison with the Navier-Stokes compliant surface tension will be presented further. For the Navier-Stokes there is one additional constant k which controls the interface width. Therefore, the comparison can be done for different parameters k in order to obtain the best match to the original Shan-Chen model. The next section defines the surface tension and critical parameters for the original and the Navier-Stokes compliant surface tension Shan-Chen model.

4.1.6 Critical values for density and parameters. Surface tension σ

Let us obtain critical values from equation (4.8). For the most popular function (4.14) one can obtain $G_{crit} = -4$ and $\rho_{crit} = \ln 2$. For function defined as $\psi(\rho) = \frac{1}{C+\frac{1}{\rho}}$ one can obtain that $\rho_{crit} = \frac{1}{2C}$ and $G_{crit} = -\frac{27}{4}C$.

If the interface is diffusive and it has the certain width, then all fluxes are continuous. In the discontinuous case, the surface tension is defined as stated in (Landau and Lifshitz, 1987) as follows:

$$n_k(P_{ik}^{(1)} - P_{ik}^{(2)}) = \sigma\left(\frac{1}{R_1} + \frac{1}{R_2}\right)n_i, \tag{4.17}$$

where indexes 1 and 2 are related to the different phases, R_1 and R_2 are the main radiuses of the interface surface, and $\boldsymbol{n}$ is the surface interface normal vector. If the discontinuous definition is applied for the planare case, then the surface tension obtained equals zero, which coincides with the physics of the problem. In the case of diffusive models, the surface tension for the Shan-Chen model is defined as follows (Sbragaglia et al., 2007):

$$\sigma = -\frac{G}{18}\int_{-\infty}^{+\infty}|\partial_n\psi|^2\mathrm{d}\boldsymbol{n}$$

The additional surface tension factor, k, should be taken from the fact that the Maxwellian profile should be close to the Shan-Chen profile for any given G. There are a few approaches to the issue:

- One is the estimation of the factor z:

$$\begin{aligned} z_{Maxwell} &= -\frac{2\rho}{k}\int\left(p_0 - c_s^2\rho - \frac{G}{6}\psi^2\right)\frac{\mathrm{d}\rho}{\rho^2} \\ z_{SC} &= \frac{\psi}{\psi'^2}\frac{36}{G}\int\left(p_0 - c_s^2\rho - \frac{G}{6}\psi^2\right)\frac{\psi'}{\psi^2}\mathrm{d}\rho. \end{aligned} \tag{4.18}$$

  The values of ρ_g and ρ_l are almost the same for the Maxwellian and the Shan-Chen models. Thus, the integrals in the equation (4.18) are close. Therefore, one needs to compare the integration coefficients in order to obtain the proper scaled surface tension coefficient, k:

$$-\frac{2\rho}{k} \approx \frac{\psi}{\psi'^2}\frac{36}{G}. \tag{4.19}$$

  The estimation of $\frac{\psi}{\psi'^2}$ can be taken for small densities, ρ, located on the gas branch near ρ_g:

$$\frac{\psi}{\psi'^2} = \frac{1-\exp\left(-\rho\right)}{\exp\left(-2\rho\right)} \approx \rho. \tag{4.20}$$

  Then the coefficient k can be estimated as:

$$\begin{aligned} -\frac{2\rho}{k} &\approx \frac{\psi}{\psi'^2}\frac{36}{G} \\ k &\approx -\frac{G}{18}. \end{aligned} \tag{4.21}$$

- Another approach is presented by Benzi et al. (2006). They suggested the following scaling for $k \approx -\frac{1}{G}$ to match the surface tension.

- However, the numerical observations show that, for k varying in the least-square sense, the best matching k parameter ranges from $-\frac{1}{3G}$ to $-\frac{1}{4G}$.

For comparison reason, the different profiles are showed in Fig. 4.5. The profile developed here is referred as "Work scaling", the least-square matched parameter is referred as

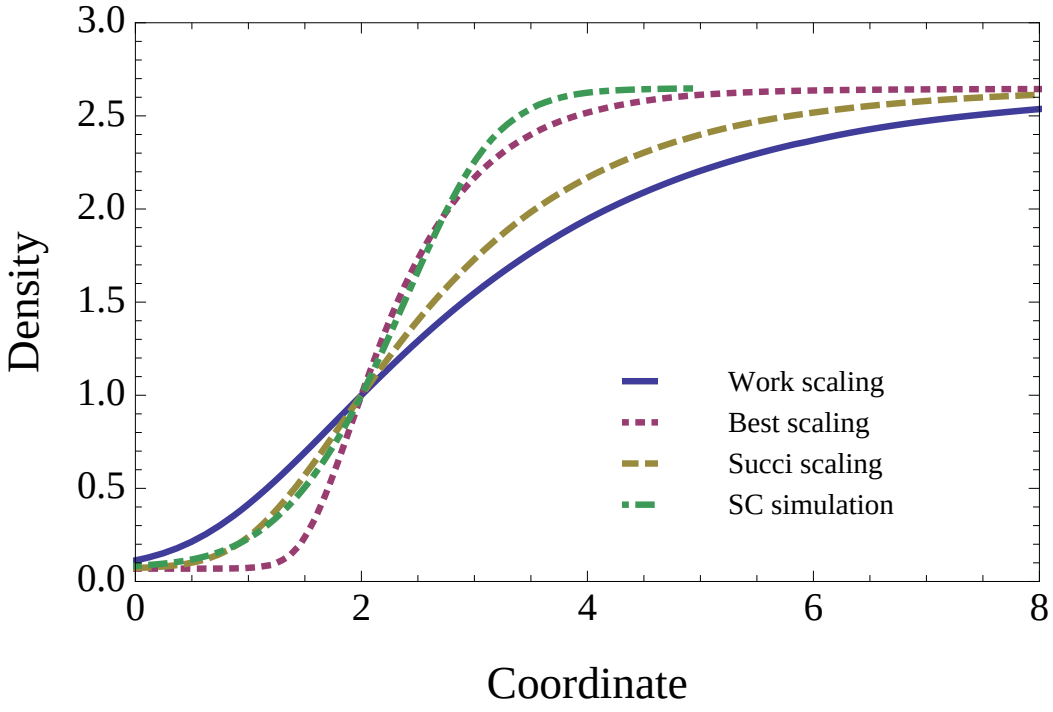

Figure 4.5: Density profile dependency on the surface tension factor k taken as $-G/18$ for the present work scaling, $-1/G$ for the scaling from (Benzi et al., 2006) ("Succi scaling"), $G = -1/(4G)$ for the best scaling in the least-square sense. Notice the better performance of the "Succi scaling" in a low density regime and the better performance of the "Best scaling" curve overall in the least-square sense. $G = -6.0$ was taken for the simulation.

"Best scaling", and the referenced scaling of Benzi et al. (2006) is referenced as "Succi scaling". Overall, one can adopt the surface tension parameter $k = -1/(4G)$ as giving the closest curve to the original Shan-Chen simulations. Note that the parameter is taken as $G < -4$, because the separation begins for $G < G_{crit}$. Thus, the collapse for $k = -1/(4G)$ is avoided.

Once the best scaling is adopted, i.e. $k = -\dfrac{1}{4G}$, it is possible to reconstruct the Maxwellian interfaces for different G and compare them with the simulation results with the original Shan-Chen model. For example, the restored profiles for different G for the Maxwell reconstruction are presented in Fig. 4.6. The comparison between Maxwell reconstruction profiles for $k = -\frac{1}{4G}$ and Shan-Chen theoretical profiles are illustrated in

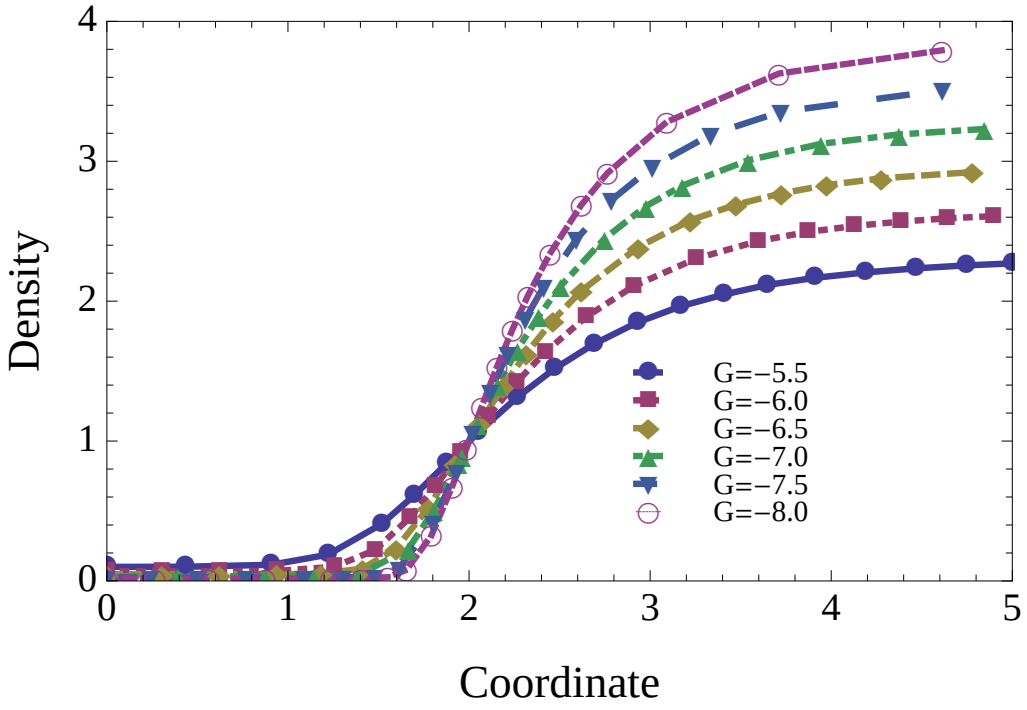

Figure 4.6: Density profile dependency on G for the Maxwell reconstruction in compliance with Navier-Stokes equation. Notice the interface width decrease with the gas-liquid density increase while G increases.

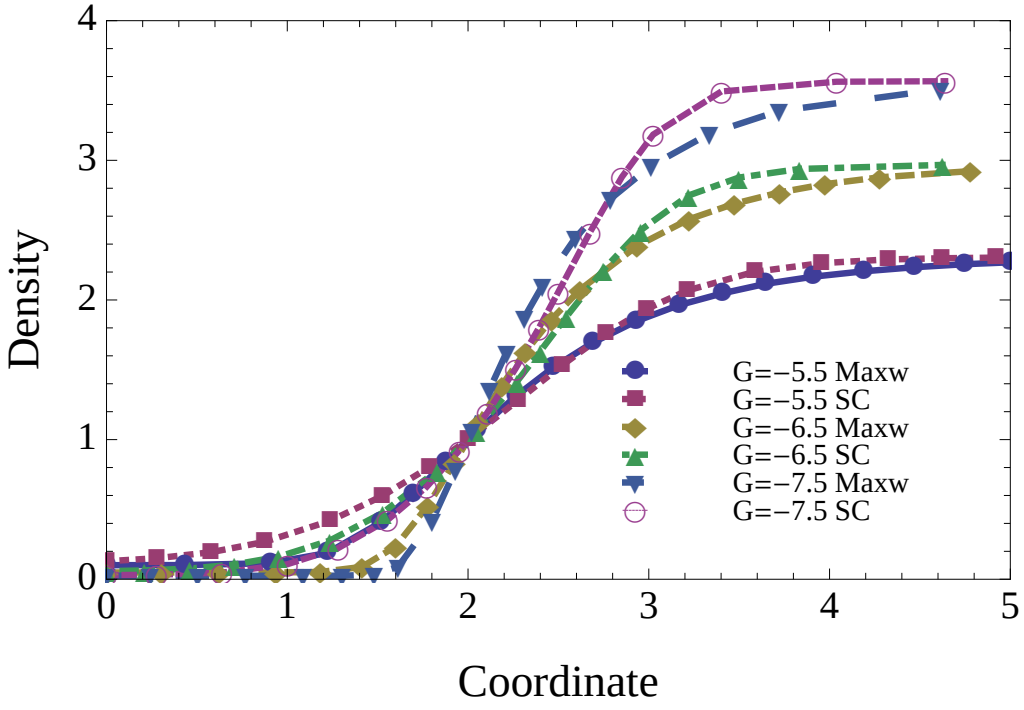

Figure 4.7: Density profile dependency on G for the Maxwell reconstruction and Shan-Chen theoretical reconstruction. One can see the difference between the profiles' widths. However, the equation of state density values are almost the same as in the original Shan-Chen model.

Fig. 4.7.

4.1.7 Limitations of the Shan-Chen model

Note that the surface tension and the equation of state depend on the same parameter G, which is clearly a limitation of the Shan-Chen model. Therefore, by taking a larger parameter G the gas-liquid density ratio is not only increased, as shown in Fig. 4.8 for the droplet profiles, but the interface width is decreased because of the larger surface tension. This is one reason for the stability failure with the large G parameter. As the interface is narrowed and the scheme fails due to large density gradients. Sbragaglia et al. (2007) introduced the multirange potential to separate the equation of state and the surface tension. However, it is not compliant with the Navier-Stokes surface tension term.

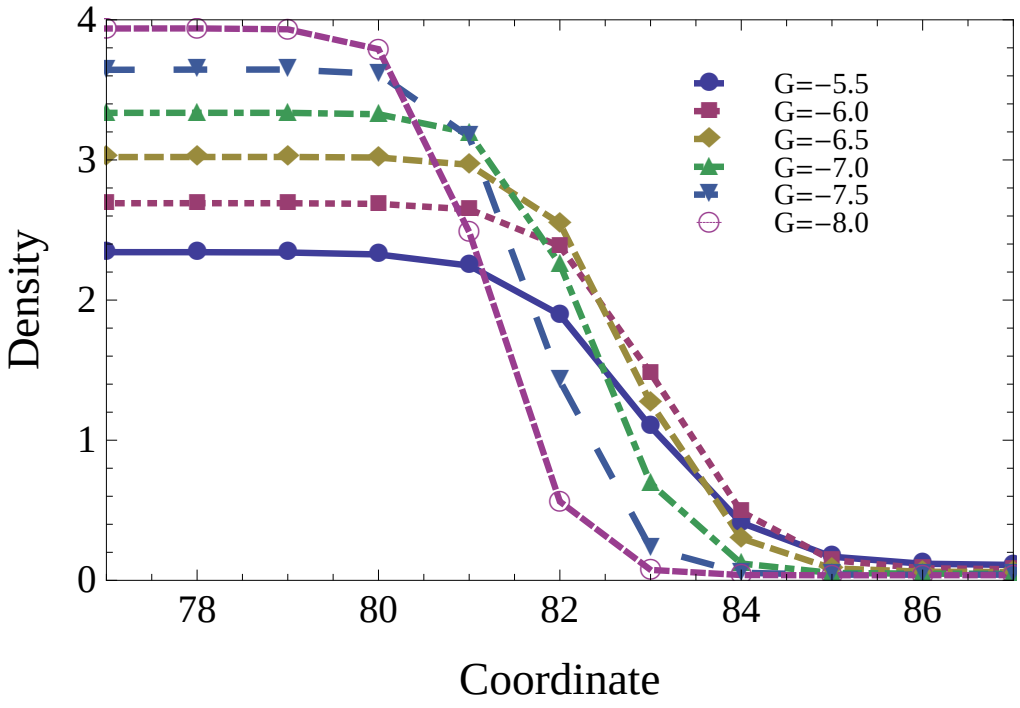

Figure 4.8: Density profile dependency on G. Note that the interface width decreases with a gas-liquid density increase while G increases. The simulations are made for the droplet put in the centre of the 128x128 domain with radius 20 lattice units initialized with the ρ_g and ρ_l obtained from the equation of state and the Maxwell reconstruction law.

This work introduces a modified Shan-Chen multirange potential, which can separate the equation of state and the surface tension term, and to include the surface tension term in compliance with the Navier-Stokes equation.

For the original pseudopotential function, Eq. (4.14), the Maxwell reconstruction is not fulfilled. Instead of the latter one, equation (4.12) is used to restore profiles which are close but not exact to the obtained by the Maxwell reconstruction. This limitation is stated as thermodynamical inconsistency (Nourgaliev et al., 2003). The same goes for the surface tension which is for the difusion interface in compliance with the Navier-Stokes equation can be represented as:

$$\sigma = k \int_{-\infty}^{+\infty} |\partial_n \rho|^2 \mathrm{d}\boldsymbol{n} \tag{4.22}$$

Even the latter expression (4.22) is proportional to the Navier-Stokes surface tension term, as stated in (Sbragaglia et al., 2007), the Shan-Chen surface tension is deviated from the latter. This is also one of the limitations of the Shan-Chen model, so-called thermodynamical inconsistency. It will be examined closer in the multirange section.

As mentioned before, the equilibrium distribution function defined before can be represented as the low Mach expansion for the Boltzmann continuous distribution. The lattice Boltzmann method operates in the limit of slightly compressible flow region. The Shan-Chen method produces the spurious currents around the droplet, which for the large gas-liquid density ratio make the numerical scheme unstable. One can refer to Fig. 4.9, where the Mach number map, $Ma = \frac{u}{c_s}$, is presented for the droplet of radius 20 units with $G = -8.0$ on the grid 128x128 units. Fig. 4.9 shows that there are places on the interface where the Mach number is close to c_s, the stability limit for the LBM.

Some authors suggested that the instability comes from the poor discretization of the surface tension term. They propose the better numerical schemes to tackle with the instabilities (Sbragaglia et al., 2007; Shan, 2006; Wu et al., 2008). Others suggested modification of the pseudopotential to include other equations of states (Yuan and Schaefer, 2006a). This allows inclusion of the Peng-Robinson, Carnahan-Sterling, van der Waals equations of states, giving lower spurious currents for the same gas-liquid density ratio.

This work presents a method to overcome some of the mentioned problems. The combination of the multi-relaxation time collision operator and the modified multirange potential overcomes limitations of the original Shan-Chen model, i.e. stability and the thermodynamical inconsistency.

The original Shan-Chen model cannot simulate anisotropic phenomena, thus, the generalized Shan-Chen model will be used to simulate anisotropic phenomena, mainly occurring in ferro-fluidics.

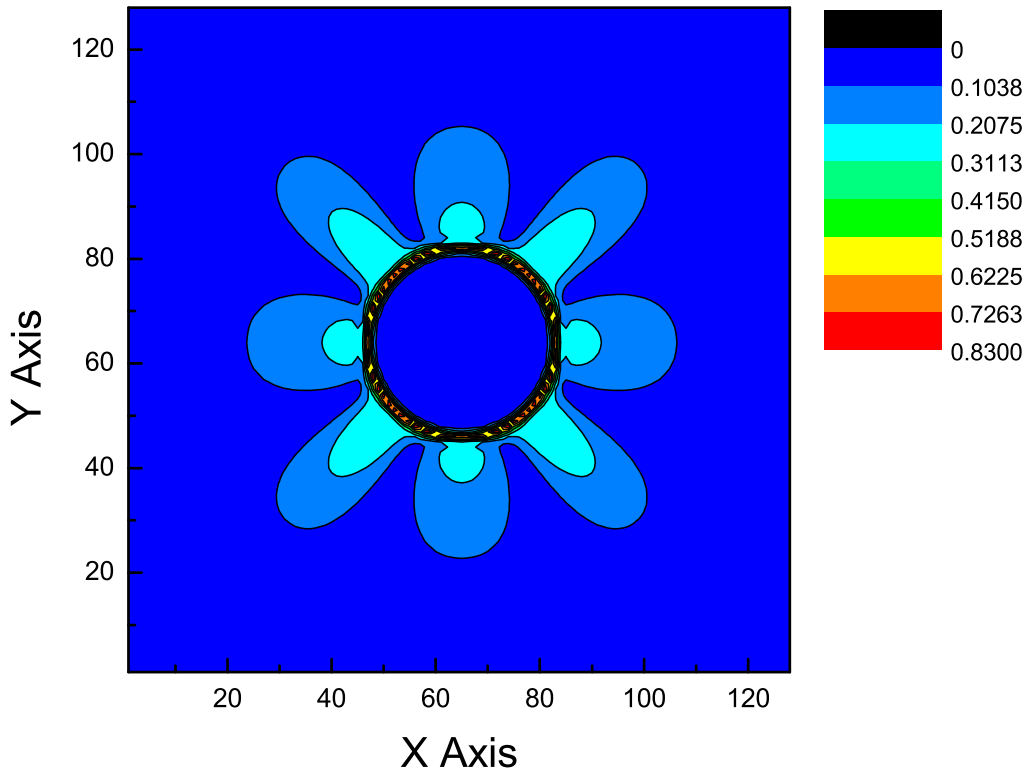

Figure 4.9: Mach number for the droplet of radius 20 after 3000 steps. Mach number is defined as $\frac{\sqrt{u_x^2+u_y^2}}{c_s}$. One can see the quadrupole structure of the spurious currents.

4.2 Multirange Shan-Chen model

The section presents the modified Shan-Chen model with the multirange potential. The method overcomes some limitations of the Shan-Chen model stated earlier, such as the non-thermodynamical behaviour (Fig. 4.7), the proper inclusion of the Navier-Stokes compliant surface tension term and the reduction of spurious currents. The section is divided into several parts. First, the explanation of the multirange potential will be given, followed by the proper inclusion of the surface tension coefficient k through numerical stencils. The section is concluded by numerical simulation results.

4.2.1 Multirange potential

As stated in equation (4.5), the obtained equation of state and the surface tension term depend on the discretization of the Shan-Chen force. Once the different discretization is introduced, the latter can help in obtaining better discretizations of the surface tension term and even to include the Navier-Stokes compliant surface tension term. Therefore, the multirange Shan-Chen force can be introduced as follows:

$$\boldsymbol{F} = -G \sum_{i=1..n} w_i^{SC}(\|\boldsymbol{c_i}\|)\psi(\boldsymbol{r})\boldsymbol{c_i}, \tag{4.23}$$

where weights w^{SC} are the corresponding discretization weights for the Shan-Chen force, and n is the number of discretization points. Weights, w^{SC}, depend on the modulus of velocity $\boldsymbol{c_i}$ fulfilling the isotropy of the problem. The larger number of points are used for the discretization of the Shan-Chen force, the better isotropic approximations are possible. That means the model becomes not the nearest neighbours model, but two or more layers can be taken for the discretization. The multirange model presented here attempts to decrease the spurious currents amplitude, and to include the Navier-Stokes surface tension term.

4.2.2 Spurious currents

The spurious currents for one of the simulations are presented in Fig. 4.9. It is known that the spurious currents are related to the discretization of the surface tension term and nonisotropy of the Shan-Chen force (Benzi et al., 2006; Shan, 2006). For instance, the Shan-Chen force in the usual form presented above can be expanded into a Taylor series to the fifth order as follows:

$$\begin{aligned} F_x &= \frac{G}{3}\boldsymbol{\nabla}\psi + \frac{G}{18}\boldsymbol{\nabla}\Delta\psi + \frac{G}{216}\boldsymbol{\nabla}\Delta^2\psi - \frac{G}{520}\partial_x^5\psi \\ F_y &= \frac{G}{3}\boldsymbol{\nabla}\psi + \frac{G}{18}\boldsymbol{\nabla}\Delta\psi + \frac{G}{216}\boldsymbol{\nabla}\Delta^2\psi - \frac{G}{520}\partial_y^5\psi. \end{aligned} \tag{4.24}$$

Note that terms $-\frac{G}{520}\partial_x^5\psi$ and $-\frac{G}{520}\partial_x^5\psi$ are nonisotropic and introduce the quadrupole structure of the spurious currents presented in Fig.4.9. Sbragaglia et al. (2007) introduced the different discretizations for the Shan-Chen force, where certain isotropies are fulfilled. Fig. 4.10 presents the Sbragaglia et al. (2007) discretization schemes. The model overcomes the problem with inability of the Shan-Chen force to control the surface tension and the equation of state separately. But the problem with thermodynamical consistency still remains. Kuzmin and Mohamad (2009) suggested a modified version of the multirange potential to include the Navier-Stokes surface tension. This work shows that the degree of isotropy can be even further improved. The method introduced below can overcome the isotropy problem and separates the equation of state and the surface tension term.

4.2.3 2^{nd} layer multirange potential

Fig. 4.11 illustrates the 2^{nd} layer multigrid velocity vectors. Velocity directions are sorted by the amplitude. Directions 1,2,3,4 have amplitude 1 and have weight w_1; directions 5,6,7,8 have amplitude 2 with weight w_2; directions 9,10,11,12 have amplitude 4 with weight w_4, directions 13,14,15,16,17,18,19,20 - amplitude 5 with weight w_5; directions 21,22,23,24 - amplitude 8 with weight w_8. Therefore, the second layer Shan-Chen force

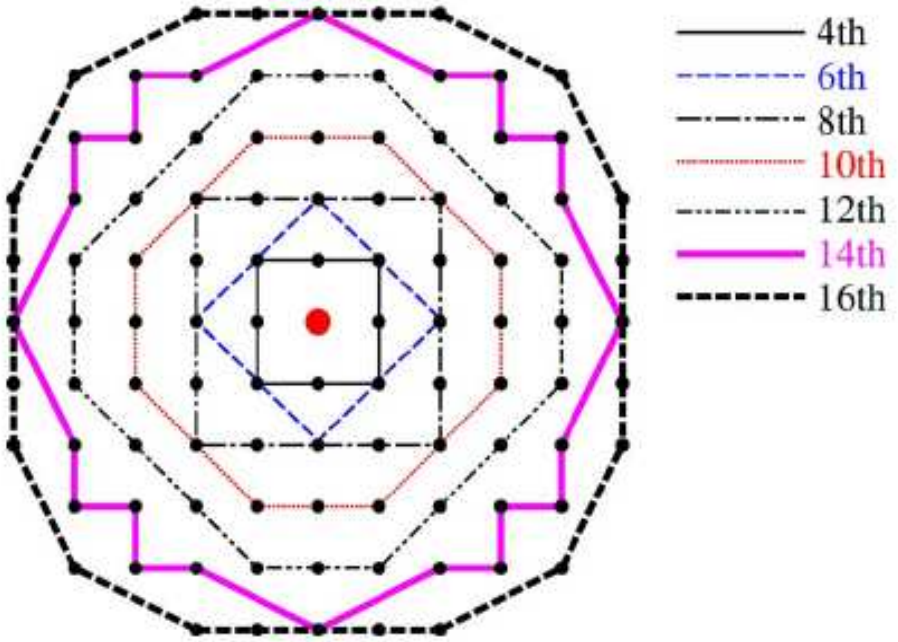

Figure 4.10: The multirange discretization of Shan-Chen model (courtesy of Sbragaglia et al. (2007)). The achieved isotropy is also presented.

can be expanded by Taylor series as:

$$\begin{aligned}\boldsymbol{F} = \quad & G\psi(\boldsymbol{r}) \sum_{i=1..4} w_1 \psi(\boldsymbol{r}+\boldsymbol{c_i})\boldsymbol{c_i} + G\psi(\boldsymbol{r}) \sum_{i=5..8} w_2 \psi(\boldsymbol{r}+\boldsymbol{c_i})\boldsymbol{c_i} + \\ & G\psi(\boldsymbol{r}) \sum_{i=9..12} w_4 \psi(\boldsymbol{r}+\boldsymbol{c_i})\boldsymbol{c_i} + G\psi(\boldsymbol{r}) \sum_{i=13..20} w_5 \psi(\boldsymbol{r}+\boldsymbol{c_i})\boldsymbol{c_i} + \\ & G\psi(\boldsymbol{r}) \sum_{i=21..24} w_8 \psi(\boldsymbol{r}+\boldsymbol{c_i})\boldsymbol{c_i}\end{aligned} \tag{4.25}$$

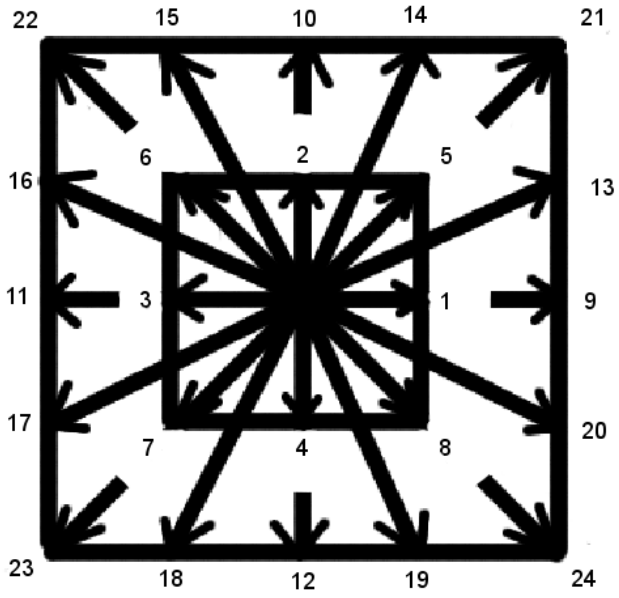

Figure 4.11: Second layer discretization Shan-Chen scheme. All velocity directions are numbered.

The latter expression reveals the internal structure of the multirange force:

$$
\begin{aligned}
F_x = \;& 2G\psi\partial_x\psi(w_1 + 2w_2 + 4w_4 + 10w_5 + 8w_8) + \\
& \left(\frac{G}{3}\psi\partial_x^3\psi(w_1 + 2w_2 + 16w_4 + 34w_5 + 32w_8) + 2(w_2 + 8(w_5 + 2w_8))\psi\partial_x\partial_y^2\psi\right) + \\
& \frac{G}{60}\Big(\psi\partial_x^5\psi(2(w_2 + 32w_4 + 65w_5 + 64w_8) + w_1) + \\
& 10(w_2 + 20w_5 + 64w_8)\left(\psi\partial_x\partial_y^4\psi + 2\psi\partial_x^3\partial_y^2\psi\right)\Big) \\
F_y = \;& 2\psi\partial_y\psi(w_1 + 2w_2 + 4w_4 + 10w_5 + 8w_8) + \\
& \left(\frac{G}{3}\psi\partial_y^3\psi(w_1 + 2w_2 + 16w_4 + 34w_5 + 32w_8) + 2(w_2 + 8(w_5 + 2w_8))\psi\partial_x^2\partial_y\psi\right) + \\
& \frac{G}{60}\Big(\psi\partial_y^5\psi(2(w_2 + 32w_4 + 65w_5 + 64w_8) + w_1) + \\
& 10(w_2 + 20w_5 + 64w_8)\left(2\psi\partial_x^2\partial_y^3\psi + \psi\partial_x^4\partial_y\psi\right)\Big)
\end{aligned}
\tag{4.26}
$$

The structure of the force implies additional equations for weights w_1, w_2, w_4, w_5 and w_8. The aim for the discretization is to satisfy the equation of state, to cancel the third order derivatives, as the proper Navier-Stokes term should be included, and to fulfill the isotropy of the higher order derivatives. The first condition is related to the equation of state:

$$\begin{aligned} p_0 &= \frac{\rho}{3} + \frac{G}{6}\psi(\rho)^2 \\ 2(w_1 + 2w_2 + 4w_4 + 10w_5 + 8w_8) &= \frac{1}{3} \end{aligned} \tag{4.27}$$

The Navier-Stokes compliant surface tension is defined through the force as:

$$\boldsymbol{F} = \frac{G}{3}\psi\boldsymbol{\nabla}\psi + k\rho\boldsymbol{\nabla}\Delta\rho. \tag{4.28}$$

The aim is to include the surface tension term $k\rho\boldsymbol{\nabla}\Delta\rho$ in the Shan-Chen force. It can be fulfilled when the third order derivatives are cancelled in equation (4.26). Thus, two more equations for weights can be obtained:

$$\begin{aligned} w_1 + 2w_2 + 16w_4 + 34w_5 + 32w_8 &= 0 \\ w_2 + 8(w_5 + 2w_8) &= 0 \end{aligned} \tag{4.29}$$

The fifth order terms in the equation (4.26) is to obtain the isotropic structure, i.e. $\boldsymbol{\nabla}\Delta^2\psi$. The condition gives one additional equation for the weights:

$$(2(w_2 + 32w_4 + 65w_5 + 64w_8) + w_1) = 10(w_2 + 20w_5 + 64w_8) \tag{4.30}$$

Therefore, the whole system of equations can be rewritten as:

$$\begin{aligned} 2(w_1 + 2w_2 + 4w_4 + 10w_5 + 8w_8) &= \frac{1}{3} \\ w_1 + 2w_2 + 16w_4 + 34w_5 + 32w_8 &= 0 \\ w_2 + 8(w_5 + 2w_8) &= 0 \\ (2(w_2 + 32w_4 + 65w_5 + 64w_8) + w_1) &= 10(w_2 + 20w_5 + 64w_8) \end{aligned} \tag{4.31}$$

The system consists of four equations with five unknown variables. Therefore, there is one degree of freedom, w_1 in this case. One cannot constrain w_1 with the isotropy of the

7th order tensor. Therefore, w_1 is the free parameter to be defined later. The solution of the system (4.31) is straightforward:

$$\begin{aligned} w_2 &= \frac{1}{135}(19 - 90w_1) \\ w_4 &= \frac{1}{60}(2 - 15w_1) \\ w_5 &= \frac{1}{270}(45w_1 - 8) \\ w_8 &= \frac{13 - 90w_1}{2160} \end{aligned} \tag{4.32}$$

There are three possibilities to obtain parameter w_1 as follows:

- The 7th order Taylor expansion of the Shan-Chen force reveals:

$$\begin{aligned} O(F_x) &= -\frac{7\left((90w_1 - 11)\partial_x^3\partial_y^4\psi + \partial_x\partial_y^6\psi + 3\partial_x^5\partial_y^2\psi\right) + 5\partial_x^7\psi}{3780} \\ O(F_y) &= -\frac{7\left((90w_1 - 11)\partial_y^4\partial_x^3\psi + 3\psi\partial_x^2\partial_y^5 + \partial_x^6\partial_y\psi\right) + 5\partial_y^7\psi}{3780} \end{aligned} \tag{4.33}$$

  Equation (4.33) almost restores the seventh order isotropy and is stated as:

$$O(\boldsymbol{F}) \approx \boldsymbol{\nabla}\Delta^3\psi = \boldsymbol{\nabla}\partial_x^6 + 3\partial_x^4\partial_y^2 + 3\partial_x^2\partial_y^2 + \partial_y^6 \tag{4.34}$$

  To approximate the isotropy one can equalize $90w_1 - 11 = 3$. Then $w_1 = \frac{7}{45}$. All other parameters can be found from previous equations, $w_2 = \frac{1}{27}$,$w_4 = -\frac{1}{180}$,$w_5 = -\frac{1}{270}$,$w_8 = -\frac{1}{2160}$. For the sake of simplicity, the discretization scheme is formulated through the matrix containing weights coefficients on certain velocity directions:

$$\begin{pmatrix} -\frac{1}{2160} & -\frac{1}{270} & -\frac{1}{180} & -\frac{1}{270} & -\frac{1}{2160} \\ -\frac{1}{270} & \frac{1}{27} & \frac{7}{45} & \frac{1}{27} & -\frac{1}{270} \\ -\frac{1}{180} & \frac{7}{45} & 0 & \frac{7}{45} & -\frac{1}{180} \\ -\frac{1}{270} & \frac{1}{27} & \frac{7}{45} & \frac{1}{27} & -\frac{1}{270} \\ -\frac{1}{2160} & -\frac{1}{270} & -\frac{1}{180} & -\frac{1}{270} & -\frac{1}{2160} \end{pmatrix}. \tag{4.35}$$

- Another possibility to be distinguished is the choice of w_1, when the numerical scheme is efficient in terms of computational simplicity. We consider the

computational simplicity if the same order of the isotropiness can be achieved with some weights coefficients equal to zero. Eight velocity directions have the weight w_5, representing the biggest group for the discretization. The purpose is to force w_5 to equal zero. The solution is $w_1 = \frac{8}{45}$. Then, the parameters are $w_2 = \frac{1}{45}$,$w_4 = -\frac{1}{90}$,$w_5 = 0$,$w_8 = -\frac{1}{720}$. It can be represented in the matrix form as:

$$\begin{pmatrix} -\frac{1}{720} & 0 & -\frac{1}{90} & 0 & -\frac{1}{720} \\ 0 & \frac{1}{45} & \frac{8}{45} & \frac{1}{45} & 0 \\ -\frac{1}{90} & \frac{8}{45} & 0 & \frac{8}{45} & -\frac{1}{90} \\ 0 & \frac{1}{45} & \frac{8}{45} & \frac{1}{45} & 0 \\ -\frac{1}{720} & 0 & -\frac{1}{90} & 0 & -\frac{1}{720} \end{pmatrix} . \tag{4.36}$$

The discretization scheme with $w_5 = 0$ utilizes the original set of $D2Q9$ scheme, as follows:

$$\begin{aligned} \boldsymbol{F} = \quad & w_1 G\psi \sum_{i=1..4} \psi(\boldsymbol{r} + \boldsymbol{c_i})\boldsymbol{c_i} + w_2 G\psi \sum_{i=5..8} \psi(\boldsymbol{r} + \boldsymbol{c_i})\boldsymbol{c_i} + \\ & 2w_4 G\psi \sum_{i=1..4} \psi(\boldsymbol{r} + 2\boldsymbol{c_i})\boldsymbol{c_i} + 2w_8 G\psi \sum_{i=5..8} \psi(\boldsymbol{r} + 2\boldsymbol{c_i})\boldsymbol{c_i} \end{aligned} \tag{4.37}$$

The discretization of the equation of state requires only a 16-point stencil scheme. This form is close to the one presented in (Kuzmin and Mohamad, 2009). Although it provides better isotropy in the fifth order terms. The advantage of using the multirange potential is into obtaining a pure potential of the equation of state without additional surface tension terms at a reasonable computational cost.

- The latter discretization can be compared with the suggested by Kuzmin and Mohamad (2009) multirange potential, which is:

$$\boldsymbol{F} = G_1\psi(\boldsymbol{r}) \sum_i \psi(\boldsymbol{r} + \boldsymbol{c_i}\Delta t)\boldsymbol{c_i} + G_2\psi(\boldsymbol{r}) \sum_i \psi(\boldsymbol{r} + 2\boldsymbol{c_i}\Delta t)\boldsymbol{c_i}, \tag{4.38}$$

By the Taylor series expansion, the following formula is obtained:

$$F_\alpha = \frac{G_1 + 2G_2}{3}\psi\partial_\alpha\psi + \frac{G_1 + 8G_2}{6}\psi\partial_\alpha\Delta\psi\,. \tag{4.39}$$

By taking $G_2 = -G_1/8$, the surface tension force term equals zero. Therefore, equating $G_2 = -G_1/8$ also allows the proper equation of state to be obtained by multiplying the force by 4/3:

$$\begin{aligned} F_\alpha =& \frac{4}{3}(F_1 + F_2) = \frac{4}{3}\frac{G_1 + 2G_2}{3}\psi\partial_\alpha\psi \\ =& \frac{G_1}{3}\psi\partial_\alpha\psi \quad , \end{aligned}$$

which refers to the equation of state $p = c_s^2\rho + \frac{G_1}{6}\psi^2$ without any additional terms from the surface tension. In the notations introduced above, the scheme is represented with the following parameters $w_1 = 4/27$, $w_2 = 1/27$,$w_4 = -1/108$,$w_5 = 0$,$w_8 = -1/432$. The matrix form for this choice of the potential is:

$$\begin{pmatrix} -\frac{1}{432} & 0 & -\frac{1}{108} & 0 & -\frac{1}{432} \\ 0 & \frac{1}{27} & \frac{4}{27} & \frac{1}{27} & 0 \\ -\frac{1}{108} & \frac{4}{27} & 0 & \frac{4}{27} & -\frac{1}{108} \\ 0 & \frac{1}{27} & \frac{4}{27} & \frac{1}{27} & 0 \\ -\frac{1}{432} & 0 & -\frac{1}{108} & 0 & -\frac{1}{432} \end{pmatrix} . \tag{4.40}$$

However, the latter expression doesn't restore the isotropy of even 5th order expansion.

All the cases can be compared with each other, but firstly the surface tension discretization should be introduced.

4.2.4 Surface tension term discretization

Once the potential for the equation of state is known, the force term can be split into two parts. One part is related to the potential, and the other is to the surface tension:

$$\boldsymbol{F} = \boldsymbol{F}_{pot} + \boldsymbol{F}_s, \tag{4.41}$$

where $\boldsymbol{F}_s = \frac{G}{18}\psi\boldsymbol{\nabla}\Delta\psi$. This term will be replaced by $\boldsymbol{F}_s = k\rho\boldsymbol{\nabla}\Delta\rho$. When using the extended multirange potential, the surface tension term will be discretized through a 25-point stencil discretization scheme.

Different numerical schemes may be used for the discretization of the Laplacian or the gradient. Let us represent the stencil through the matrix below, where every element applies to the corresponding point in the lattice. Any 25-point stencil has the following form:

$$\begin{pmatrix} a_{11} & a_{12} & a_{13} & a_{14} & a_{15} \\ a_{21} & a_{22} & a_{23} & a_{24} & a_{25} \\ a_{31} & a_{32} & a_{33} & a_{34} & a_{35} \\ a_{41} & a_{42} & a_{43} & a_{44} & a_{45} \\ a_{51} & a_{52} & a_{53} & a_{54} & a_{55} \end{pmatrix}. \tag{4.42}$$

For the gradient of the Laplacian in the x-direction ($\partial_x\Delta$) the following conditions apply. First of all, it is asymmetric in the x-direction and symmetric in the y-direction:

$$\begin{pmatrix} a_{11} & a_{12} & 0 & -a_{12} & -a_{11} \\ a_{21} & a_{22} & 0 & -a_{22} & -a_{21} \\ a_{31} & a_{32} & 0 & -a_{32} & -a_{31} \\ a_{21} & a_{22} & 0 & -a_{22} & -a_{21} \\ a_{11} & a_{12} & 0 & -a_{12} & -a_{11} \end{pmatrix}. \tag{4.43}$$

After expanding, using the Taylor series about the central point, the expression can be obtained:

$$\begin{aligned} &\partial_x\Delta = -2\left(\partial_x(4a_{11} + 2(a_{12} + 2a_{21} + a_{22} + a_{31}) + a_{32})\right) + \\ &\left(-\frac{1}{3}\partial_x^3\psi(2(8a_{11} + a_{12} + 8a_{21} + a_{22} + 4a_{31}) + a_{32}) - 2\partial_x\partial_y^2\psi(8a_{11} + 4a_{12} + 2a_{21} + a_{22})\right) + \\ &\frac{1}{60}\Bigg(-\partial_x^5\psi(2(32a_{11} + a_{12} + 32a_{21} + a_{22} + 16a_{31}) + a_{32}) \\ &- 10\partial_x\partial_y^4\psi(32a_{11} + 16a_{12} + 2a_{21} + a_{22}) - 20\partial_x^3\partial_y^2\psi(32a_{11} + 4a_{12} + 8a_{21} + a_{22})\Bigg) \end{aligned} \tag{4.44}$$

From equation (4.44), the following equations are developed to obtain third order derivative:

$$\begin{aligned} 8a_{11}+4a_{12}+8a_{21}+4a_{22}+4a_{31}+2a_{32} &= 0 \\ -16a_{11}-8a_{12}-4a_{21}-2a_{22} &= -\frac{16}{3}a_{11}-\frac{2}{3}a_{12}- \\ & \quad \frac{16}{3}a_{21}-\frac{2}{3}a_{22}-\frac{8}{3}a_{31}-\frac{1}{3}a_{32} \\ -16a_{11}-8a_{12}-4a_{21}-2a_{22} &= 1. \end{aligned} \tag{4.45}$$

To insure the isotropy of the problem one needs to impose two more conditions:

$$\begin{aligned} (2(32a_{11}+a_{12}+32a_{21}+a_{22}+16a_{31})+a_{32}) &= -10\partial_x\partial_y^4\psi(32a_{11}+16a_{12}+2a_{21}+a_{22}) \\ -20\partial_x\partial_y^4\psi(32a_{11}+16a_{12}+2a_{21}+a_{22}) &= -20\partial_x^3\partial_y^2\psi(32a_{11}+4a_{12}+8a_{21}+a_{22}) \end{aligned} \tag{4.46}$$

The solution of the systems (4.45) and (4.46) is the following:

$$\begin{aligned} a_{11} &= \frac{1}{72}(5-6a_{32}) \\ a_{12} &= \frac{1}{18}(-4+3a_{32}) \\ a_{21} &= \frac{1}{9}(-4+3a_{32}) \\ a_{22} &= \frac{1}{18}(13-12a_{32}) \\ a_{31} &= \frac{1}{4}(1-2a_{32}) \end{aligned} \tag{4.47}$$

With the parametrization as $a_{32}=1$ the discretization scheme for $\partial_x\Delta$ can be obtained:

$$\partial_x\Delta = \frac{1}{72}\begin{pmatrix} -1 & -4 & 0 & 4 & 1 \\ -8 & 4 & 0 & -4 & 8 \\ -18 & 72 & 0 & -72 & 18 \\ -8 & 4 & 0 & -4 & 8 \\ -1 & -4 & 0 & 4 & 1 \end{pmatrix}, \tag{4.48}$$

which is the same as used in number of works (Kuzmin and Mohamad, 2009; Pooley and Furtado, 2008). Another parametrization scheme is with $a_{32}=\frac{29}{30}$ which gives better

isotropy:

$$\partial_x \Delta = \frac{1}{180} \begin{pmatrix} -2 & -11 & 0 & 11 & 2 \\ -22 & 14 & 0 & -14 & 22 \\ -42 & 174 & 0 & -174 & 42 \\ -22 & 14 & 0 & -14 & 22 \\ -2 & -11 & 0 & 11 & 2 \end{pmatrix} \tag{4.49}$$

4.2.5 Numerical simulation results

The droplet of radius 20 lattice units is initialized with $\rho_l = 3.273$ in the centre of domain with $\rho_g = 0.0386$. The parameter of Shan-Chen model was taken as -7.0. One of the examples where the interface thickness is controlled by the surface tension parameter k is given in Fig. 4.12, where the original method of shifting velocity with $\tau = 1$ is applied to the numerical scheme as in (Kuzmin and Mohamad, 2009).

As shown in Fig. 4.12, even parameter k controls the interface width, however with increase of k the width becomes larger. This certainly conflicts with physics. The irregularities come from either additional contribution of the force, or the higher order of Shan-Chen force are larger than the proper surface tension contributions. To ensure that the contribution of the additional force term due to the shifting velocity is not involved, the proper forcing was implemented with the model suggested by Kuzmin and Mohamad (2009). The parameters were taken as $G = -5.5$, $\rho_l = 2.26$ and $\rho_g = 0.1$ for the droplet with radius 20 lattice units. Fig. 4.13 shows the same tendency as the shifting velocity method. Therefore, one needs to account for the higher orders of the force expansion, and more complicated numerical schemes are needed to be used in order to restore proper interface behaviour.

To check the validity of the statement that the higher order involved, and not the discretization of the Navier-Stokes term, $\boldsymbol{F_s} = k\rho\boldsymbol{\nabla}\Delta\rho$, causes the interface misbehaviour,

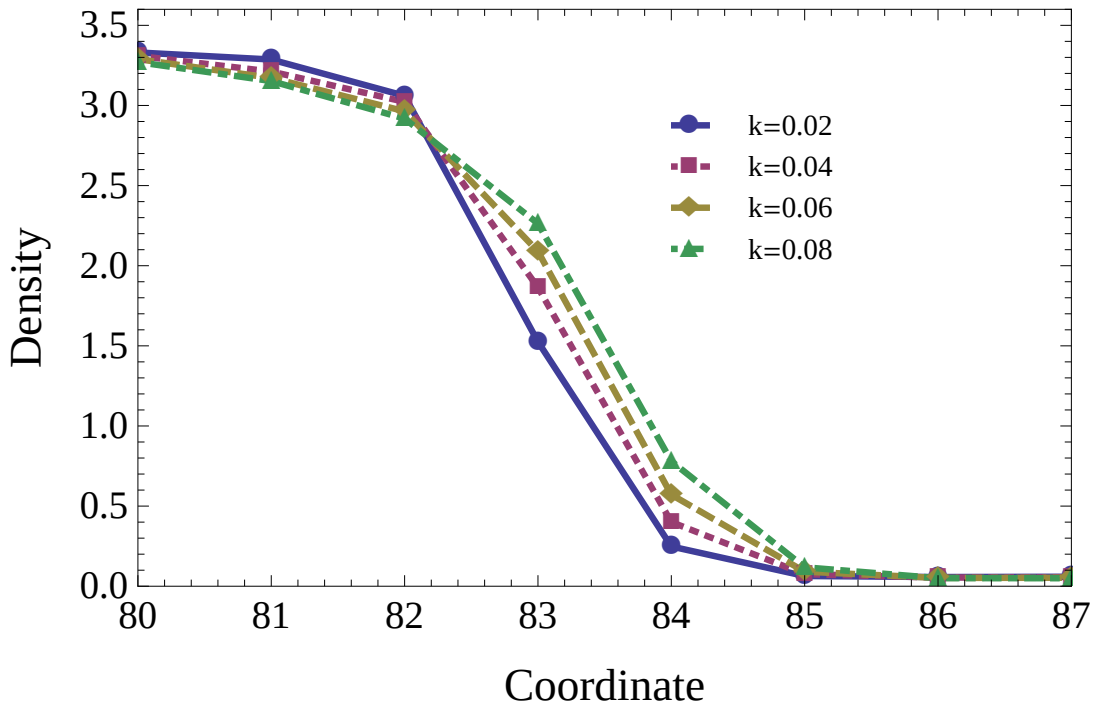

Figure 4.12: Interface density profiles are controlled by the surface tension parameter k. The method used is the shifting velocity procedure as in (Kuzmin and Mohamad, 2009).

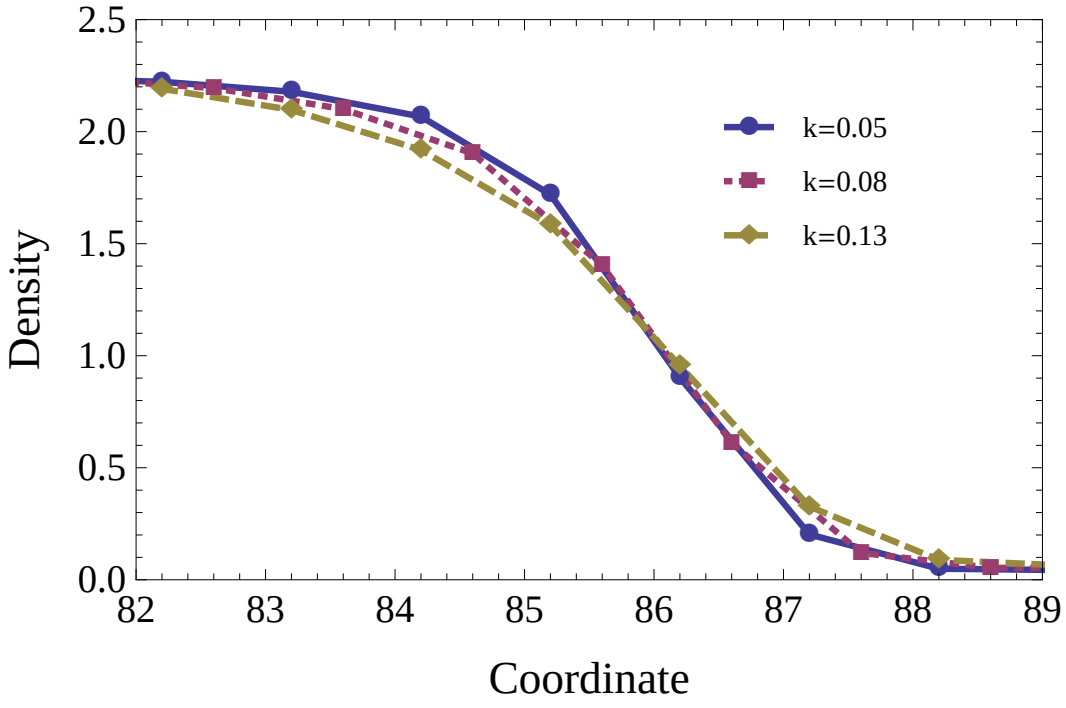

Figure 4.13: Interface density profiles are controlled by the surface tension parameter k. The method used is the proper incorporation of the force described earlier.

the original surface tension, $\boldsymbol{F_s} = G_2 \boldsymbol{\nabla} \Delta\psi$, was discretized through the schemes given. One, so-called isotropy scheme, refers to equations (4.35) and (4.49). Another is used by Kuzmin and Mohamad (2009), so-called "paper" discretization, is the combination of the equations (4.48) and (4.40). By varying G_2 we expect the proper behaviour of the interface width, i.e. the increase of G_2 invokes the decrease of the interface width. However, Fig. 4.14 and Fig. 4.15 indicate that the interface width increases at the same time that the surface tension factor G_2 does. Therefore, better numerical schemes which account for the fifth and seventh order of the force expansion are needed.

The numerical simulations show that the isotropy scheme is better in terms of the stability. However, Fig. 4.16 shows almost the same density profiles between the isotropy and the paper schemes. Despite of the misbehaviour of the interface, the model is still valid for the macroscale, i.e. the Laplace law is satisfied. Therefore, the following nu-

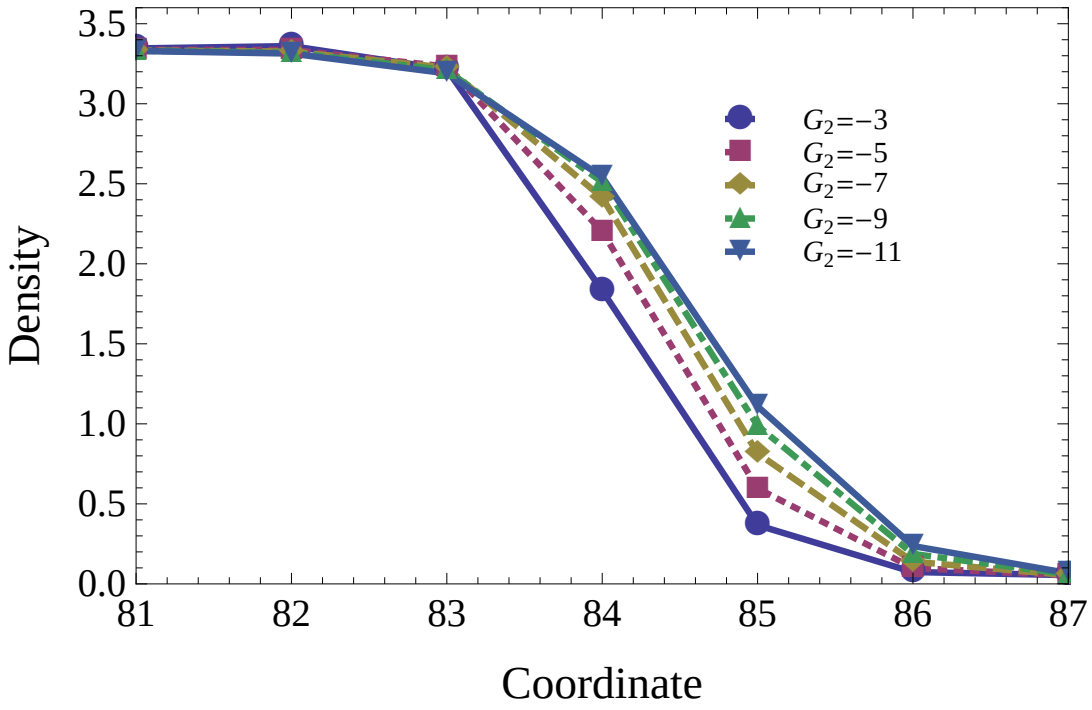

Figure 4.14: Interface density profiles are controlled by the surface tension parameter G_2. The model discretizes the surface tension and the equation for state separately. The isotropy discretization scheme is used for the potential and the surface tension.

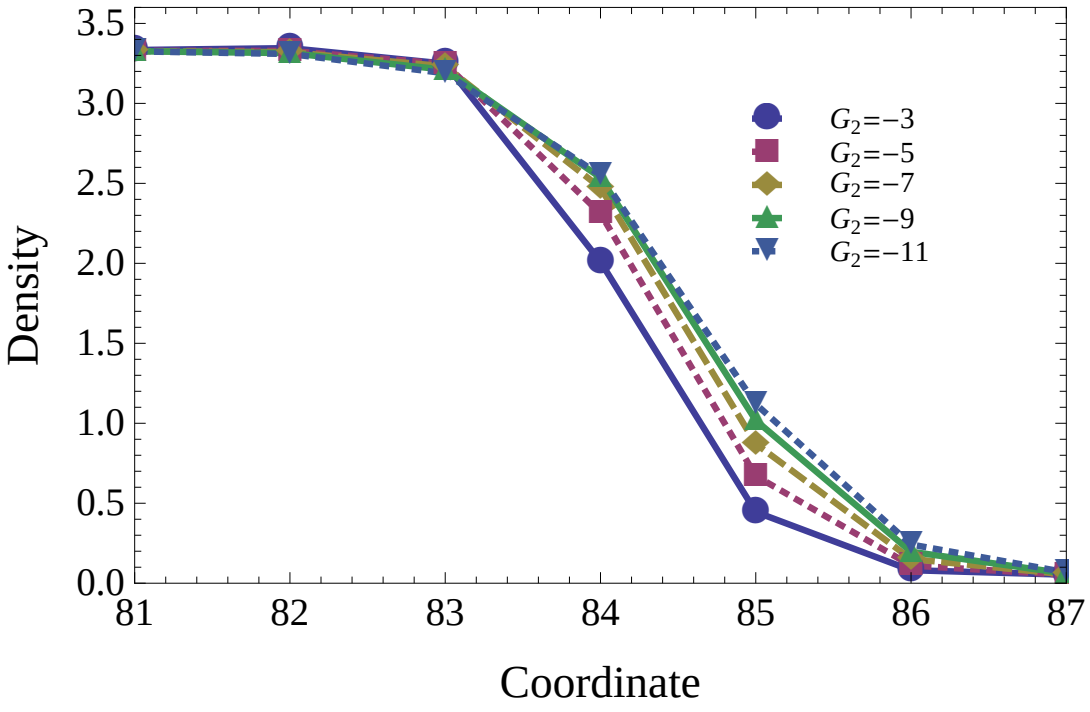

Figure 4.15: Interface density profiles are controlled by surface tension parameter G_2. The discretization is done as in (Kuzmin and Mohamad, 2009) for $G = -7.0$.

merical schemes with the discretized Navier-Stokes surface tension are used:

- The isotropy scheme refers to the equations (4.35) and (4.49). Equation (4.35) is used to calculate the force which accounts for the equation of state. Equation (4.49) is used to obtain $\nabla\Delta\rho$, then it's multiplied on $k\rho$ to obtain the Navier-Stokes surface tension. This scheme is better in isotropy to reduce the spurious currents, thus it's better in stability. However, the improvements are minor and do not give tangible effects in the simulation tests.

- The paper scheme, equations (4.48) and (4.40), goes through the same procedure. Another one used in the (Kuzmin and Mohamad, 2009), so-called paper discretization, is the combination of the equations (4.48) and (4.40).

Although there are some problems with interface behaviour one can check the Laplace Law, which states that the difference between pressures inside and outside the droplet

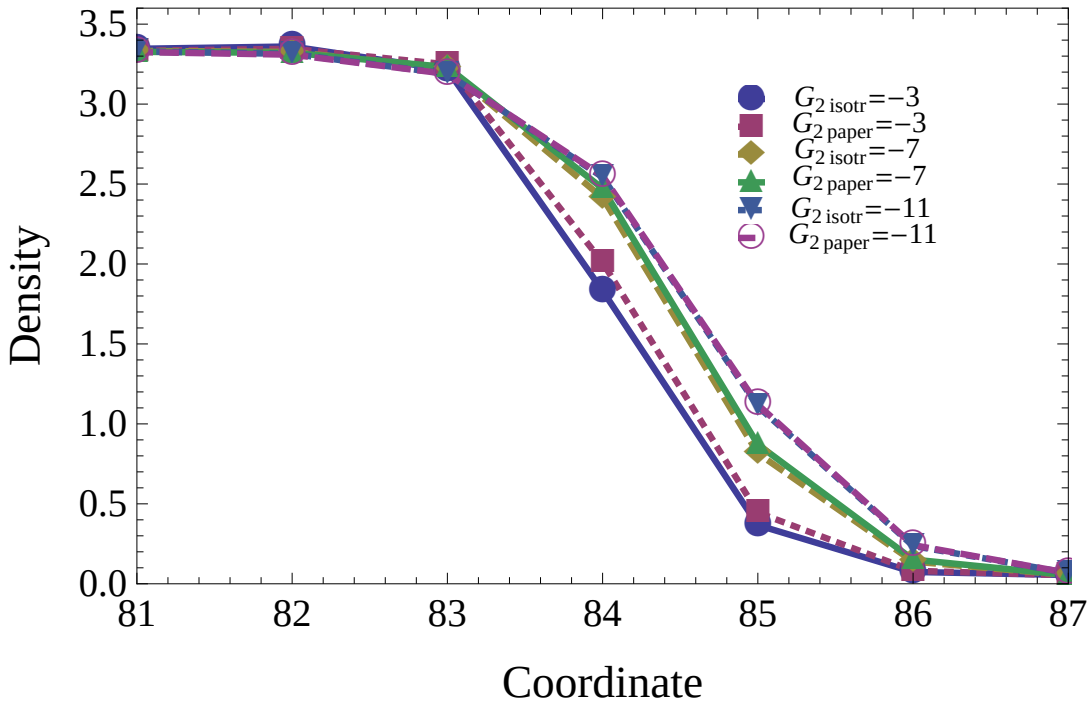

Figure 4.16: Interface density profiles comparison controlled for the isotropy discretization and discretization as mentioned in (Kuzmin and Mohamad, 2009). Surface tension is controlled by parameter G_2. The equation of state is taken with $G = -7.0$. The difference between the numerical schemes is minor.

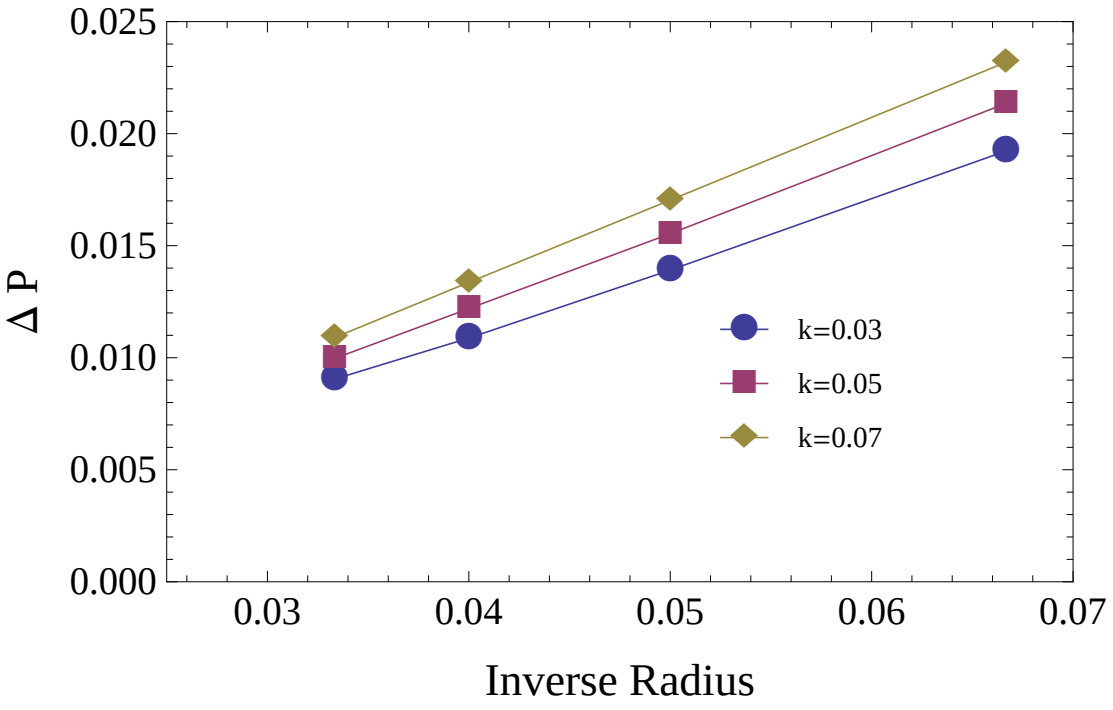

Figure 4.17: The Laplace law for the isotropy discretization with the different surface tensions k parameters. The equation of state is taken with $G = -7.0$.

should be proportional to the surface tension and be reversely proportional to the radius of the droplet. The pressure difference is defined through the equation of state:

$$\Delta P = \frac{\rho_l - \rho_g}{3} + \frac{G}{6}(\psi(\rho_l)^2 - \psi(\rho_g)^2). \tag{4.50}$$

The Laplace law is verified and shown in Fig. 4.17 for the isotropy discretization and Fig. 4.18 for the paper discretization. Even the interface is increased with the increase of the parameters k, but the Laplace law is verified given the proper surface tension. The linear regression was performed for the data to prove the linearity of the law:

- Paper discretization (Kuzmin and Mohamad, 2009):

  $k = 0.03$: $\Delta P = -0.0016350763744534622 + 0.3083195063230295\frac{1}{R}$

  $k = 0.05$: $\Delta P = -0.0011243361919483427 + 0.3313945272432076\frac{1}{R}$

  $k = 0.07$: $\Delta P = -0.0012378359795153053 + 0.3623552892211475\frac{1}{R}$

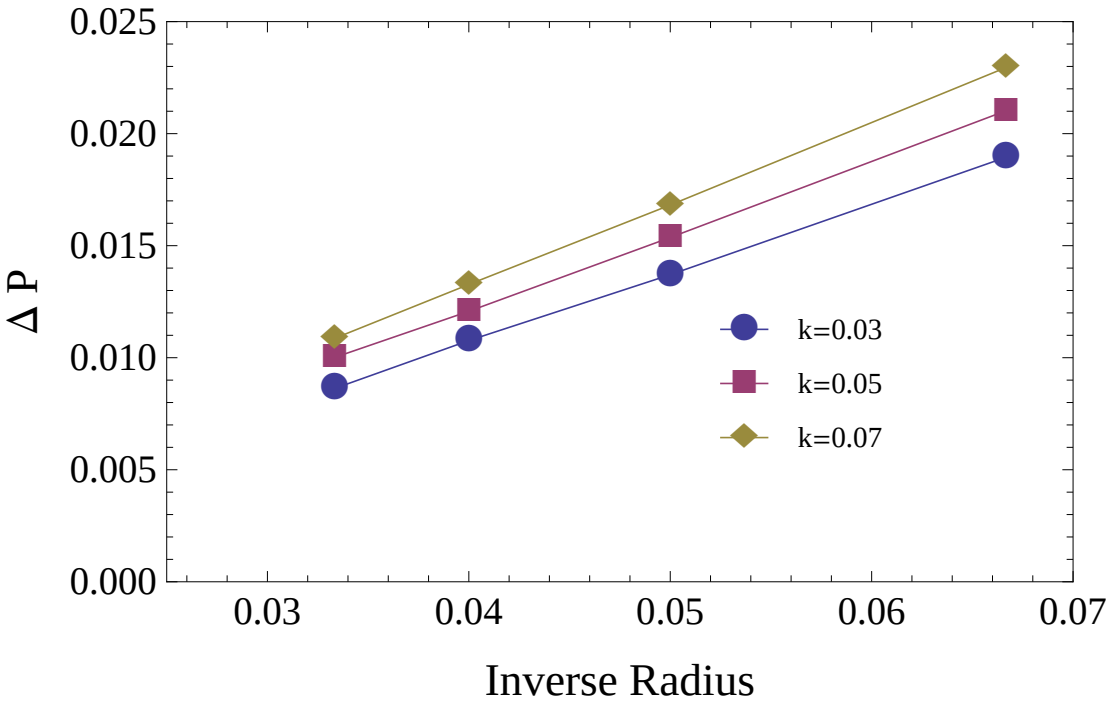

Figure 4.18: The Laplace law for the isotropy discretization for the different surface tensions k parameters. The equation of state is taken with $G = -7.0$.

- Isotropy discretization:

  $k = 0.03$: $\Delta P = -0.0013146878905434612 + 0.3069269489962196\frac{1}{R}$

  $k = 0.05$: $\Delta P = -0.0014663292967228153 + 0.3416053168811372\frac{1}{R}$

  $k = 0.07$: $\Delta P = -0.0013855521651597296 + 0.3685459029535829\frac{1}{R}$

4.2.6 Discussion

It can be concluded that the multirange model presented here gives adequate surface tension, although the interface is controlled by higher order approximations in the Shan-Chen force. The model can be used to control separately the surface tension and the equation of state. To give the entire picture for the model it is necessary to establish the surface tension dependency on the surface tension parameter k. The performed calculations are done for $G = -7.0$ for the isotropy model and presented in Fig. 4.19.

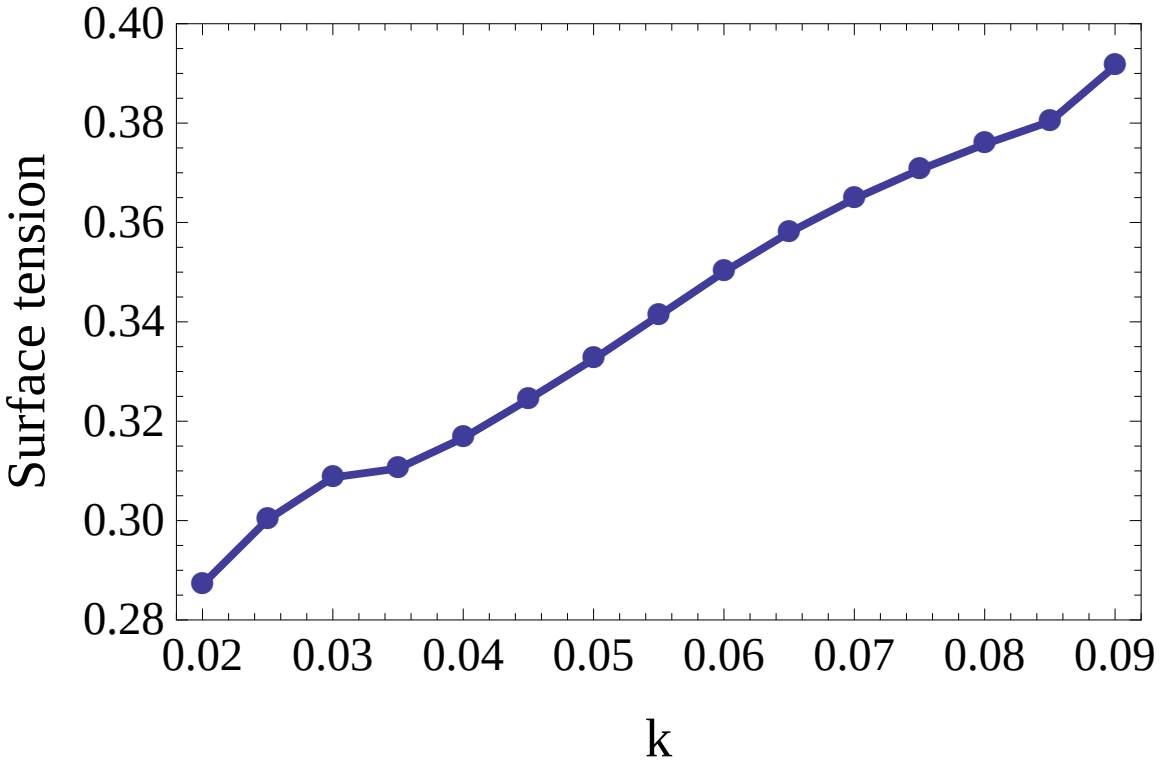

Figure 4.19: Surface tension dependency on k with $G = -7.0$ for the isotropy model.

The complicated dependency of the parameters due to influences of the higher orders in the Shan-Chen force Taylor expansion are shown.

The model can be used in various simulations of phenomena where there is a need for the anisotropic dependency of the surface tension. One of the examples is a droplet behaviour in a temperature field. The droplet of radius 20 units is initialized in the centre of domain 128x128, which has the temperature surface tension dependency in y-direction as follows:

$$k = 0.01 + 0.05 \left\| y/H - \frac{1}{2} \right\|, \tag{4.51}$$

which describes the droplet located on the cold substrate which has heat sources at the top and the bottom. The example is shown in Fig. 4.20. The surface tension anisotropy influences the droplet shape, which has an elliptic shape.

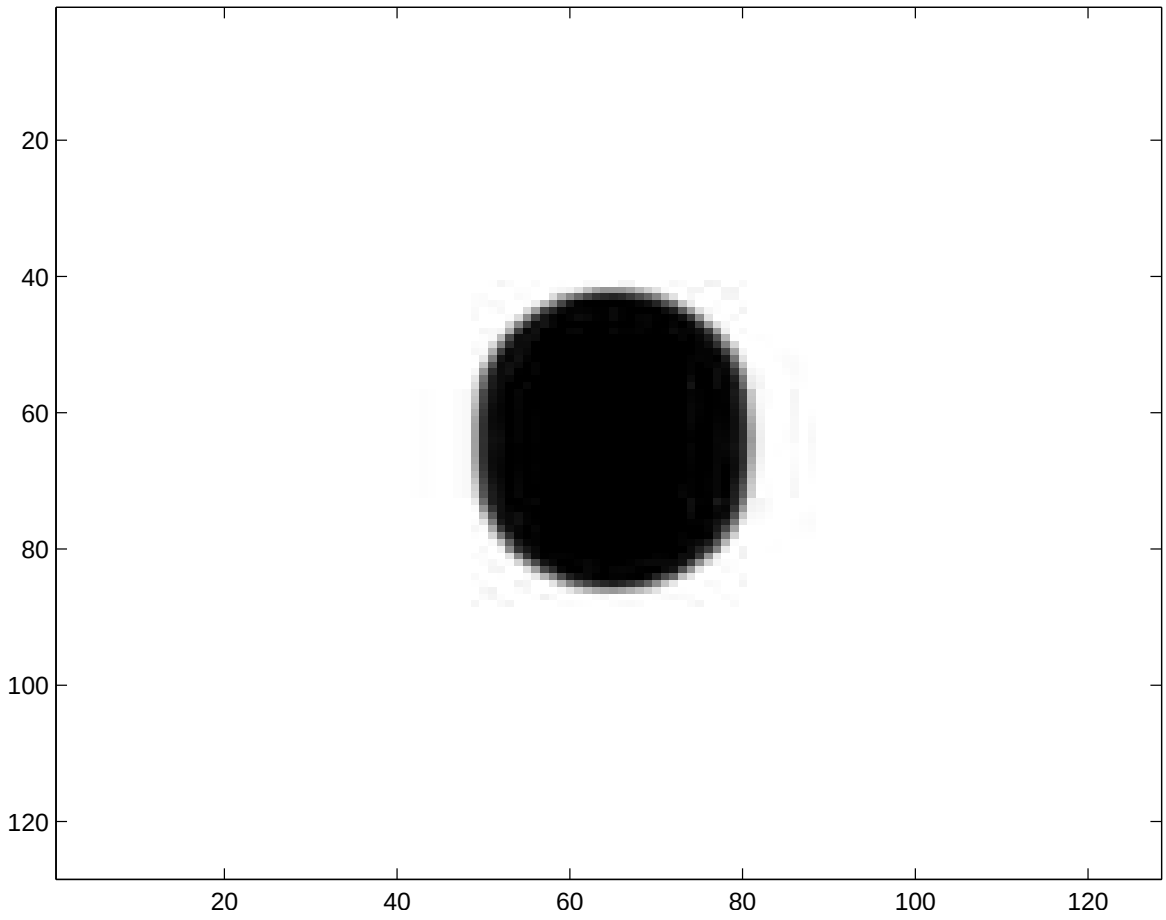

Figure 4.20: Axisymmetric controlled droplet with $G = -7.0$. The droplet is located on the substrate with the top and the bottom heated. The elongation of the top and bottom part are presented.

4.3 Generalized Lattice Boltzmann System

This section introduces the generalized Shan-Chen model, which has the ability to simulate anisotropic phenomena, such as the behaviour of ferrofluid droplet, which is a colloidal suspension oriented by the magnetic field (Rosensweig, 1997). The ability to simulate ferrofluids can help to describe the behaviour of biomedical nanoparticles, as targeted drug delivery. The proposed model has the ability to simulate difficult phenomena, i.e. the fingering phenomena in a ferrofluid (Jackson et al., 1994), which are hard to analytically analyze, and itself is the challenging phenomenon. Therefore, computational methods for the simulation are in high demand (Lavrova et al., 2004; Polevikov, 2004). By introducing the generalized Shan-Chen model for the single-phase transition, which is rather simple, the highly complicated multicomponent simulations for ferrofluids can be avoided. The model is capable of deformation and rupture of a magnetic droplet simulations under the influence of a magnetic field. The magnetic field forces the ferrofluid to change shape in an anisotropic way.

Falcucci et al. (2009) formulated the general Shan-Chen model for D2Q9 model:

$$\boldsymbol{F} = -\psi(x,y)\sum_i w_i G_i \psi(x+c_{ix}, y+c_{iy})\boldsymbol{c_i} \quad , \tag{4.52}$$

where weights are $w_i = \left(\frac{4}{9},\frac{1}{9},\frac{1}{9},\frac{1}{9},\frac{1}{9},\frac{1}{36},\frac{1}{36},\frac{1}{36},\frac{1}{36}\right)$ with vectors of velocities $c_{ix} = (0,\ 1,\ 0,\ -1,\ 0,\ 1,\ -1,\ -1,\ 1)$ and $c_{iy} = (0,\ 0,\ 1,\ 0,\ -1,\ 1,\ 1,\ -1,\ -1)$. Close examination of the

model reveals the following structure:

$$
\begin{aligned}
F_x = &-\frac{1}{36}(4G_1 - 4G_3 + G_5 - G_6 - G_7 + G_8)\psi(x,y)^2 - \\
&\frac{1}{36}(G_5 - G_6 + G_7 - G_8)\psi(x,y)\partial_y\psi(x,y) - \\
&\frac{1}{36}(4G_1 + 4G_3 + G_5 + G_6 + G_7 + G_8)\psi(x,y)\partial_x\psi(x,y) - \\
&\frac{1}{72}(G_5 - G_6 - G_7 + G_8)\psi(x,y)\partial_y^2\psi(x,y) - \\
&\frac{1}{72}(2G_5 + 2G_6 - 2G_7 - 2G_8)\psi(x,y)\partial_x\partial_y\psi(x,y) - \\
&\frac{1}{72}(4G_1 - 4G_3 + G_5 - G_6 - G_7 + G_8)\psi(x,y)\partial_x^2\psi(x,y) \\
&\frac{1}{216}(G_5 - G_6 + G_7 - G_8)\psi(x,y)\partial_y^3\psi(x,y) - \\
&\frac{1}{216}(3G_5 + 3G_6 + 3G_7 + 3G_8)\psi(x,y)\partial_x\partial_y^2\psi(x,y) - \\
&\frac{1}{216}(3G_5 - 3G_6 + 3G_7 - 3G_8)\psi(x,y)\partial_x^2\partial_y\psi(x,y) - \\
&\frac{1}{216}(4G_1 + 4G_3 + G_5 + G_6 + G_7 + G_8)\psi(x,y)\partial_x^3\psi(x,y) \\
F_y = &-\frac{1}{36}(4G_2 - 4G_4 + G_5 + G_6 - G_7 - G_8)\psi(x,y)^2 - \\
&\frac{1}{36}(4G_2 + 4G_4 + G_5 + G_6 + G_7 + G_8)\psi(x,y)\partial_y\psi(x,y) - \\
&\frac{1}{36}(G_5 - G_6 + G_7 - G_8)\psi(x,y)\partial_x\psi(x,y) - \\
&\frac{1}{72}(4G_2 - 4G_4 + G_5 + G_6 - G_7 - G_8)\psi(x,y)\partial_y^2\psi(x,y) - \\
&\frac{1}{72}(2G_5 - 2G_6 - 2G_7 + 2G_8)\psi(x,y)\partial_x\partial_y\psi(x,y) - \\
&\frac{1}{72}(G_5 + G_6 - G_7 - G_8)\psi(x,y)\partial_x^2\psi(x,y) - \\
&\frac{1}{216}(4G_2 + 4G_4 + G_5 + G_6 + G_7 + G_8)\psi(x,y)\partial_y^3\psi(x,y) - \\
&\frac{1}{216}(3G_5 - 3G_6 + 3G_7 - 3G_8)\psi(x,y)\partial_x\partial_y^2\psi(x,y) - \\
&\frac{1}{216}(3G_5 + 3G_6 + 3G_7 + 3G_8)\psi(x,y)\partial_x^2\partial_y\psi(x,y) - \\
&\frac{1}{216}(G_5 - G_6 + G_7 - G_8)\psi(x,y)\partial_x^3\psi(x,y).
\end{aligned}
\tag{4.53}
$$

Let us examine more thoroughly on the forces F_x and F_y, where there is a mass term with $\psi(x,y)^2$. To eliminate those terms the linkwise general Shan-Chen model can be introduced, i.e. one coefficient for c_i and opposite velocity $\bar{c}_i$. Therefore we will have:

$$\boldsymbol{c_1}, \boldsymbol{c_3} \rightarrow G_x \tag{4.54}$$

$$\boldsymbol{c_2}, \boldsymbol{c_4} \rightarrow G_y \tag{4.55}$$

$$\boldsymbol{c_5}, \boldsymbol{c_7} \rightarrow G_{xy} \tag{4.56}$$

$$\boldsymbol{c_6}, \boldsymbol{c_8} \rightarrow G_{yx}. \tag{4.57}$$

After substitution equations for forces this can be rewritten as follows:

$$\begin{aligned} F_x = &-\frac{2}{36}(G_{xy}-G_{yx})\psi(x,y)\partial_y\psi(x,y)- \\ &\frac{1}{36}(8G_x+2G_{xy}+2G_{yx})\psi(x,y)\partial_x\psi(x,y)- \\ &\frac{1}{216}(2G_{xy}-2G_{yx})\psi(x,y)\partial_y^3\psi(x,y)- \\ &\frac{1}{216}(6G_{xy}+6G_{yx})\psi(x,y)\partial_x\partial_y^2\psi(x,y)- \\ &\frac{1}{216}(6G_{xy}-6G_{yx})\psi(x,y)\partial_x^2\partial_y\psi(x,y)- \\ &\frac{1}{216}(8G_x+2G_{xy}+2G_{yx})\psi(x,y)\partial_x^3\psi(x,y) \end{aligned} \tag{4.58}$$

$$\begin{aligned} F_y = &\frac{1}{36}(8G_y+2G_{xy}+G_{yx})\psi(x,y)\partial_y\psi(x,y)- \\ &\frac{2}{36}(G_{xy}-G_{yx})\psi(x,y)\partial_x\psi(x,y)- \\ &\frac{1}{216}(8G_y+2G_{xy}+2G_{yx})\psi(x,y)\partial_y^3\psi(x,y)- \\ &\frac{1}{216}(6G_{xy}-6G_{yx})\psi(x,y)\partial_x\partial_y^2\psi(x,y)- \\ &\frac{1}{216}(6G_{xy}+6G_{yx})\psi(x,y)\partial_x^2\partial_y\psi(x,y)- \\ &\frac{1}{216}(2G_{xy}-2G_{yx})\psi(x,y)\partial_x^3\psi(x,y). \end{aligned}$$

4.3.1 Anisotropic droplets

Anisotropic droplets are formed on a mesoscopic level due to the difference between momentum flux components (Rosensweig, 1997):

$$P_{xx} - P_{yy} = \frac{B^2}{2\mu_0}, \tag{4.59}$$

where B is the external magnetic field, directed along x-direction, responsible for a non-isotropic contribution to the fluid pressure. The generalized model brings the nonideal contribution to the pressure. Previously, it was suggested that the multicomponent lattice Boltzmann models could be used to simulate the ferrofluids behaviour, however, the present model simulates it with only one set of populations.

The easiest example of the magnetic field directed along x-direction can be simulated by taking $G_y \neq G_x$ and $G_{xy} = G_{yx} = G_x$ (Falcucci et al., 2009). Then the force (4.58) is simplified as follows:

$$\begin{aligned} F_x = &-\frac{G_x}{3}\psi(x,y)\partial_x\psi(x,y) && -\frac{G_x}{18}\psi(x,y)\partial_x\partial_y^2\psi(x,y) \\ & && -\frac{G_x}{18}\psi(x,y)\partial_x^3\psi(x,y) \\ F_y = &-\frac{1}{36}(8G_y + 4G_x)\psi(x,y)\partial_y\psi(x,y) && -\frac{1}{216}(8G_y + 4G_x)\psi(x,y)\partial_y^3\psi(x,y) \\ & && -\frac{G_x}{18}\psi(x,y)\partial_x^2\partial_y\psi(x,y). \end{aligned} \tag{4.60}$$

By recombining terms with G_x and G_y the equation (4.60) can be rewritten as follows:

$$\begin{aligned} F_x = &-\frac{G_x}{3}\psi(x,y)\partial_x\psi(x,y) - && \frac{1}{18}G_x\psi(x,y)\partial_x\Delta\psi(x,y) \\ F_y = &-\frac{1}{36}(8G_y + 4G_x)\psi(x,y)\partial_y\psi(x,y) - && \frac{1}{54}G_x\psi(x,y)\partial_y\Delta\psi(x,y) - \\ & \frac{1}{27}G_y\psi(x,y)\partial_y^3\psi(x,y) - && \frac{1}{27}G_x\psi(x,y)\partial_x^2\partial_y\psi(x,y). \end{aligned} \tag{4.61}$$

Terms in (4.61) containing $\psi(x,y)\partial_x\Delta\psi(x,y)$ and $\psi(x,y)\partial_y\Delta\psi(x,y)$ are the surface tension terms. Here the anisotropy of surface tension terms can be observed, i.e. in for F_y we have terms proportional to the $G_y\psi(x,y)\partial_y^3\psi(x,y)$ and $G_x\partial_x^2\partial_y\psi$, which bring the anisotropy into surface tension terms.

To obtain momentum fluxes,a steady-state problem has to be solved to examine surface tension terms more thoroughly:

$$\partial_x P_{xx} + \partial_y P_{xy} = -F_x + \partial_x(c_s^2\rho)$$
$$\partial_x P_{yx} + \partial_y P_{yy} = -F_y + \partial_y(c_s^2\rho).$$

After algebraic computations and using equations

$$\psi\partial_y\partial_x^2\psi = \partial_y(\psi\partial_x^2\psi) - \partial_x(\partial_x\psi\partial_y\psi) + \frac{1}{2}\partial_y(\partial_x\psi)^2$$
$$\psi\partial_y^3\psi = \partial_y(\psi\partial_y^2\psi) - \frac{1}{2}\partial_y(\partial_y\psi)^2$$

the following expressions for momentum fluxes can be obtained:

$$\begin{aligned}
\partial_x P_{xx} + \partial_y P_{xy} =& \partial_x(c_s^2\rho) + \frac{G_x}{6}\partial_x\psi^2 + \frac{G_x}{18}\partial_x(\psi\Delta\psi) - \\
& \frac{G_x}{18}\partial_x(\partial_x\psi)^2 - \frac{G_x}{18}\partial_y(\partial_x\psi\partial_y\psi) \\
\partial_x P_{yx} + \partial_y P_{yy} =& \partial_y(c_s^2\rho) + \frac{8G_y + 4G_x}{72}\partial_y\psi^2 + \frac{4G_x}{216}\partial_y(\psi\Delta\psi) + \\
& \frac{8G_y}{216}\partial_y(\psi\partial_y^2\psi) + \frac{8G_x}{216}\partial_y(\psi\partial_x^2\psi) - \frac{12G_x}{216}\partial_x(\partial_x\psi\partial_y\psi) + \\
& \frac{6G_x}{216}\partial_y(\partial_x\psi)^2 - \frac{2G_x}{216}\partial_y(\partial_y\psi)^2 - \frac{4G_y}{216}\partial_y(\partial_y\psi)^2.
\end{aligned} \tag{4.62}$$

Therefore, the momentum fluxes P_{xx}, $P_{xy} = P_{yx}$, P_{yy} can be found from equation (4.62) as:

$$\begin{aligned}
P_{xx} =& \frac{G_x}{6}\psi^2 + \frac{G_x}{18}\psi\Delta\psi + \frac{G_x}{36}(\nabla\psi)^2 - \frac{G_x}{18}(\partial_x\psi)^2 \\
P_{xy} = P_{yx} =& -\frac{G_x}{18}\partial_x\psi\partial_y\psi \\
P_{yy} =& \frac{8G_y + 4G_x}{72}\psi^2 + \frac{4G_x}{216}\psi\Delta\psi + \frac{8G_y}{216}\psi\partial_y^2\psi + \\
& \frac{8G_x}{216}\psi\partial_x^2\psi + \frac{6G_x}{216}(\partial_x\psi)^2 - \frac{2G_x}{216}(\partial_y\psi)^2 - \frac{4G_y}{216}(\partial_y\psi)^2,
\end{aligned}$$

or without the surface tension terms in the first approximation as:

$$\begin{aligned} P_{xx} =& \frac{G_x}{6}\psi^2 \\ P_{xy} =& P_{yx} = 0 \\ P_{yy} =& \frac{8G_y + 4G_x}{72}\psi^2 \end{aligned} \tag{4.63}$$

4.3.2 Numerical results

Therefore, in terms of $G_y = G_x + \delta G$, the difference $P_{yy} - P_{xx} = \frac{\delta G}{9}\psi^2$. One of the possible shapes for $G_x = -5.0$ and $G_y = -5.03$ is presented in Fig. 4.21.

Comparison of the simulation results can be made with the published experimental results for ferrofluids (Flament et al., 1996). The extra component due to the nonisotropy of the magnetic pressure equals the Shan-Chen model contribution:

$$\frac{B^2}{2\mu_0} = \frac{\delta G}{9}\psi^2, \tag{4.64}$$

where $\psi^2 = \frac{\psi_g^2 + \psi_l^2}{2}$ is averaged pseudopotential value. The results are in excellent agreement. The process is controlled by the Bond number which is for a magnetic droplet refers to the ratio of an amplitude of a magnetic field to the capillary pressure:

$$Bo = \frac{\delta G \psi^2 / 9}{\frac{\sigma}{D}}, \tag{4.65}$$

where D is the diameter, and σ is the surface tension. The experimental results compared with simulation data for the eccentricity factor, defined as $e^2 = 1 - \frac{b^2}{a^2}$ with a and b being axes radius, as a function of Bond number, are presented in Fig. 4.22.

4.4 Discussion

This chapter introduced the Shan-Chen model concept. The model was examined thoroughly with theoretical and simulation results compared. The limitations of the Shan-Chen model were discussed. Also, the chapter presented some extensions of the Shan-

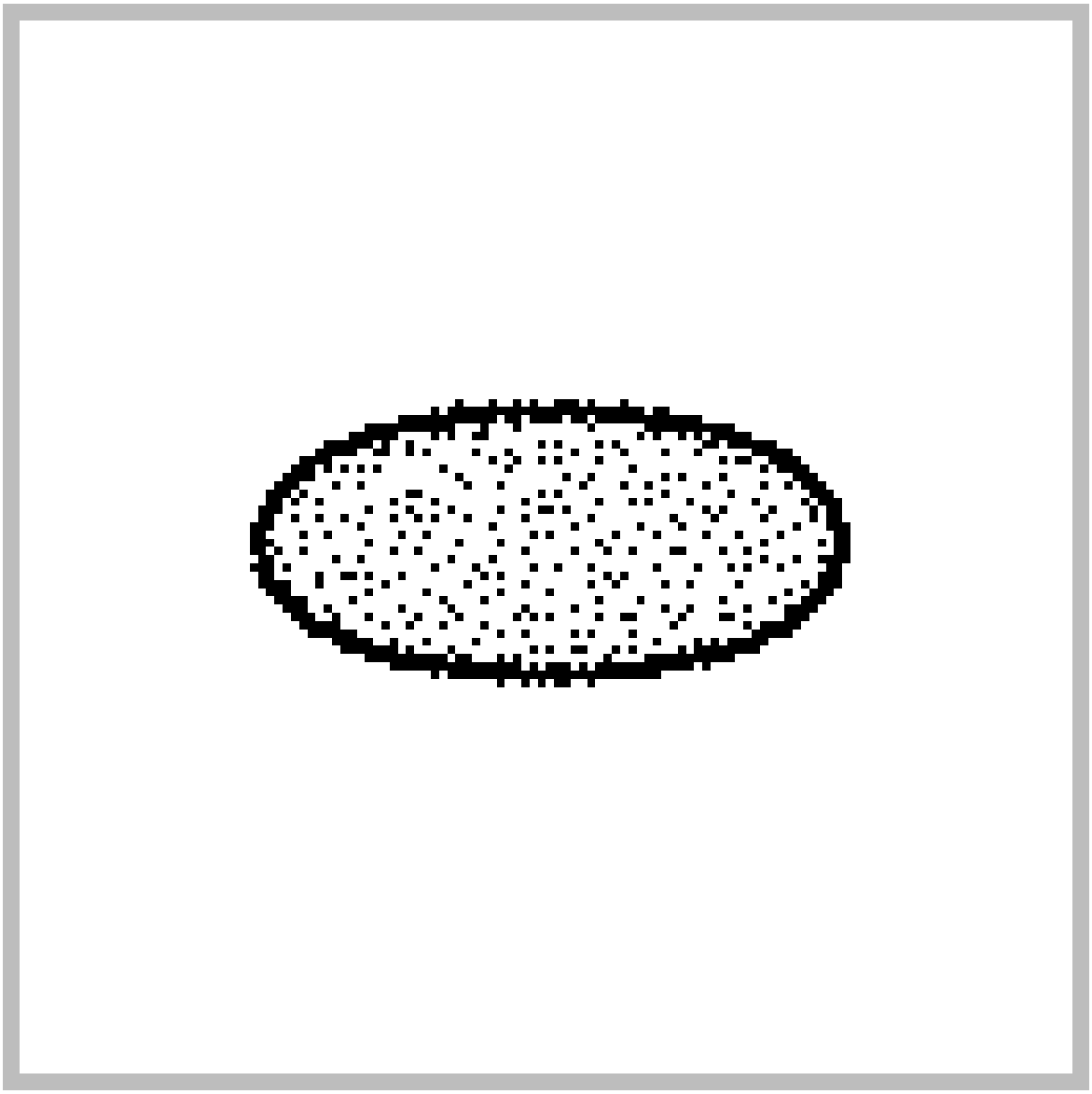

Figure 4.21: Anisotropic droplet with $G_x = -5.00$ and $G_y = -5.03$.

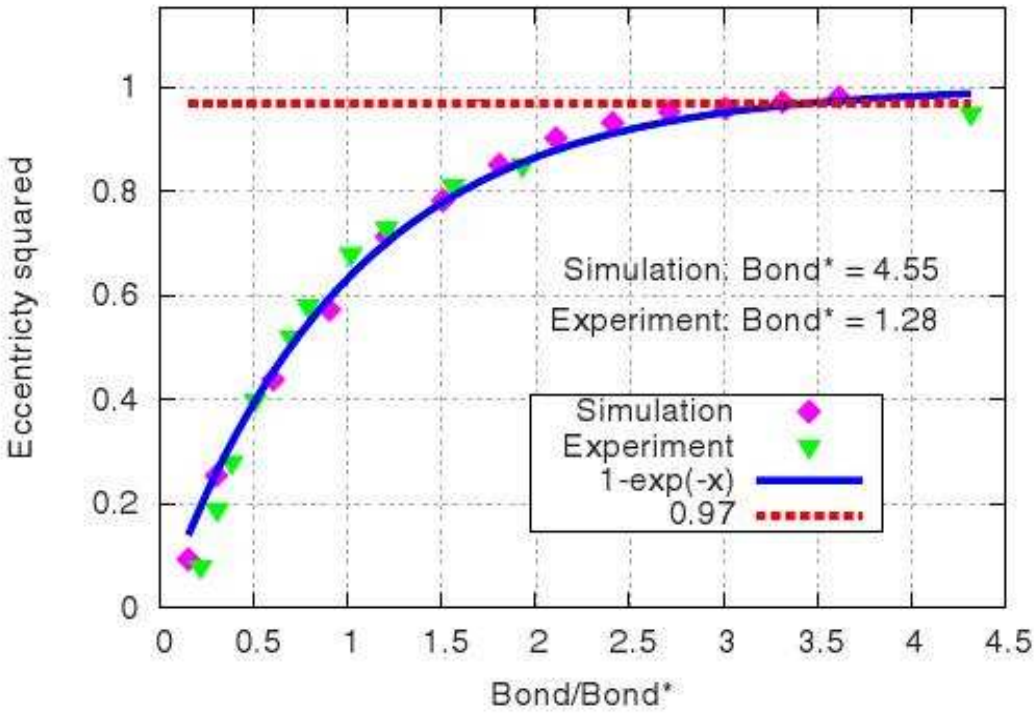

Figure 4.22: Comparison of simulations for the ferrofluid droplet with the experimental data. The figure shows the eccentricity dependency on the Bond number. Courtesy of Falcucci et al. (2009).

Chen model, the so-called multirange model and the generalized Shan-Chen model, which allow extension of the original Shan-Chen model in terms of stability and ability to simulate anisotropic phenomena. Also, the multirange model allows separation of the equation of state from the surface tension term. Even the width of the interface behaves not in the physical way because of the influence higher-order expansion terms, the macrophysics is fulfilled.

The next chapter brings attention to the Multi-Relaxation Time (MRT) collision operator, being able to improve stability and to overcome some limitations of the Shan-Chen model, i.e. the same dynamic and bulk viscosities, viscosity dependence of the surface tension.

Chapter 5

Multi-Relaxation time collision operator

5.1 Introduction

The lattice Boltzmann method based on a Single Relaxation Time (SRT) model (Bhatnagar et al., 1954) is limited by numerical instabilities, unsteadiness, and the porous media viscosity dependence on τ (Ginzburg, 2009).

The Multi-Relaxation Time (MRT) and Two Relaxation Time (TRT) models (Ginzburg, 2005b) operate with multiple parameters in the collision operator. Additional free parameters allow tuning the model. The MRT collision operator works with hydrodynamic moments not distribution function populations, therefore, the tuning of the parameters for the model to restore the hydrodynamic limits of the Navier-Stokes equation (Dellar, 2003) becomes straightforward and simple. The model shows better numerical stability (Lallemand and Luo, 2000), the ability to simulate the hydrodynamic problems with different bulk and shear viscosities (Dellar, 2001).

The MRT model was introduced by d'Humières (1992), based on the matrix formulation of Higuera and Jimenez (1989); Higuera et al. (1989). Although it's only 15% to 20% slower than the BGK version of collision operator d'Humières et al. (2002), the MRT model has many advantages in comparison with the BGK collision operator. Almost, any problem modeled with MRT performs better than the BGK model. This is because of the MRT free parameters. Note that the BGK model is the limit of the MRT model when all parameters of MRT equate to a single value. The advantages of using MRT are better stability (Lallemand and Luo, 2000), low viscous multiphase flow (Premnath and Abraham, 2007), ability to simulate phenomena with Prandtl number different from

unity (d'Humières et al., 2002). Also, the MRT model results in improvement of boundary conditions (Ginzburg and d'Humières, 2003) and their effective location (Ginzburg, 2005a). The MRT model is the only one which can adequately represent the porous media simulations (Ginzburg, 2009) and microflows with Knudsen number around unity (Luo, 2009b). The model has been succesfully applied to multiphase simulations, e.g.,Poiseuille flow in inclined channels with different kinematic viscosities (Ginzbourg and Adler, 1995), for free-interface flow (Ginzburg and Steiner, 2002), for capillary waves simulations (McCracken and Abraham, 2005), for binary drop collisions (Premnath and Abraham, 2005), for a simulation of a lid-driven cavity (Wu and Shao, 2004). Tölke et al. (2006) applied the MRT model for multiphase flow simulations on adaptive grids. Mukherjee and Abraham (2007) incorporated a pressure-based MRT high-density-ratio two-phase LBM, and claimed the ability to simulate density ratios up to 1000. Ginzburg developed a collision operator requirement on the surface of two phases (Ginzburg, 2007).

All these papers demonstrate the MRT model superiority over the BGK model. However, among all the successful applications of the MRT model, the multiphase applications with the MRT model applied need to be further developed.

In the following section, the theory of MRT with the force inclusion and the Chapman-Enskog restoration of the Navier-Stokes equation will be discussed. Secondly, the application of MRT with Shan-Chen model will be examined.

5.2 Matrix representation

There are several possible ways to represent the collision operator including the BGK with single relaxation time (Qian et al., 1992), the TRT with two relaxation time (Ginzburg, 2005b), and the MRT with multiple relaxation times (Asinari, 2006; d'Humières, 1992; Lallemand and Luo, 2000; McCracken and Abraham, 2005) following the original idea of

Higuera and Jimenez (1989).

Let's reformulate the collision operator as in (Higuera and Jimenez, 1989). Instead of updating the populations separately from each other, all the populations are involved in the collision through the matrix:

$$\Omega f^{neq} = \sum_j A_{ij}(f_j^{eq} - f_j).$$

Thus, the Lattice Boltzmann Equation takes the form:

$$f_i(\boldsymbol{r} + \boldsymbol{c_i}\Delta t, t) - f_i(\boldsymbol{r}, t) = -\sum_j A_{ij}(f_j(\boldsymbol{r}, t) - f_j^{eq}(\boldsymbol{r}, t))\,. \tag{5.1}$$

The right hand side of equation (5.1) contains the matrix A_{ij}, which can be analyzed in terms of eigenvalues and eigenvectors.

5.3 Eigenvectors decomposition

Any rectangular matrix, V, can be represented in the eigendecomposition representation $V_{ij} = \sum_k V_i^{(k)} \omega_k V_j^{(k)}$, where ω_k are eigenvalues and $V^{(k)}$ are eigenvectors (provided that $V^{(k)}$ are linearly independent), and $\sum_i V_i^{(j)} V_i^{(k)} = \delta_{jk}$ is an orthogonality condition.

The collision matrix A_{ij} can be decomposed in the same manner through the set of eigenvectors but with the another othogonality condition:

$$A_{ij} = w_i \sum_k A_i^{(k)} \omega_k A_j^{(k)}, \tag{5.2}$$

where w_i are the weights defined in (3.75). Note that the equation (5.2) is weighted by w_i. This is because the orthogonality conditions are slightly different, namely

$$\begin{aligned} w_i \sum_k A_i^{(k)} A_j^{(k)} &= \delta_{ij} \\ \sum_i w_i A_i^{(j)} A_i^{(k)} &= \delta_{jk} \end{aligned} \tag{5.3}$$

It was mentioned previously that with the help of Hermite polynomials the expansion of the equilibrium distribution function can be obtained. Therefore the properties of Hermite polynomials in discrete velocity space can be used once again for the matrix construction. As we will see later, it is the excellent basis for the matrix construction. Basically the weights in the orthogonality conditions (5.3) come from the Hermite polynomials.

5.4 Matrix eigenvectors

The Hermite polynomials in the continuous space are recalled as (Shan et al., 2006):

$$\begin{aligned}
&\mathcal{H}^{(0)}(\boldsymbol{\xi}) = 1 \\
&\mathcal{H}_i^{(1)}(\boldsymbol{\xi}) = \xi_i \\
&\mathcal{H}_{ij}^{(2)}(\boldsymbol{\xi}) = \xi_i\xi_j - \delta_{ij} \\
&\mathcal{H}_{ijk}^{(3)}(\boldsymbol{\xi}) = \xi_i\xi_j\xi_k - \xi_i\delta_{jk} - \xi_j\delta_{ik} - \xi_k\delta_{ij} \\
&\xi_i\mathcal{H}_{i_1i_2\ldots i_n}^{(n)}(\boldsymbol{\xi}) = \mathcal{H}_{ii_1i_2\ldots i_n}^{(n+1)}(\boldsymbol{\xi}) + \sum_{k=1}^{n}\delta_{ii_k}\mathcal{H}_{i_1i_2\ldots i_{k-1}i_{k+1}\ldots i_n}^{(n+1)}(\boldsymbol{\xi}),
\end{aligned} \tag{5.4}$$

where indexes $i, i_1, \ldots, i_n$ indicate axes, as x, y and z. The renormalized version, Eq. 5.3, in the discretized space will imply the following eigenvectors:

$$
\begin{aligned}
|A^{(0)}\rangle &= |A_\rho\rangle = (1,1,1,1,1,1,1,1,1) && \propto H^{(0)},\\
|A^{(1)}\rangle &= |A_{J_x}\rangle = (0,1,0,-1,0,1,-1,-1,1)\sqrt{3} && \propto H^{(1)}_x,\\
|A^{(2)}\rangle &= |A_{J_y}\rangle = (0,0,1,0,-1,1,1,-1,-1)\sqrt{3} && \propto H^{(1)}_y,\\
|A^{(3)}\rangle &= |A_{P_{xx}}\rangle = (-1/3,2/3,-1/3,2/3,-1/3,2/3,2/3,2/3,2/3)3/\sqrt{2} && \propto H^{(2)}_{xx},\\
|A^{(4)}\rangle &= |A_{P_{xy}}\rangle = (0,0,0,0,0,1,-1,1,-1)3 && \propto H^{(2)}_{xy},\\
|A^{(5)}\rangle &= |A_{P_{yy}}\rangle = (-1/3,-1/3,2/3,-1/3,2/3,2/3,2/3,2/3,2/3)3/\sqrt{2} && \propto H^{(2)}_{yy},\\
|A^{(6)}\rangle &= |A_{J_\gamma}\rangle = (1,-2,-2,-2,-2,4,4,4,4)/2 && \propto H^{(4)}_{xxyy},\\
|A^{(7)}\rangle &= |A_{J_{\gamma_x}}\rangle = (0,-2,0,2,0,4,-4,-4,4)\sqrt{3}/\sqrt{8} && \propto H^{(3)}_{xyy},\\
|A^{(8)}\rangle &= |A_{J_{\gamma_y}}\rangle = (0,0,-2,0,2,4,4,-4,-4)\sqrt{3}/\sqrt{8} && \propto H^{(3)}_{xxy}.
\end{aligned}
\tag{5.5}
$$

The Hermite polynomials through the velocity set can be expressed as follows:

$$
\begin{aligned}
H^{(0)} &= 1 \quad ,\\
H^{(1)}_x &= c_{ix} \quad ,\\
H^{(1)}_y &= c_{iy} \quad ,\\
H^{(2)}_{xx} &= c_{ix}c_{ix} - \frac{1}{3} \quad ,\\
H^{(2)}_{xy} &= c_{ix}c_{iy} \quad ,\\
H^{(2)}_{yy} &= c_{iy}c_{iy} - \frac{1}{3} \quad ,\\
H^{(4)}_{xxyy} &= c_{ix}c_{ix}c_{iy}c_{iy} - \frac{1}{3}c_{ix}c_{ix} - \frac{1}{3}c_{iy}c_{iy} + \frac{1}{9} \quad ,\\
H^{(3)}_{xyy} &= c_{ix}c_{iy}c_{iy} - \frac{1}{3}c_{ix} \quad ,\\
H^{(3)}_{xxy} &= c_{iy}c_{ix}c_{ix} - \frac{1}{3}c_{iy}\,.
\end{aligned}
\tag{5.6}
$$

5.5 Moments of Navier-Stokes equation

Matrix A perform the transformation from population space to the moment space. The moment is introduced in the following way:

$$F_k = \sum_i f_i A_i^{(k)}. \tag{5.7}$$

F_k are the kinetic moments. As it will be shown later, all the moments can be divided into hydrodynamics and kinetic moments. The inverse formula explicitly includes the weights:

$$f_i = w_i \sum_i F_k A_i^{(k)} \tag{5.8}$$

To insure that equations (5.7) and (5.8) are consistent:

$$f_i = w_i \sum_k F_k A_i^{(k)} = w_i \sum_k \sum_j f_j A_j^{(k)} A_i^{(k)} =$$
$$= \sum_j f_j \sum_k w_i A_j^{(k)} A_i^{(k)} = \sum_j f_j \delta_{ij} = f_i$$

Note that for BGK, all eigenvalues equal $\omega = \frac{1}{\tau}$. For this case, from the orthogonality of the eigenvectors, it follows that:

$$A_{ij} = w_i \sum_k A_i^{(k)} \omega_k A_j^{(k)} = \omega \sum_k A_i^{(k)} w_i A_j^{(k)} = \omega \delta_{ij}$$

This matrix representation differs from the matrix presented in (d'Humières et al., 2002; Lallemand and Luo, 2000). Usage of this matrix representation can be found in works of Asinari (2006); Higuera and Jimenez (1989); Kuzmin et al. (2008). Note that different representations do not affect the underlying physics. The eigenvectors choice is arbitrary in some subgroups taken from group theory (Rubinstein and Luo, 2008) and may influence the analysis of eigenvalue problems and overall stability. However, the presented matrix representation is based on the Hermite polynomial basis and has a solid basis.

5.6 Equilibrium moments

As far as the eigenvectors were chosen as Hermite polynomials, one can recognise in the equilibrium moments the coefficients $\boldsymbol{a}_i$ defined earlier in equation (3.24). Therefore, the equilibrium moments are:

$$\begin{aligned}
\sum_i f_i^{eq} A_i^{(0)} &= \rho \\
\sum_i f_i^{eq} A_i^{(1)} &= \sqrt{3}\rho u_x \\
\sum_i f_i^{eq} A_i^{(2)} &= \sqrt{3}\rho u_y \\
\sum_i f_i^{eq} A_i^{(3)} &= \frac{3}{\sqrt{2}}\rho u_x u_x \\
\sum_i f_i^{eq} A_i^{(4)} &= 3\rho u_x u_y \\
\sum_i f_i^{eq} A_i^{(5)} &= \frac{3}{\sqrt{2}}\rho u_y u_y \\
\sum_i f_i^{eq} A_i^{(6)} &= \frac{9}{2}\rho u_x^2 u_y^2 \\
\sum_i f_i^{eq} A_i^{(7)} &= 3\frac{\sqrt{3}}{\sqrt{2}}\rho u_x^2 u_y \\
\sum_i f_i^{eq} A_i^{(8)} &= 3\frac{\sqrt{3}}{\sqrt{2}}\rho u_y^2 u_x.
\end{aligned} \tag{5.9}$$

The equilibrium distribution function is recalled to be:

$$\begin{aligned}
f_i^{eq} =& w_i\rho\bigg(1 + 3c_{i\alpha}u_\alpha + \frac{9}{2}Q_{i\alpha\beta}u_\alpha u_\beta + \\
& C_3^1\frac{27}{6}\Big(c_{ix}c_{ix}c_{iy} - \frac{1}{3}c_{iy}\Big)u_x^2 u_y + \frac{27}{2}\Big(c_{iy}c_{iy}c_{ix} - \frac{1}{3}c_{ix}\Big)u_y^2 u_x + \\
& C_4^2\frac{81}{24}\Big(c_{ix}c_{ix}c_{iy}c_{iy} - \frac{1}{3}c_{ix}c_{ix} - \frac{1}{3}c_{iy}c_{iy} + \frac{1}{9}\Big)u_x^2 u_y^2\bigg),
\end{aligned} \tag{5.10}$$

where $C_\alpha^\beta = \frac{\beta!}{(\alpha-\beta)!\beta!}$ the quantity of substitutes. This is because the Hermite polynomial which leads to the presented equilibrium are not unique, i.e. $H_{xyy} = H_{yxy} = H_{yyx}$, which is needed to be accounted for. The same goes for $H_{xxyy} = H_{xyxy} = H_{yxxy} = H_{yxyx} = H_{xyyx} = H_{xxyy}$ giving the factor 6 in the equilibrium.

5.7 Collision operator representation

The collision operator can then be written in terms of eigenvectors, eigenvalues and kinetic moments equation as follows,

$$
\begin{aligned}
&-\sum_j A_{ij}(f_j - f_j^{eq}) = -\sum_j (f_j - f_j^{eq}) w_i \sum_k A_i^{(k)} \omega_k A_j^{(k)} = \\
&-\sum_k w_i A_i^{(k)} \omega_k \sum_j (f_j - f_j^{eq}) A_j^{(k)} = -\sum_k w_i A_i^{(k)} \omega_k (F_k - F_k^{eq}) = \\
&= -w_i \big(\omega_0 A_i^{(1)} (\rho - \rho^{eq}) + \sqrt{3}\omega_1 A_i^{(2)} (\mathcal{J}_x - \mathcal{J}_x^{eq}) + \sqrt{3}\omega_2 A^{(3)} (\mathcal{J}_y - \mathcal{J}_y^{eq}) + \\
&+ \frac{3}{\sqrt{2}} \omega_3 A_i^{(3)} (\mathcal{P}_{xx} - \mathcal{P}_{xx}^{eq}) + 3\omega_4 A_i^{(4)} (\mathcal{P}_{xy} - \mathcal{P}_{xy}^{eq}) + \frac{3}{\sqrt{2}} \omega_5 A_i^{(5)} (\mathcal{P}_{yy} - \mathcal{P}_{yy}^{eq}) + \\
&+ \frac{9}{2} \omega_6 A^{(6)} (\mathcal{J}_\gamma - \mathcal{J}_\gamma^{eq}) + 3\sqrt{\frac{3}{2}} \omega_7 A_i^{(7)} (\mathcal{J}_{\gamma_x} - \mathcal{J}_{\gamma_x}^{eq}) + 3\sqrt{\frac{3}{2}} \omega_8 A_i^{(8)} (\mathcal{J}_{\gamma_y} - \mathcal{J}_{\gamma_y}^{eq}) \big) \\
&= -w_i \big(\omega_0 1_i (\rho - \rho^{eq}) + 3\omega_1 c_{ix} (\mathcal{J}_x - \mathcal{J}_x^{eq}) + 3\omega_2 c_{iy} (\mathcal{J}_y - \mathcal{J}_y^{eq}) + \\
&+ \frac{9}{2} \omega_3 Q_{ixx} (\mathcal{P}_{xx} - \mathcal{P}_{xx}^{eq}) + 9\omega_4 Q_{ixy} (\mathcal{P}_{xy} - \mathcal{P}_{xy}^{eq}) + \frac{9}{2} \omega_5 Q_{iyy} (\mathcal{P}_{yy} - \mathcal{P}_{yy}^{eq}) + \\
&+ \frac{81}{4} \omega_6 g_i (\mathcal{J}_\gamma - \mathcal{J}_\gamma^{eq}) + \frac{27}{2} \omega_7 g_i c_{ix} (J_{\gamma_x} - J_{\gamma_x}^{eq}) + \frac{27}{2} \omega_8 g_i c_{iy} (J_{\gamma_y} - J_{\gamma_y}^{eq}) \big).
\end{aligned}
\tag{5.11}
$$

One can examine the action of the eigenvectors on the collision operator, which is needed for the Chapman-Enskog expansion:

$$
\begin{aligned}
&-\sum_i A_i^{(l)} \sum_j A_{ij} (f_j - f_j^{eq}) = -\sum_i A_i^{(l)} \sum_j (f_j - f_j^{eq}) w_i \sum_k A_i^{(k)} \omega_k A_j^{(k)} = \\
&-\sum_k \omega_k (F_k - F_k^{eq}) \sum_i w_i A_i^{(k)} A_i^{(l)} = -\sum_k \omega_k (F_k - F_k^{eq}) \sum_i w_i A_i^{(k)} A_i^{(l)} = \\
&-\sum_k \omega_k (F_k - F_k^{eq}) \delta_{kl} = -\omega_l (F_l - F_l^{eq}).
\end{aligned}
\tag{5.12}
$$

5.8 Conservation laws

The matrix A should force the conservation laws. The three conservation laws for the incompressible limit are the density,ρ, conservation and momentum fluxes,$\mathcal{J}_\S$ and $\mathcal{J}_\dagger$, conservation. Therefore, the collision operator $-\sum_j A_{ij}(f_j - f_j^{eq})$ shouldn't change the

density or momentum fluxes. The following is fulfilled by allowing the equilibrium moments equal to the non-equilbrium moments, i.e. $\rho = \rho^{eq}$, $J_\alpha = J_\alpha^{eq}$. Therefore, the collision procedure doesn't involve the corresponding eigenvalues ω_0, ω_1 and ω_2, as the quantity, which they are multiplied by, equals zero. Those eigenvalues can be taken arbitrarily.

5.9 Chapman-Enskog expansion

To examine the difference between the restored macroscopic equations with the MRT and the SRT collisions operators, the MRT LBE without the force incorporated will be first examined as:

$$\begin{aligned}
&\epsilon^0 : f_i^{(0)} = f_i^{eq} \\
&\epsilon^1 : (\partial_{t_0} + c_{i\alpha}\partial_\alpha) f_i^{(0)} = -\sum_j A_{ij} f_j^{(1)} \\
&\epsilon^2 : \partial_{t_1} f_i^{(0)} + (\partial_{t_0} + c_{i\alpha}\partial_\alpha) f_i^{(1)} + \frac{(\partial_{t_0} + c_{i\alpha}\partial_\alpha)^2 f_i^{(0)}}{2} = -\sum_j A_{ij} f_j^{(2)}.
\end{aligned} \tag{5.13}$$

The continuity equation can be restored by summation by i index of the second and the third equations of system (5.13):

$$\begin{aligned}
&\partial_{t_0}\rho^{eq} + \partial_\alpha \rho^{eq} u_\alpha^{eq} = -\sum_{ij} A_{ij} f_j^{(1)} = -\sum_{ij} A_i^{(0)} A_{ij} f_j^{(1)} = -\omega_0 \sum_j f_j^{(1)} = 0 \\
&\partial_{t_1}\rho^{eq} + \sum_i (\partial_{t_0} + c_{i\alpha}\partial_\alpha) f_i^{(1)} + \sum_i \frac{(\partial_{t_0} + c_{i\alpha}\partial_\alpha) A_{ij} f_j^{(1)}}{2} = -\sum_{ij} A_{ij} f_j^{(2)} = 0 \\
&\partial_{t_1}\rho^{eq} = 0.
\end{aligned} \tag{5.14}$$

By summing up the equations of the system (5.14) multiplied on ϵ^0 and ϵ^1 correspondingly, the continuity equation ($\rho = \rho^{eq}$ and $\boldsymbol{u} = \boldsymbol{u^{eq}}$ as the collision operator conserves those quantities. Therefore we omit the "eq" symbol elsewhere) can be obtained:

$$\partial_t \rho + \partial_\alpha \rho u_\alpha = 0.$$

To obtain Navier-Stokes equation it is necessary to sum up the equations with $c_{i\alpha}$:

$$\begin{aligned}
&\partial_{t_0}\rho u_\alpha + \partial_\beta \sum_i c_{i\alpha}c_{i\beta}f_i^{(0)} = -\sum_{ij} A_{ij}c_{i\alpha}f_j^{(1)} \\
&\partial_{t_1}\rho u_\alpha + \partial_\beta \sum_i c_{i\alpha}c_{i\beta}f_i^{(1)} - \sum_i \frac{(\partial_{t_0} + c_{i\beta}\partial_\beta))c_{i\alpha}A_{ij}f_j^{(1)}}{2} = -\sum_{ij} A_{ij}c_{i\alpha}f_j^{(2)}.
\end{aligned} \tag{5.15}$$

In the expression (5.15) some terms need to be figured out. The expression for the equilibrium function (5.10) is to be used to calculate them:

$$\begin{aligned}
&\partial_\beta \sum_i c_{i\alpha}c_{i\beta}f_i^{(0)} = \partial_\beta(\frac{\rho}{3}\delta_{\alpha\beta} + \rho u_\alpha u_\beta) \\
&\sum_{ij} \frac{(\partial_{t_0} + c_{i\beta}\partial_\beta)c_{i\alpha}A_{ij}f_j^{(1)}}{2} = \frac{\partial_{t_0}}{2}\sum_{ij} c_{i\alpha}A_{ij}f_j^{(1)} + \frac{\partial_\beta}{2}\sum_{ij} c_{i\alpha}c_{i\beta}A_{ij}f_j^{(1)} = \\
&\frac{1}{\sqrt{3}}\frac{\partial_{t_0}}{2}\sum_{ij} A_i^{(1,2)}A_{ij}f_j^{(1)} + \frac{(\sqrt{2}-1)\delta_{\alpha\beta}+1}{3}\frac{\partial_\beta}{2}\sum_{ij}(A_i^{(3,4,5)} + \frac{1}{3}\delta_{\alpha\beta})A_{ij}f_j^{(1)} = \\
&\frac{\partial_{t_0}}{2}\sum_i \omega_{1,2}c_{i\alpha}f_i^{(1)} + \frac{(\sqrt{2}-1)\delta_{\alpha\beta}+1}{3}\frac{3}{(\sqrt{2}-1)\delta_{\alpha\beta}+1}\frac{\partial_\beta}{2}\sum_i \omega_{3,4,5}(c_{i\alpha}c_{i\beta} - \frac{1}{3}\delta_{\alpha\beta})f_i^{(1)} + \\
&\frac{(\sqrt{2}-1)\delta_{\alpha\beta}+1}{3}\frac{\partial_\beta}{2}\sum_j \frac{1}{3}\delta_{\alpha\beta}f_i^{(1)} = \frac{\partial_{t_0}}{2}\sum_i \omega_{1,2}c_{i\alpha}f_i^{(1)} + \frac{\partial_\beta}{2}\sum_i \omega_{3,4,5}c_{i\alpha}c_{i\beta}f_i^{(1)},
\end{aligned} \tag{5.16}$$

where indexes $1, 2$ are taken for indexes α, β correspondingly and $3, 4, 5$ are taken for the following combination of tensor indexes xx, xy, yy. The Navier-Stokes equation can be restored from the following system:

$$\begin{aligned}
&\partial_{t_0}\rho u_\alpha + \partial_\beta \sum_i c_{i\alpha}c_{i\beta}f_i^{(0)} = 0 \\
&\partial_{t_1}\rho u_\alpha + \left(1 - \frac{\omega_{3,4,5}}{2}\right)\partial_\beta \sum_i f_i^{(1)}c_{i\alpha}c_{i\beta} = 0.
\end{aligned} \tag{5.17}$$

The main challenge is to calculate $\sum_i f_i^{(1)} c_{i\alpha}c_{i\beta} = \sum_i f_i^{(1)} \left(\frac{(\sqrt{2}-1)\delta_{\alpha\beta}+1}{3} A_i^{3,4,5} + \frac{1}{3}\delta_{\alpha\beta} A_i^{(0)} \right)$:

$$
\begin{aligned}
&(\partial_{t_0} + c_{i\alpha}\partial_\alpha) f_i^{(0)} = -\sum_j A_{ij} f_j^{(1)} \\
&\sum_i (\partial_{t_0} + c_{i\gamma}\partial_\gamma) c_{i\alpha}c_{i\beta} f_i^{(0)} = \\
&-\sum_{ij} \left(\frac{(\sqrt{2}-1)\delta_{\alpha\beta}+1}{3} A_i^{(3,4,5)} + \frac{1}{3}\delta_{\alpha\beta} A_i^{(0)} \right) A_{ij} f_j^{(1)} \\
&-\frac{(\sqrt{2}-1)\delta_{\alpha\beta}+1}{3}\omega_{3,4,5} \sum_j A_j^{(3,4,5)} f_j - \frac{\omega_0}{3}\delta_{\alpha\beta} \sum_j f_j^{(1)} = \\
&-\frac{(\sqrt{2}-1)\omega_{3,4,5}\delta_{\alpha\beta}+1}{3} \sum_j \frac{3}{(\sqrt{2}-1)\delta_{\alpha\beta}+1} (c_{j\alpha}c_{j\beta} + \frac{1}{3}\delta_{\alpha\beta}) f_j - \frac{\omega_0}{3}\delta_{\alpha\beta} \sum_j f_j^{(1)} = \\
&-\omega_{3,4,5} \sum_j c_{j\alpha}c_{j\beta} f_j^{(1)} - \frac{\omega_0 - \omega_{3,4,5}}{3}\delta_{\alpha\beta} \sum_j f_j^{(1)} = -\omega_{3,4,5} \sum_j c_{j\alpha}c_{j\beta} f_j^{(1)},
\end{aligned}
\tag{5.18}
$$

where indexes $3, 4, 5$ are corresponing to xx, xy, yy. As far as the equilibrium function is given, one can calculates all the expression in equation (5.18):

$$
\begin{aligned}
\sum c_{ix}c_{ix}c_{ix} f_i^{(0)} &= \rho u_x \\
\sum c_{ix}c_{ix}c_{iy} f_i^{(0)} &= \frac{\rho u_y}{3} + \rho u_x^2 u_y \\
\sum c_{ix}c_{iy}c_{iy} f_i^{(0)} &= \frac{\rho u_x}{3} + \rho u_x u_y^2 \\
\sum c_{iy}c_{iy}c_{iy} f_i^{(0)} &= \rho u_x.
\end{aligned}
\tag{5.19}
$$

As far as the restored equations are in the low Mach limit, terms with the third order velocities ($\rho u_\alpha^m u_\beta^n$, where $m+n=3$) are neglected. The quite general formula eligible for the Chapman-Enskog expansion is obtained:

$$
\sum c_{i\alpha}c_{i\beta}c_{i\gamma} f_i^{(0)} = \frac{\rho}{3}(u_\gamma\delta_{\alpha\beta} + u_\alpha\delta_{\beta\gamma} + u_\beta\delta_{\alpha\gamma}). \tag{5.20}
$$

Therefore, for the equilbrium moments all the expressions are summarized as follows:

$$
\begin{aligned}
\partial_{t_0} \sum_i c_{i\alpha}c_{i\beta} f_i^{(0)} &= \partial_{t_0} \big(\rho u_\alpha u_\beta + \frac{\rho}{3}\delta_{\alpha\beta} \big) \\
\partial_\gamma \sum_i c_{i\alpha}c_{i\beta}c_{i\gamma} f_i^{(0)} &= \partial_\gamma \frac{\rho}{3} \big(u_\gamma\delta_{\alpha\beta} + u_\alpha\delta_{\beta\gamma} + u_\beta\delta_{\alpha\gamma} \big).
\end{aligned}
\tag{5.21}
$$

The term $\partial_{t_0}\rho u_\alpha u_\beta$ can be found from the previous expressions:

$$\begin{aligned}\partial_{t_0}\left(\frac{\rho u_\alpha \rho u_\beta}{\rho}\right) = &- u_\alpha u_\beta \partial_{t_0}\rho + u_\alpha \partial_{t_0}\rho u_\beta + u_\beta \partial_{t_0}\rho u_\alpha = \\ &u_\alpha u_\beta \partial_\gamma \rho u_\gamma + u_\alpha\Big(-\partial_\beta \frac{\rho}{3} - \partial_\gamma \rho u_\beta u_\gamma\Big) + u_\beta\Big(-\partial_\alpha \frac{\rho}{3} - \partial_\gamma \rho u_\alpha u_\gamma\Big).\end{aligned} \tag{5.22}$$

We neglect the terms with the third order magnitude of the velocity and obtain:

$$\partial_{t_0}\left(\frac{\rho u_\alpha \rho u_\beta}{\rho}\right) = -\frac{1}{3}u_\alpha \partial_\beta \rho - \frac{1}{3}u_\beta \partial_\alpha \rho. \tag{5.23}$$

Also, one can calculate the expression $\partial_{t_0}\left(\frac{\rho}{3}\delta_{\alpha\beta}\right)$:

$$\partial_{t_0}\left(\frac{\rho}{3}\delta_{\alpha\beta}\right) = -\frac{1}{3}\partial_\gamma \rho u_\gamma \delta_{\alpha\beta}. \tag{5.24}$$

Combining the equations (5.18), (5.21), (5.23), and (5.24) together, the momentum fluxes for the $f_i^{(1)}$ can be obtained:

$$\begin{aligned}-\omega_{3,4,5}\sum_i c_{i\alpha}c_{i\beta}f_i^{(1)} = &\quad \sum_i (\partial_{t_0} + c_{i\gamma}\partial_\gamma)c_{i\alpha}c_{i\beta}f_i^{(0)} \\ -\omega_{3,4,5}\sum_i c_{i\alpha}c_{i\beta}f_i^{(1)} = &\quad \sum_i \partial_{t_0}c_{i\alpha}c_{i\beta}f_i^{(0)} + \sum_i \partial_\gamma c_{i\gamma}c_{i\alpha}c_{i\beta}f_i^{(0)} \\ -\omega_{3,4,5}\sum_i c_{i\alpha}c_{i\beta}f_i^{(1)} = &\quad -\frac{\delta_{\alpha\beta}}{3}\partial_\gamma \rho u_\gamma - \frac{1}{3}u_\alpha \partial_\beta \rho - \frac{1}{3}u_\beta \partial_\alpha \rho + \\ \partial_\gamma \frac{\rho}{3}\big(u_\gamma \delta_{\alpha\beta} + u_\alpha \delta_{\beta\gamma} + u_\beta \delta_{\alpha\gamma}\big) = &\quad -\frac{1}{3}u_\alpha \partial_\beta \rho - \frac{1}{3}u_\beta \partial_\alpha \rho + \partial_\gamma \frac{\rho}{3}\big(u_\alpha \delta_{\beta\gamma} + u_\beta \delta_{\alpha\gamma}\big) = \\ &\rho\frac{\partial_\beta u_\alpha}{3} + \rho\frac{\partial_\alpha u_\beta}{3}.\end{aligned} \tag{5.25}$$

After substituting indexes $3, 4, 5$ through the components xx, yy, xy, the momentum fluxes can be restored as:

$$\begin{aligned}\sum_i c_{ix}c_{ix}f_i^{(1)} &= -\frac{\frac{2}{3}\rho\partial_x u_x}{\omega_3} \\ \sum_i c_{ix}c_{iy}f_i^{(1)} &= -\frac{\frac{1}{3}\rho(\partial_x u_y + \partial_y u_x)}{\omega_4} \\ \sum_i c_{ix}c_{ix}f_i^{(1)} &= -\frac{\frac{2}{3}\rho\partial_y u_y}{\omega_5}.\end{aligned} \tag{5.26}$$

Then the system (5.17) can be rewritten in the following manner:

$$\begin{aligned}
&\partial_{t_0}\rho u_\alpha + \partial_\beta \sum_i c_{i\alpha}c_{i\beta}f_i^{(0)} = 0\\
&\partial_{t_1}\rho u_\alpha + \left(1-\frac{\omega_{3,4,5}}{2}\right)\partial_\beta \sum_i f_i^{(1)}c_{i\alpha}c_{i\beta} = 0\\
&\partial_{t_1}\rho u_\alpha - \left(1-\frac{\omega_{3,4,5}}{2}\right)\partial_\beta \frac{\rho\frac{\partial_\beta u_\alpha}{3}+\rho\frac{\partial_\alpha u_\beta}{3}}{\omega_{3,4,5}} = 0\\
&\partial_{t_1}\rho u_\alpha - \left(\frac{1}{\omega_{3,4,5}}-\frac{1}{2}\right)\partial_\beta \frac{\rho\frac{\partial_\beta u_\alpha}{3}+\rho\frac{\partial_\alpha u_\beta}{3}}{\omega_{3,4,5}} = 0.
\end{aligned} \tag{5.27}$$

Therefore, the Navier-Stokes equation is restored by summing up the first and the second equation of the system (5.27) multiplied on ϵ and ϵ^2:

$$\begin{aligned}
\partial_t\rho u_x + \partial_x\rho u_x u_x + \partial_y\rho u_x u_y = &-\frac{1}{3}\partial_x\rho + \left(\frac{1}{\omega_3}-\frac{1}{2}\right)\frac{2}{3}\partial_x\rho\partial_x u_x +\\
&\left(\frac{1}{\omega_4}-\frac{1}{2}\right)\frac{1}{3}\partial_y(\rho\partial_y u_x + \rho\partial_x u_y)\\
\partial_t\rho u_y + \partial_x\rho u_y u_x + \partial_y\rho u_y u_y = &-\frac{1}{3}\partial_y\rho + \left(\frac{1}{\omega_5}-\frac{1}{2}\right)\frac{2}{3}\partial_y\rho\partial_y u_y +\\
&\left(\frac{1}{\omega_4}-\frac{1}{2}\right)\frac{1}{3}\partial_x(\rho\partial_x u_y + \rho\partial_y u_x).
\end{aligned} \tag{5.28}$$

By introducing conventions $\omega_3 = \omega_5 = \omega_{bulk}$ and $\omega_4 = \omega_{kin}$ one can restore the Navier-Stokes equation with different bulk and kinematic viscosities:

$$\partial_t\rho u_\alpha + \partial_\beta\rho u_\alpha u_\beta = -\frac{1}{3}\partial_\alpha\rho + \frac{1}{3}\left(\frac{1}{\omega_{bulk}}-\frac{1}{2}\right)\partial_\beta(\rho\partial_\beta u_\alpha) + \frac{1}{3}\left(\frac{1}{\omega_{kin}}-\frac{1}{2}\right)\partial_\beta(\rho\partial_\alpha u_\beta). \tag{5.29}$$

In that sense, the scheme has one free parameter, and it is close to the TRT scheme formulated by Ginzburg (2005b). As will be shown later, the MRT formulation has not only the proper restoration of the Navier-Stokes equation, but also the stability improvement. The three eigenvalues $\gamma = \omega_6$, $\gamma_x = \omega_7$ and $\gamma_y = \omega_8$ are called "ghost" eigenvalues, because they are not required for restoration of the Navier-Stokes equation (Benzi et al., 1992). The eigenvalues γ, γ_x and γ_y can be tuned to improve the stability of LBM.

5.10 Force incorporation for the mass and force sources

There are many approaches to the force incorporation with the MRT collision operator. One constructs the force moments through the equilibrium distribution function and incorporate them by applying the matrix of the collision operator (Premnath and Abraham, 2007). Another approach is to incorporate it by adding the half force momenta before and after the collision (Lallemand and Luo, 2003). Thorough analysis of the force incorporation in MRT case is needed. The analysis presented here is to assist researchers who want to incorporate the force term in the MRT model.

As in the case with the BGK, the restored equations will be for the shifted density $\rho^m = \rho + \epsilon M/2$ and the velocity $\boldsymbol{u_m} = \boldsymbol{u} + \epsilon \boldsymbol{F}/2$. Hence, the expressions for the first and second moments of the $f^{(1)}$ functions:

$$\begin{aligned} \sum_i f_i^{(1)} &= -M/2 \\ \sum_i f_i^{(1)} c_{i\alpha} &= -F_\alpha/2. \end{aligned} \tag{5.30}$$

The Chapman-Enskog system with the force inclusion is rewritten as:

$$\begin{aligned} &\epsilon^0 : f_i^{(0)} = f_i^{eq} \\ &\epsilon^1 : (\partial_{t_0} + c_{i\alpha}\partial_\alpha) f_i^{(0)} = -\sum_j A_{ij} f_j^{(1)} + F_i \\ &\epsilon^2 : \partial_{t_1} f_i^{(0)} + (\partial_{t_0} + c_{i\alpha}\partial_\alpha) f_i^{(1)} + \frac{(\partial_{t_0} + c_{i\alpha}\partial_\alpha)^2 f_i^{(0)}}{2} = -\sum_j A_{ij} f_j^{(2)} \\ &\epsilon^2 : \partial_{t_1} f_i^{(0)} + (\partial_{t_0} + c_{i\alpha}\partial_\alpha) f_i^{(1)} + \frac{(\partial_{t_0} + c_{i\alpha}\partial_\alpha)(-\sum_j A_{ij} f_j^{(1)} + F_i)}{2} = -\sum_j A_{ij} f_j^{(2)}. \end{aligned} \tag{5.31}$$

As in the case with the BGK we summarize the second and the third equations in system

(5.31) by index i, obtaining:

$$\begin{aligned}
&\partial_{t_0}\rho^m + \partial_\alpha \rho^m u_\alpha^m = -\sum_{ij} A_{ij} f_j^{(1)} + \sum_i F_i \\
&\partial_{t_1}\rho^m + \partial_{t_0}\sum_i f_i^{(1)} + \partial_\alpha \sum_i c_{i\alpha} f_i^{(1)} - \partial_{t_0}\frac{\sum_{ij} A_{ij} f_j^{(1)}}{2} - \partial_\alpha \frac{\sum_{ij} c_i A_{ij} f_j^{(1)}}{2} + \\
&\partial_{t_0}\frac{\sum_i F_i}{2} + \partial_\alpha \frac{\sum_i c_{i\alpha} F_i}{2} = -\sum_{ij} A_{ij} f_j^{(2)}.
\end{aligned} \tag{5.32}$$

We plug the known moments of $\sum_i f_i^{(1)}$ and $\sum_i c_{i\alpha} f_i^{(1)}$ from (5.30) to the system (5.32). Also, the expression for the collision operator $\sum_i A_i^{(k)} A_{ij} = \omega_k A_j^{(k)}$ is used:

$$\begin{aligned}
&\partial_{t_0}\rho^m + \partial_\alpha \rho^m u_\alpha^m = -\omega_0 \sum_i f_j^{(1)} + \sum_i F_i \\
&\partial_{t_0}\rho^m + \partial_\alpha \rho^m u_\alpha^m = \omega_0 \frac{M}{2} + \sum_i F_i \\
&\partial_{t_1}\rho^m - \partial_{t_0}\frac{M}{2} - \partial_\alpha \frac{F_\alpha}{2} - \omega_0 \partial_{t_0} \frac{\sum_i f_i^{(1)}}{2} - \omega_{1,2}\partial_\alpha \frac{\sum_i c_{i\alpha} f_i^{(1)}}{2} + \\
&\partial_{t_0}\frac{\sum_i F_i}{2} + \partial_\alpha \frac{\sum_i c_{i\alpha} F_i}{2} = -\omega_0 \sum_i f_i^{(2)} = 0 \\
&\partial_{t_1}\rho^m - \partial_{t_0}\frac{M}{2} - \partial_\alpha \frac{F_\alpha}{2} + \omega_0 \partial_{t_0}\frac{M}{4} + \omega_{1,2}\partial_\alpha \frac{F_\alpha}{4} + \partial_{t_0}\frac{\sum_i F_i}{2} + \partial_\alpha \frac{\sum_i c_{i\alpha} F_i}{2} = 0.
\end{aligned} \tag{5.33}$$

The following terms are set to simplify the equation (5.33):

$$\begin{aligned}
&\sum_i F_i = \left(1 - \frac{\omega_0}{2}\right) M \\
&\sum_i F_i c_{i\alpha} = \left(1 - \frac{\omega_{1,2}}{2}\right) F_\alpha.
\end{aligned} \tag{5.34}$$

After substitutions the continuity equation with the mass term can be restored by multiplying the second equation on ϵ and summing it up with the first equation of the following system:

$$\begin{aligned}
&\partial_{t_0}\rho^m + \partial_\alpha \rho^m u_\alpha^m = M \\
&\partial_{t_1}\rho^m = 0 \\
&\partial_t \rho^m + \partial_\alpha \rho^m u_\alpha^m = M
\end{aligned} \tag{5.35}$$

The Navier-Stokes equation with the source term can be restored from multiplying the Chapman-Enskog system on $c_{i\alpha}$ and summing it up by the i index:

$$\begin{aligned}
\epsilon^1: \quad & \partial_{t_0}\rho^m u^m_\alpha + \partial_\beta \sum_i c_{i\alpha}c_{i\beta}f_i^{(0)} = -\sum_{ij} c_{i\alpha}A_{ij}f_j^{(1)} + \sum_i F_i c_{i\alpha} \\
\epsilon^2: \quad & \partial_{t_1}\rho^m u^m_\alpha + \partial_{t_0}\sum_i c_{i\alpha}f_i^{(1)} + \partial_\beta \sum_i c_{i\alpha}c_{i\beta}f_i^{(1)} - \\
& \frac{1}{2}\partial_{t_0}\sum_{ij} c_{i\alpha}A_{ij}f_j^{(1)} - \frac{1}{2}\partial_\beta \sum_{ij} c_{i\alpha}c_{i\beta}A_{ij}f_j^{(1)} + \frac{1}{2}\partial_{t_0}\sum_i c_{i\alpha}F_i + \\
& \frac{1}{2}\partial_\beta \sum_i c_{i\alpha}c_{i\beta}F_i = -\sum_{ij} c_{i\alpha}A_{ij}f_j^{(2)}
\end{aligned} \tag{5.36}$$

Let's examine some terms in the system (5.36):

$$\begin{aligned}
& \sum_i c_{i\alpha}c_{i\beta}f_i^{(0)} = \rho u^m_\alpha u^m_\beta + \frac{\rho^m}{3}\delta_{\alpha\beta} \\
& \sum_{ij} c_{i\alpha}A_{ij}f_j^{(1)} = \omega_{1,2}\sum_i c_{i\alpha}f_i^{(1)} = -\omega_{1,2}\frac{F_\alpha}{2} \\
& \sum_i F_i c_{i\alpha} = \left(1 - \frac{\omega_{1,2}}{2}\right)F_\alpha \\
& \partial_{t_0}\sum_i c_{i\alpha}f_i^{(1)} = -\frac{1}{2}\partial_{t_0}F_\alpha \\
& \frac{1}{2}\partial_{t_0}\sum_{ij} c_{i\alpha}A_{ij}f_j^{(1)} = \frac{\omega_{1,2}}{2}\partial_{t_0}\sum_i c_{i\alpha}f_i^{(1)} = -\frac{\omega_{1,2}}{4}\partial_{t_0}F_\alpha \\
& \frac{1}{2}\partial_\beta \sum_{ij} c_{i\alpha}c_{i\beta}A_{ij}f_j^{(1)} = \frac{\omega_{3,4,5}}{2}\partial_\beta \sum_i c_{i\alpha}c_{i\beta}f_j^{(1)} \\
& \frac{1}{2}\partial_{t_0}\sum_i c_{i\alpha}F_i = \frac{1}{2}\partial_{t_0}F_\alpha\left(1 - \frac{\omega_{1,2}}{2}\right) \\
& \sum_{ij} c_{i\alpha}A_{ij}f_j^{(2)} = \omega_{1,2}\sum_i c_{i\alpha}f_i^{(2)} = 0
\end{aligned} \tag{5.37}$$

Overall, the system (5.36) is represented as:

$$\begin{aligned}
\epsilon^1: \;& \partial_{t_0}\rho^m u^m_\alpha + \partial_\beta(\rho u^m_\alpha u^m_\beta + \frac{\rho^m}{3}\delta_{\alpha\beta}) = \omega_{1,2}\frac{F_\alpha}{2} + \left(1 - \frac{\omega_{1,2}}{2}\right)F_\alpha = F_\alpha \\
\epsilon^2: \;& \partial_{t_1}\rho^m u^m_\alpha - \frac{1}{2}\partial_{t_0}F_\alpha + \partial_\beta \sum_i c_{i\alpha}c_{i\beta}f_i^{(1)} - \\
& \frac{\omega_{1,2}}{4}\partial_{t_0}F_\alpha - \frac{\omega_{3,4,5}}{2}\partial_\beta \sum_i c_{i\alpha}c_{i\beta}f_j^{(1)} + \frac{1}{2}\partial_{t_0}F_\alpha\left(1 - \frac{\omega_{1,2}}{2}\right) + \\
& \frac{1}{2}\partial_\beta \sum_i c_{i\alpha}c_{i\beta}F_i = 0
\end{aligned} \tag{5.38}$$

The terms with ∂_{t_0} are eliminated giving:

$$\begin{aligned}
\varepsilon^1: \;& \partial_{t_0}\rho^m u^m_\alpha + \partial_\beta\Big(\rho u^m_\alpha u^m_\beta + \frac{\rho^m}{3}\delta_{\alpha\beta}\Big) = F_\alpha \\
\varepsilon^2: \;& \partial_{t_1}\rho^m u^m_\alpha + \Big(1 - \frac{\omega_{3,4,5}}{2}\Big)\partial_\beta \sum_i c_{i\alpha}c_{i\beta}f_i^{(1)} + \frac{1}{2}\partial_\beta \sum_i c_{i\alpha}c_{i\beta}F_i = 0
\end{aligned} \tag{5.39}$$

Let's find $\sum_i f_i c_{i\alpha}c_{i\beta}$ in the presence of the external force. This can be performed by summing up the second equation of (5.31) multiplied by $c_{i\alpha}c_{i\beta}$:

$$\begin{aligned}
& \partial_{t_0}\sum_i f_i^{(0)}c_{i\alpha}c_{i\beta} + \partial_\gamma \sum_i f_i^{(0)}c_{i\alpha}c_{i\beta}c_{i\gamma} = -\sum_{ij} c_{i\alpha}c_{i\beta}A_{ij}f_i^{(1)} + \sum_i c_{i\alpha}c_{i\beta}F_i = \\
& = -\omega_{3,4,5}\sum_i c_{i\alpha}c_{i\beta}f_i^{(1)} - \frac{\omega_0 - \omega_{3,4,5}}{3}\sum_i f_i^{(0)} + \sum_i c_{i\alpha}c_{i\beta}F_i = -\omega_{3,4,5}\sum_i c_{i\alpha}c_{i\beta}f_i^{(1)} + \\
& (\omega_0 - \omega_{3,4,5})\delta_{\alpha\beta}\frac{M}{6} + \sum_i c_{i\alpha}c_{i\beta}F_i
\end{aligned} \tag{5.40}$$

The left hand side of the equation (5.40) can be calculated using the moments of the

equilibrium distribution function as it was done in the equation (5.25):

$$\partial_{t_0}\sum_i f_i^{(0)}c_{i\alpha}c_{i\beta} = \partial_{t_0}\left(\frac{1}{3}\rho\delta_{\alpha\beta} + \rho u_\alpha u_\beta\right)$$
$$\partial_{t_0}\left(\frac{1}{3}\rho\delta_{\alpha\beta}\right) = \frac{M}{3}\delta_{\alpha\beta} - \frac{\delta_{\alpha\beta}}{3}\partial_\gamma\rho^m u_\gamma^m$$

$$\begin{aligned}
&\partial_{t_0}\rho u_\alpha u_\beta = -u_\alpha u_\beta\partial_{t_0}\rho + u_\alpha\partial_{t_0}\rho u_\beta + u_\beta\partial_{t_0}\rho u_\alpha = \\
&- u_\alpha u_\beta(M - \partial_\gamma\rho^m u_\gamma) + u_\alpha(F_\beta - \partial_\gamma(\rho u_\beta u_\gamma + \frac{\rho^m}{3}\delta_{\beta\gamma})) + \\
&u_\beta(F_\alpha - \partial_\gamma(\rho^m u_\alpha^m u_\gamma^m + \frac{\rho^m}{3}\delta_{\alpha\gamma})) \\
&\partial_{t_0}\rho u_\alpha u_\beta \approx u_\alpha F_\beta + u_\beta F_\alpha - \frac{u_\alpha}{3}\partial_\beta\rho^m - \frac{u_\beta}{3}\partial_\alpha\rho^m
\end{aligned} \tag{5.41}$$

$$\partial_\gamma\sum_i f_i^{(0)}c_{i\alpha}c_{i\beta}c_{i\gamma} = \partial_\gamma\left(\frac{\rho^m}{3}u_\alpha\delta_{\beta\gamma} + \frac{\rho^m}{3}u_\beta\delta_{\alpha\gamma} + \frac{\rho^m}{3}u_\gamma\delta_{\alpha\beta}\right) =$$
$$\frac{\delta_{\alpha\beta}}{3}\partial_\gamma\rho^m u_\gamma + \frac{1}{3}\partial_\beta\rho^m u_\alpha + \frac{1}{3}\partial_\alpha\rho^m u_\alpha$$

Altogether,

$$\partial_{t_0}\sum_i c_{i\alpha}c_{i\beta}f_i^{(0)} + \partial_\gamma\sum_i c_{i\alpha}c_{i\beta}c_{i\gamma}f_i^{(0)} = \frac{M}{3}\delta_{\alpha\beta} + u_\alpha F_\beta + u_\beta F_\alpha + \frac{\rho}{3}\partial_\beta u_\alpha + \frac{\rho}{3}\partial_\alpha u_\beta \tag{5.42}$$

$$\sum_i c_{i\alpha}c_{i\beta}f_i^{(1)} = \frac{\frac{\delta_{\alpha\beta}}{6}(\omega_0 - \omega_{3,4,5})M + \sum_i c_{i\alpha}c_{i\beta}F_i - \frac{1}{3}\rho^m\partial_\beta u_\alpha - \frac{1}{3}\rho^m\partial_\alpha u_\beta - \frac{M}{3}\delta_{\alpha\beta} - u_\alpha F_\beta - u_\beta F_\alpha}{\omega_{3,4,5}} \tag{5.43}$$

After substitution to (5.39):

$$\begin{aligned}
&\partial_{t_1}\rho^m u^m_\alpha + \left(1-\frac{\omega_{3,4,5}}{2}\right)\partial_\beta \sum_i c_{i\alpha}c_{i\beta}f_i^{(1)} + \frac{1}{2}\partial_\beta \sum_i c_{i\alpha}c_{i\beta}F_i = 0\\
&\partial_{t_1}\rho^m u^m_\alpha + \left(1-\frac{\omega_{3,4,5}}{2}\right)\partial_\beta \frac{\frac{\delta_{\alpha\beta}}{6}(\omega_0-\omega_{3,4,5})M + \sum_i c_{i\alpha}c_{i\beta}F_i - \frac{1}{3}\rho^m\partial_\beta u_\alpha -}{}\\
&\frac{\frac{1}{3}\rho^m\partial_\alpha u_\beta - \frac{M}{3}\delta_{\alpha\beta} - u_\alpha F_\beta - u_\beta F_\alpha}{\omega_{3,4,5}} + \frac{1}{2}\partial_\beta \sum_i c_{i\alpha}c_{i\beta}F_i = 0\\
&\partial_{t_1}\rho^m u^m_\alpha - \left(\frac{1}{w_{3,4,5}}-\frac{1}{2}\right)\left(1-\frac{\omega_0-\omega_{3,4,5}}{2}\right)\partial_\alpha\frac{M}{3} + \left(\frac{1}{2}+\frac{1}{w_{3,4,5}}-\frac{1}{2}\right)\partial_\beta\sum_i c_{i\alpha}c_{i\beta}F_i =\\
&\left(\frac{1}{w_{3,4,5}}-\frac{1}{2}\right)\partial_\beta\left(\frac{1}{3}\rho^m\partial_\beta u_\alpha + \frac{1}{3}\rho^m\partial_\alpha u_\beta + u_\alpha F_\beta + u_\beta F_\alpha\right)
\end{aligned} \tag{5.44}$$

Let's impose the second moment of the force:

$$\sum_i c_{i\alpha}c_{i\beta}F_i = \left(1-\frac{w_{3,4,5}}{2}\right)\left[\left(1-\frac{\omega_0-\omega_{3,4,5}}{2}\right)\frac{M}{3}\delta_{\alpha\beta} + u_\alpha F_\beta + u_\beta F_\alpha\right] \tag{5.45}$$

Then, the Navier-Stokes equation is restored with the external force:

$$\begin{aligned}
&\partial_{t_0}\rho^m u^m_\alpha + \partial_\beta \rho^m u_\alpha u_\beta = -\frac{1}{3}\partial_\alpha\rho + F_\alpha\\
&\partial_{t_1}\rho^m u^m_\alpha = \left(1-\frac{w_{3,4,5}}{2}\right)\frac{\partial_\beta}{3}\rho^m\left(\partial_\alpha u_\beta + \partial_\alpha u_\beta\right)
\end{aligned} \tag{5.46}$$

The force populations are restored as follows:

$$\begin{aligned}
F_i = \quad & w_i\Bigg(\left(1-\frac{\omega_0}{2}\right)M + 3\left(1-\frac{\omega_{1,2}}{2}\right)\boldsymbol{F}\cdot\boldsymbol{c_i} + \left(1-\frac{\omega_{3,4,5}}{2}\right)Q_{i\alpha\beta}(F_\alpha u_\beta + F_\beta u_\alpha) +\\
& \frac{3}{4}M\omega_3(\omega 0-\omega 3)\left(c_{ix}c_{ix}-\frac{1}{3}\right) + \frac{3}{4}M\omega_5(\omega_0-\omega_5)\left(c_{iy}c_{iy}-\frac{1}{3}\right)\Bigg)\\
F_0 = \quad & M\left(1-\frac{\omega_0}{2}\right) - \sum_{i=1}^{8}F_i =\\
& \frac{1}{9}\left(6F_x(\omega_3-2)u_x + 6F_y(\omega_5-2)u_y + M\left(-\omega_0(\omega_3+\omega_5+2)+\omega_3^2+\omega_5^2+4\right)\right)
\end{aligned} \tag{5.47}$$

The result is of importance in the proper implementation of the force and mass term to the LBM. The next section tests the results obtained on the simplest Poiseuille flow case.

5.11 Numerical Results

The MRT formulation of the force population coincides with the BGK case thoroughly described by Guo et al. (2002). To check the validity of the code we implemented the simplest case as Pouseiuelle flow. For the given pressure gradient $\frac{\mathrm{d}P}{\mathrm{d}x}$ the flow velocity profile has the parabolic view:

$$u(y) = \frac{H^2}{8\nu}\frac{\mathrm{d}P}{\mathrm{d}x}\left(1 - \frac{2y}{H}\right). \tag{5.48}$$

However, for numerical setup with bounceback nodes (coming populations equal leaving populations) on boundaries and the body force equivalent to $F = -\frac{\mathrm{d}P}{\mathrm{d}x}$, the exact width of the channel doesn't equal H, but depends on the relaxation time τ, and it is viscosity dependant (Ginzburg and d'Humières, 2003) for TRT model:

$$H_{eff}^2 = N_y^2 + \frac{16}{3}\left(\frac{1}{\lambda^+} - \frac{1}{2}\right)\left(\frac{1}{\lambda^-} - \frac{1}{2}\right), \tag{5.49}$$

where λ^+ and λ^- are the eigenvalues of the TRT model. Notice that $\omega = \lambda^+ = \lambda^-$ restores the BGK model collision operator. The proper inclusion of the force has to lead to a result consistent with the analytical formulae indicated. The LBM is simulated on the rectangular grid, thus, the analytical velocity profile through the grid coordinate is as follows:

$$u(j) = \frac{4u_{max}}{N_y^2}\left(j - \frac{1}{2}\right)\left(N_y + \frac{1}{2} - j\right), \tag{5.50}$$

where j is the vertical index of the node and $u_{max} = \dfrac{N_y^2\dfrac{\mathrm{d}P}{\mathrm{d}x}}{8\nu}$. Our goal is to check the validity of the u_{max} equation along with the analytical calculation of the effective width of the channel. A few cases were studied:

- The Guo implementation of the force (Guo et al., 2002) for BGK with the macro velocity shifted as $\rho\boldsymbol{u^m} = \sum_i f_i\boldsymbol{c_i} + \frac{\boldsymbol{F}}{2}$ and the force population equation is as

follows:

$$F_i = w_i\left(1-\frac{\omega}{2}\right)\left(3(\boldsymbol{c_i}-\boldsymbol{u^m})+9(\boldsymbol{c_i}\cdot\boldsymbol{u^m})\boldsymbol{c_i}\right)\cdot\boldsymbol{F} \tag{5.51}$$

- The shift velocity implementation adopted by Shan and Chen (1994), where force implemented by the construction of the equilibrium function, as:

$$f_i^{eq} = w_i\rho\left(1+3\boldsymbol{c_i}\cdot\boldsymbol{u^{eq}}+\frac{9}{2}\left(c_{i\alpha}c_{i\beta}-\frac{\delta_{\alpha\beta}}{3}\right)u_\alpha^{eq}u_\beta^{eq}\right) \tag{5.52}$$

  where $\rho\boldsymbol{u^{eq}} = \sum_i f_i\boldsymbol{c_i} + \frac{\boldsymbol{F}}{\omega}$ and macroscopic velocity is restored as $\rho\boldsymbol{u^m} = \sum_i f_i\boldsymbol{c_i}$.

- The popular method used often in literature (Luo, 2009a; Succi, 2001) is to add the force population as $F_i = 3\boldsymbol{F_i}\boldsymbol{c_i}$. The macroscopic velocity is not changed from the original definition $\rho\boldsymbol{u^m} = \sum_i f_i\boldsymbol{c_i}$.

- The MRT implementation is as stated in this work. Note that by taking all eigenvalues equal to the BGK parameter ω the MRT implementation fully coincides with Guo's implementation of the force. Also, if one takes the $\omega_7 = \omega_8 = 8\dfrac{2-\omega_{BGK}}{8-\omega_{BGK}}$ as stated in (Ginzburg and d'Humières, 2003; Luo, 2009a) the profile should be restored with the machine accuracy.

For numerical simulations the maximum velocity in the centre is fixed by varying the force, $\dfrac{\mathrm{d}P}{\mathrm{d}x}$; grid number, $Ny \propto H$; and viscosity, ν:

$$u_{max} = \frac{H^2}{8\nu}\frac{\mathrm{d}P}{\mathrm{d}x} \tag{5.53}$$

A few grids were chosen as $N_y = 7$, $N_y = 21$, $N_y = 35$,$N_y = 49$ as the multiples of 7, and $N_x = 4$. The N_y was taken as the odd number to insure that the maximum is achieved right in the centre. The system comes to the equilibrium after 120000 time steps. The force F_x was taken to insure that the analytical velocity (5.53) doesn't depend on the viscosity and grid number N_y:

$$F_x = 0.0001\frac{7}{Ny}\frac{2-\omega}{\omega}. \tag{5.54}$$

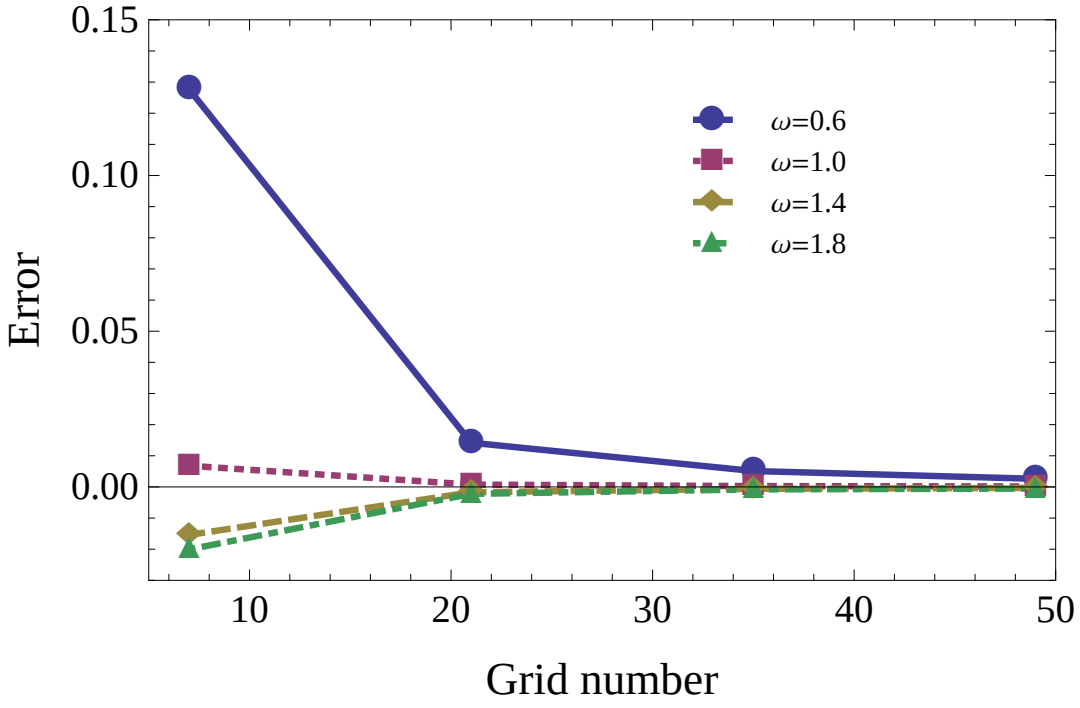

Figure 5.1: The relative error of the centre velocity for the proper force implementation depending on the grid number for different BGK parameter ω. The figure shows that the error is viscosity dependent.

The forcing term (5.54) implies the max velocity in the centre $u_{max} = 0.003675$, which is certainly in the low Mach regime. Few figures represent the error given for different methods on grid number. Figure 5.1 shows the dependency of the proper incorporation force velocity error depending on the grid number. The error is viscosity dependent, because the effective width of the channel (5.49) is viscosity dependent (ω parameter). Figure 5.2 shows the error of the different force incorporation depending on the grid number for the specific parameter $\omega = 1.0$. The error depends on the force implementation. Only MRT gives the exact velocity profile which doesn't depend on the viscosity, ω, and grid number, H.

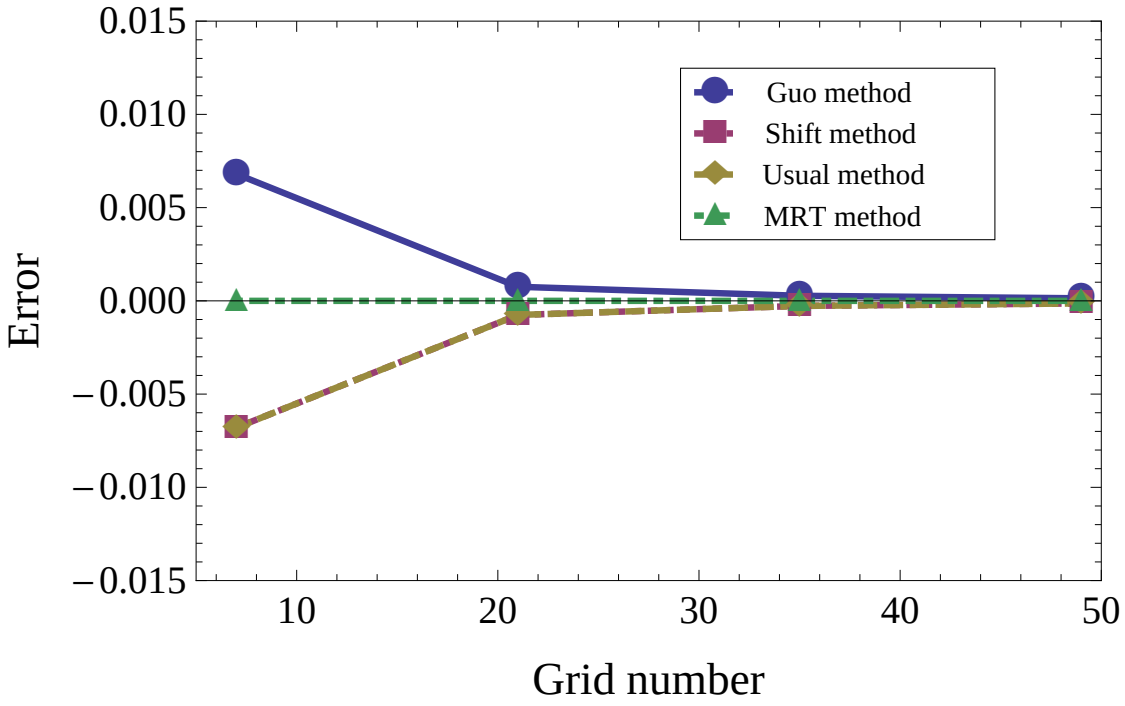

Figure 5.2: The relative error of the centre velocity for the different methods force implementation depending on the grid number for $\omega = 1.0$. The figure shows that the error depends on the implementation of the force. The MRT force incorporation method for the given parameter gives the error within the machine accuracy.

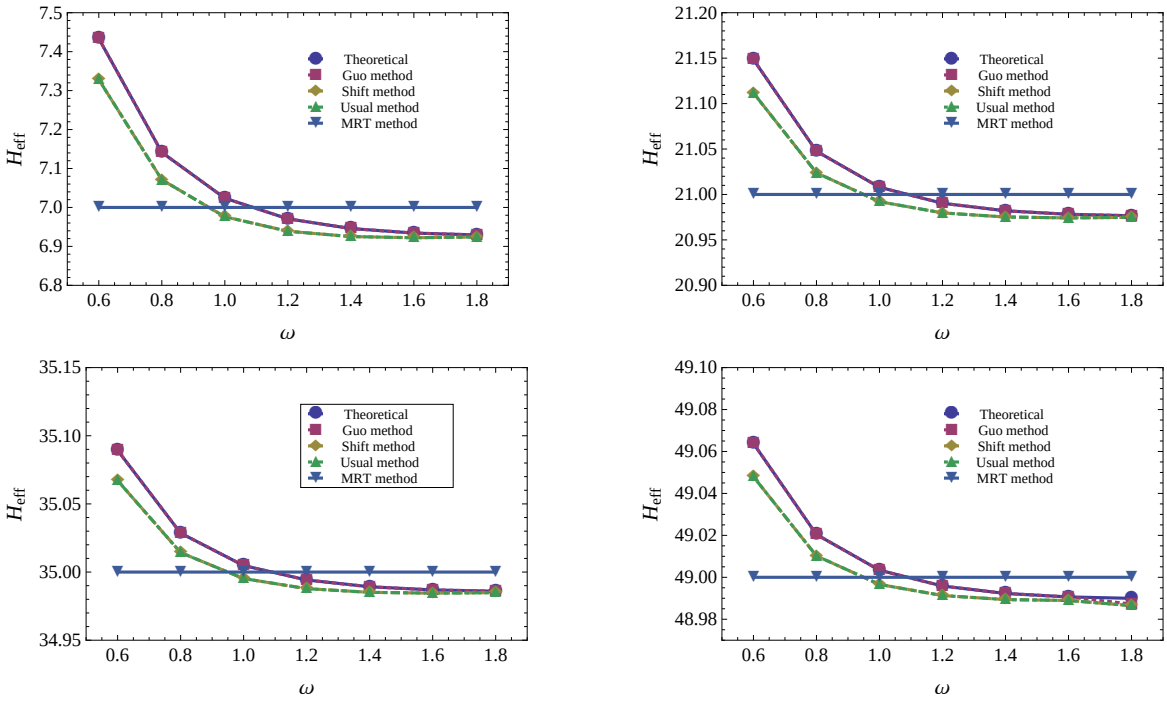

Figure 5.3: The effective width for different methods. Notice that we change the grid number and the viscosity to keep the centre velocity the same. The Guo method gives the same results as theoretical calculations (5.49) for the effective width of the channel. The shifting velocity method gives the same result as the usual force incorporation.

However, the Guo et al. (2002) force implementation restores the exact behaviour of the effective channel width H_{eff}, which can be calculated from the centre velocity:

$$H_{eff} = \sqrt{\frac{8\nu u_{max}}{\frac{\mathrm{d}P}{\mathrm{d}x}}} \tag{5.55}$$

The results for effective channel width for different methods of the force implementation are presented in Fig. 5.3 depending on the BGK parameter ω. The results of Guo implementation coincides with the theoretical curve obtained for BGK. The results of the shifting velocity method coincide with the usual force implementation. However, they do not give the same results as theoretical considerations. The MRT method with the energy flux eigenvalues taken appropriately, $\omega_7 = \omega_8 = 8\dfrac{2-\omega_{BGK}}{8-\omega_{BGK}}$ and $\omega_3 = \omega_4 = \omega_5 = \omega$, give the machine accurate exact result for the H_{eff}.

The outline of the section is that the force implementation given here is consistent, and the results are within machine accuracy. The MRT force implementation coincides with the Guo method force incorporation if all eigenvalues have the same value. The Guo method is defined only for BGK and coincides with the theoretical equations for the Poiseulle flow for the BGK model. However, it's not able to obtain the machine accuracy Poiseuille profile. The improper choice of the ω parameter can lead to the relative error of 5-10% in the centre velocity for small grid numbers. The increase of the grid number improves the accuracy for all mentioned methods. The usage of the bounce-back boundary conditions for performing porous media calculations for all methods except for the Guo or MRT force incorporation should be avoided as far as the certain location of the solid wall is viscosity dependant. To check further the validity of the method, few numerical experiments can be suggested, i.e. Taylor-Green vortex decay.

Chapter 6

MRT with Shan-Chen model

6.1 Introduction

Section 2.2 outlines the fact that there are no multiphase models without drawbacks. The MRT model which invokes better properties with tuning free parameters can be the appropriate choice to improve the multiphase models. The historical development of the MRT application to multiphase models began with the color model. Note that sometimes the MRT model not only improves the stability, but it is a necessary choice to simulate physical phenomena properly. Ginzbourg and Adler (1995) implemented the MRT model to properly simulate interface conditions between two phases. The viscosity independent location of simple boundaries (Ginzbourg and Adler, 1994) and interfaces (Ginzbourg and Adler, 1995) is also possible only with the application of MRT to the multiphase. The MRT has also been applied to simulate multiphase phenomena, e.g., Poiseuille flow in inclined channels with different kinematic viscosities (Ginzbourg and Adler, 1995) and for free-interface flow (Ginzburg and Steiner, 2002). Tölke et al. (2006) applied MRT for multiphase flow simulations on adaptive grids. McCracken and Abraham (2005) incorporated the Carnahan-Sterling EOS into the force term. The model has been tested for different multiphase flows conditions, such as capillary waves, Laplace-Young test, Lamb test. Later on, Mukherjee and Abraham (2007) incorporated a pressure-based MRT high-density-ratio two-phase LBM, and claimed the ability to simulate density ratios up to 1000. The free-energy MRT model was introduced by Pooley et al. (2009), which gives the proper contact angle between solid and fluid phases.

Despite many MRT applications to the multiphase flows, the popular Shan-Chen

model has not been used with the MRT model. Kuzmin et al. (2008) and Kuzmin and Mohamad (2009) applied the MRT collision operator with the Shan-Chen model. The results showed significant improvement of the achieved gas-liquid ratio, which is a critical issue for many LBM multiphase simulations. The extended equilibrium improves the gas-liquid ratio for droplet simulations by 30%, and the MRT collision operator improves gas-liquid ratio by almost 30%. Thus, the combination of the MRT and the extended equilibrim function (3.72) permits obtaining droplets with a gas-liquid density as 160% of the original Shan-Chen model gas-liquid ratio, around 100. The following will give a thorough consequential improvements for the Shan-Chen model. We start with hte BGK original Shan-Chen implementation, then apply the proper force BGK implementation. Then the MRT model is applied to the Shan-Chen with the extended equilibrium and to the original equilibrium function. The proper implementation and original shifting velocity force implementations will be considered here.

6.2 Numerical Results

The numerical results are performed for the droplet put in the centre of domain by size 128x128 different droplets initialized with ρ_l. The remaining domain is initialized with ρ_g. The densities ρ_l and ρ_g are obtained from the equation of state, when the parameter G is given. The radiuses are varied from 10 to 30 lattice units in order to obtain the Laplace law correlation. Also, the parameters G and ω were varied during the process of simulations.

6.2.1 BGK shifting velocity

The BGK case with the shifting velocity was implemented first. The radiuses of the droplet were taken as 10, 15,20, 25, and 30 lattice units. The BGK simulation scheme with shifting velocity is stable to $G = -8.5$ giving the gas-liquid ratio around 100 with $\omega = 1.0$.

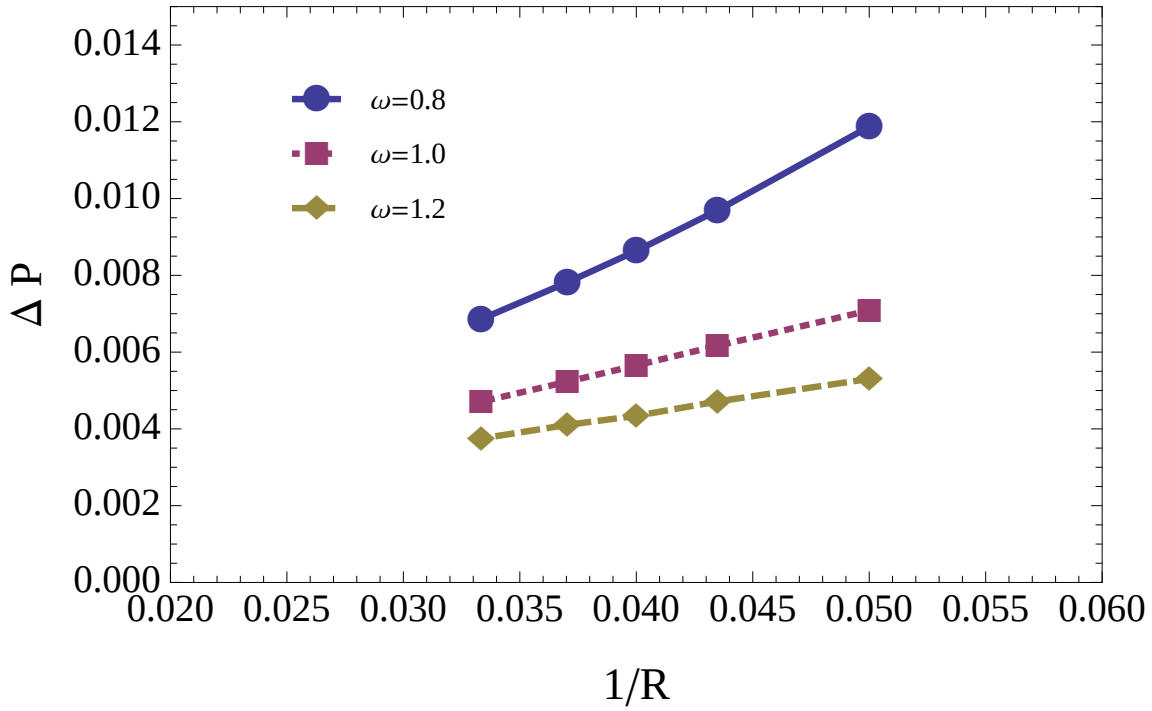

Figure 6.1: The Laplace law for different values of the relaxation parameter $\omega = \{0.8, 1.0, 1.2\}$. Notice that the results show the huge dependence of the surface tension parameter σ on the relaxation parameter ω.

The MRT model by varying ghost eigenvalues achieves the gas-liquid ratio around 160 (Kuzmin and Mohamad, 2009) with $\omega = 1.0$. However, if the omega is tuned (different from unity) when the achieved gas-liquid ratio decreases rapidly to approximately 40-60 depending on the relaxation parameter ω. This is certainly a limitation for the BGK shifting velocity method as far as the achieved gas-liquid ratio should not depend on ω. But in the case with shifting velocity, it does. Moreover, other important characteristics as the surface tension is viscosity dependent. Fig. 6.1 shows the Laplace law dependancy ($G = -6.0$) on the relaxation parameter for the set of simulations with radii 20,23,25,27 and 30 with different relaxation parameters $\omega = 0.8$, $\omega = 1.0$ and $\omega = 1.2$.

In fact, the linear regression for the curves for Fig. 6.1 reveals the following:

- $\omega = 0.8$: ΔP=-0.003337187908 + 0.3019847295 $\frac{1}{R}$

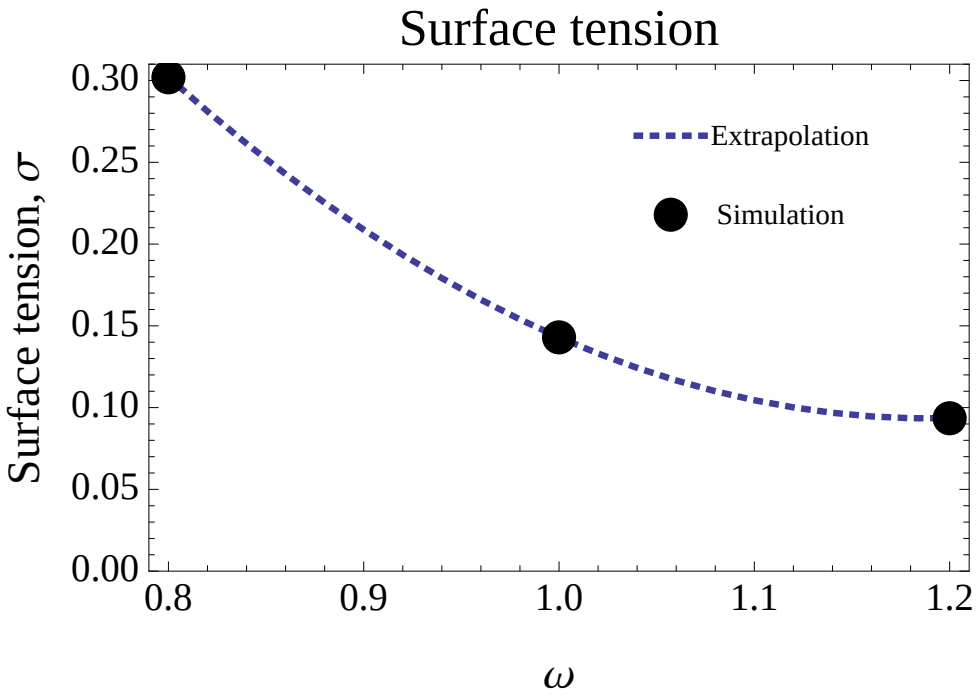

Figure 6.2: The surface tension dependency on the relaxation parameter $\omega = \{0.8, 1.0, 1.2\}$. The parabolic approximation is also shown.

- $\omega = 1.0$: ΔP=-0.00006021553023 + 0.1429528935 $\frac{1}{R}$
- $\omega = 1.2$: ΔP=0.0006300077551 + 0.0934896907 $\frac{1}{R}$

The tuning of the relaxation parameter from 0.8 to 1.2 decreases the surface tension σ by the factor of three. Figure 6.2 shows the surface tension dependency on the relaxation parameter ω. However, the viscosity dependence of the surface tension can be eliminated with the proper implementation of the force (Guo et al., 2002).

6.2.2 Proper force implementation

By taking the proposed method of Guo et al. (2002), the gas liquid ratio of approximately 60 with $G = -5.7$, with $\rho_{liq} = 4.29901$ and $\rho_{gas} = 0.04206$, can be achieved. However, the Laplace law and surface tension do not depend on the relaxation parameter, Fig. 6.3. Even the shifting velocity force implementation seems a bit more stable than the

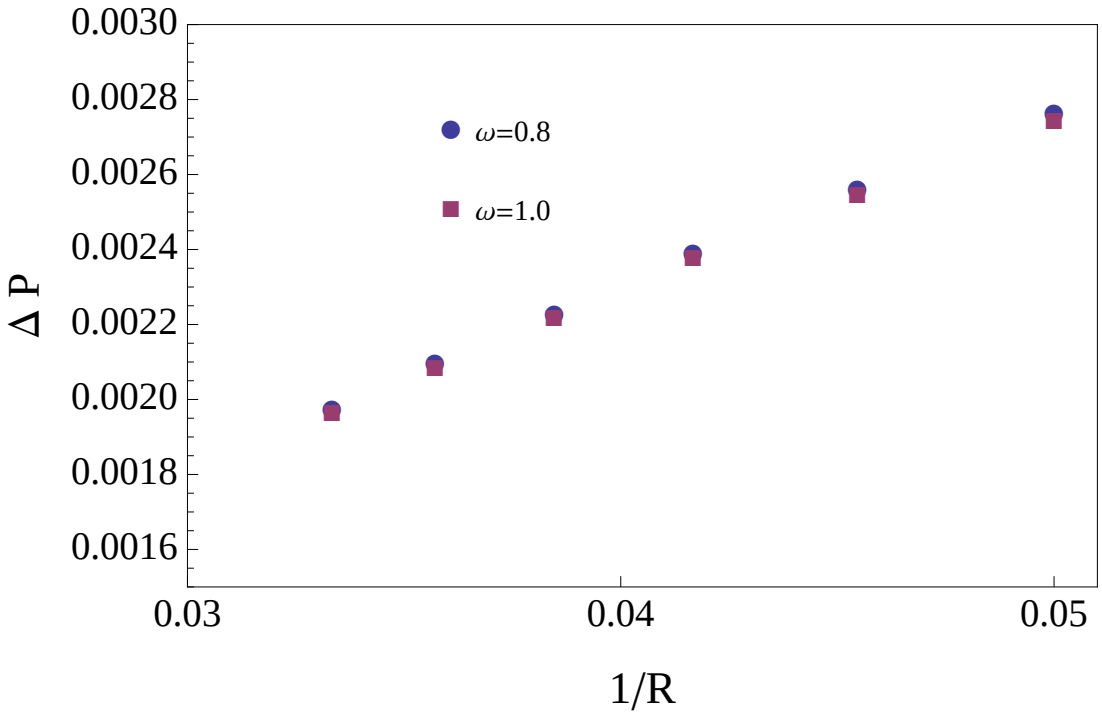

Figure 6.3: The Laplace law dependency on the relaxation parameter $\omega = \{0.8, 1.0, 1.2\}$ for Guo force implementation.

Guo force implementation, however, the Guo force implementation though not gaining in stability but it does give proper behaviour for the Laplace law.

6.2.3 Guo force implementation with extended equilibrium

We refer to the extended equilibrium presented by equation (5.10) with Guo force implementation. For the sake of completeness the table of stability for different ω is presented for Guo force implementation with extended equilibrium and usual equilibrium. Table 6.1 summarizes the stability of flow regimes. It shows that it is always good to have under-relaxed values used with Shan-Chen. The under-relaxed value of ω can be obtained through the dimensionalization procedure, when other parameters such as grid number, and velocity are varied. Also, the implication of the higher order velocity terms in the equilibrium gives a tangible stability improvement in comparison with the usual

Table 6.1: Flow regimes for the range of $G = -5.0$ to $G = -6.0$. The N/A stands for unstable regime, where simulations produce NaN values. The upper value is for the usual equilibrium. The lower value is for the extended equilibrium.

G	-5.0	-5.1	-5.2	-5.3	-5.4	-5.5	-5.6	-5.7	-5.8	-5.9	-6.0
ω											
0.6	Yes	Yes	Yes	Yes	Yes	Yes	No	No	No	No	No
	Yes	Yes	Yes	Yes	Yes	Yes	Yes	Yes	Yes	Yes	Yes
0.8	Yes	Yes	Yes	Yes	Yes	Yes	No	No	No	No	No
	Yes	Yes	Yes	Yes	Yes	Yes	Yes	Yes	Yes	Yes	Yes
1.0	Yes	Yes	Yes	Yes	Yes	Yes	No	No	No	No	No
	Yes	Yes	Yes	Yes	Yes	Yes	Yes	Yes	Yes	No	No
1.2	Yes	Yes	Yes	Yes	Yes	Yes	No	No	No	No	No
	Yes	Yes	Yes	Yes	Yes	Yes	No	No	No	No	No
1.4	Yes	Yes	Yes	Yes	No	No	No	No	No	No	No
	Yes	Yes	Yes	Yes	No	No	No	No	No	No	No
1.6	Yes	Yes	No	No	No	No	No	No	No	No	No
	Yes	Yes	No	No	No	No	No	No	No	No	No
1.8	No	No	No	No	No	No	No	No	No	No	No
	No	No	No	No	No	No	No	No	No	No	No

choice of the equilibrium function.

The consistency of the flow beyond that available for the usual force incorporation was tested. Fig. 6.4 presents two Laplace law curves when the Guo force incorporation is unstable. The Laplace law is almost ideally fulfilled when $\omega = 0.6$ and $\omega = 0.8$.

On the other hand it can be observed that the curves for the extended and usual equilibrium coincide, Fig. 6.5, for different relaxation parameter ω.

6.2.4 MRT force implementation with extended equilibrium

We aim to tune free eigenvalues to improve the stability and to increase the gas-liquid density ratio. When all the eigenvalues of the MRT model $\omega_i = \omega_{BGK}$ the BGK version is restored but with the extended equilibrium not the usual one. Even the MRT gives advantages when applied to the shifting velocity method(Kuzmin and Mohamad, 2009; Kuzmin et al., 2008), however, with the MRT proper force implementation the achieved

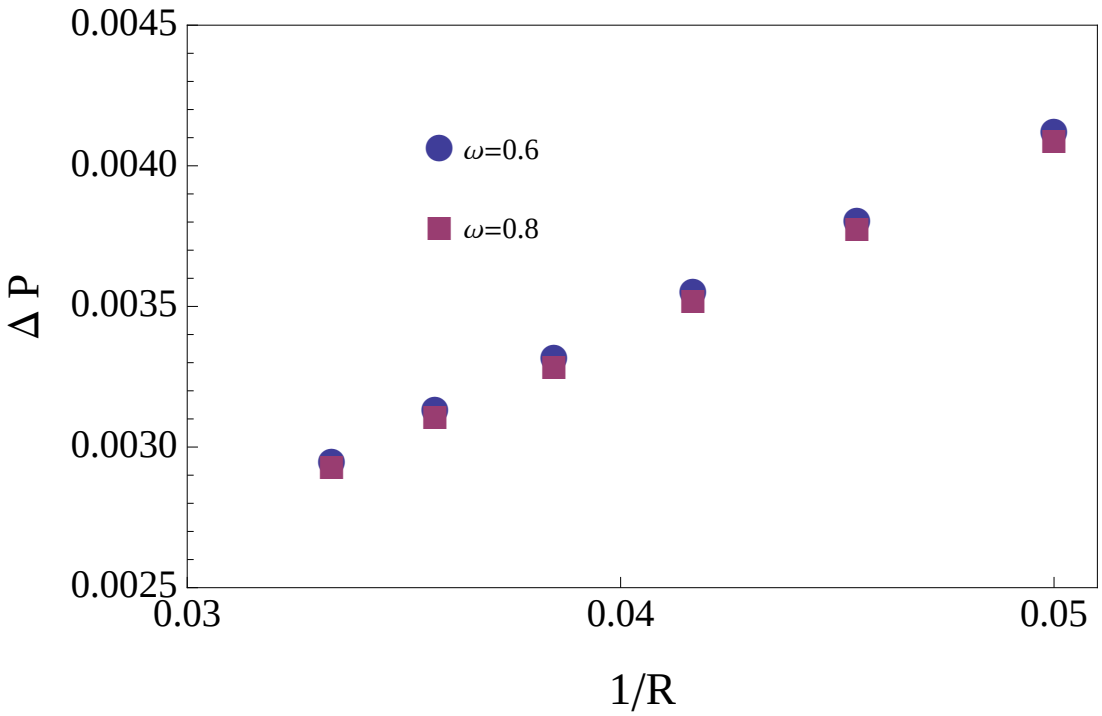

Figure 6.4: The Laplace law dependency on the relaxation parameter $\omega = \{0.6, 0.8\}$ for Guo force implementation with the extended equilibrium, $G = -5.9$, when the Guo incorporation with the usual equilibrium function is unstable. The system is consistent giving physical results.

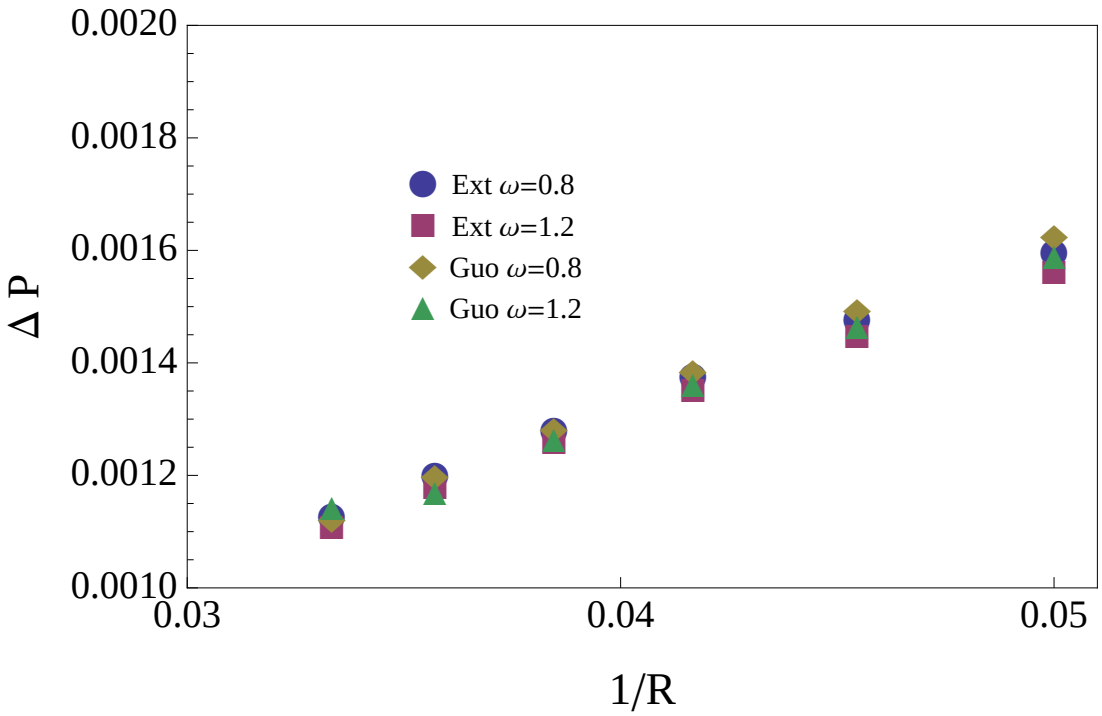

Figure 6.5: The Laplace law dependency on the relaxation parameter $\omega = \{0.8, 1.2\}$ for Guo force implementation with usual and extended equilibrium. One can see the curves coincide. $G = -5.0$ was taken to perform a simulation.

gas-liquid ratio coincides with the Guo force implementation with the extended equilibrium. During numerical experiments, the most influential factor on the stability was the eigenvalues ω_7 and ω_8 related to the energy flux. The underrelaxed values ($\omega_{7,8} \leq 1$) can improve stability but not tangibly.

6.2.5 The outline

The outline of the section is concluded in a few do's and dont's. If the simulation is planned to be carried out with dynamic droplets, the proper force implementation should be used even if the gas-liquid ratio is sacrified. The extended equilibrium should be used at any time as it gives better stability. The MRT collision operator should be used in any system involving boundary conditions as it guarantees the proper physics.

Chapter 7

Conclusion

The Shan-Chen two-phase model has had a large impact on LBM development. However, many authors apply the model to different simulations inconsistently. This work shows some advantages and disadvantages of the Shan-Chen multiphase model. The model can be used to simulate systems with moderate gas-liquid ratios around $50 - 60$. The strategy is to use the model with the better models, as the MRT model and the force inclusion method, even sacrificing the large gas-liquid ratio. It is always advantageous to use more developed models with the original Shan-Chen model in terms of proper physics behaviour. The main findings of the present work are summarized as:

- The thesis thoroughly examines the Shan-Chen model's theoretical and numerical foundations. Interface equations can help researchers to use the Shan-Chen model with the accuracy needed. Also, the developed scaling of the surface tension gives the relationship between the Shan-Chen surface tension and the Navier-Stokes surface tension. It was shown that for a fine simulation of interface conditions, the model is quite unsustainable. However, it is perfect for qualitative simulations of the interface behaviour. The Shan-Chen model gives perfect results on the macroscale level, when the interface properties are not included. This means that if the problem is described with certain macroscale parameters, including the surface tension, droplet size and gas-liquid ratio, but excluding the interface width, the Shan-Chen model predicts results consistent with both theory and experiments. Numerical experiments indicate that it is always good to have an underrelaxed BGK parameter ω for the Shan-Chen model.

- The stability can be improved with the MRT collision operator when it is applied with the original Shan-Chen method (Shan and Chen, 1994). However, the model gives the viscosity dependent surface tension. Thus, use of original Shan-Chen model is not recommended. The present work shows that the Guo method incorporation and the developed MRT force incorporation give results consistent with physics.

  Although with the developed MRT force incorporation the stability can be only slightly improved, MRT is the must choice for systems to have more realistic physical behaviour. This work found that the energy fluxes eigenvalues ω_7 and ω_8 ,when they are underrelaxed ($\omega_{7,8} \leq 1$), improve stability. The stability can also be improved by applying the developed multirange and extended equilibrium conditions, as they suppress the spurious currents around the droplet.

- The generalized Shan-Chen model is presented. It permits simulation of the systems with anisotropic momentum fluxes such as ferrofluidics systems. The model is simple to implement and has good agreement with experiment.

- The multirange potential gives the ability to separate the equation of state from the surface tension. The range of the surface tension to simulate is however limited and varies by 20% from the initial value. The interface width has some inconsistencies related to the higher order polynomials in the Shan-Chen force Taylor expansion. This is another reason that model is better to use with the macro world problems, though giving some qualitative pictures with the micro-fluidics.

- The application of the MRT collision operator with the developed MRT force implementation didn't give substantial stability improvements. However, it was shown that the proper MRT force implementation can be crucial for the systems when it is applied with the boundary conditions, i.e. bounce-back boundary conditions. The

developed MRT force implementation can be of interest for the LBM community as well as for industrial applications seeking a consistent LBM approach.

Chapter 8

Future work

There are a few of flaws in the Shan-Chen model, which can be improved. The planned future work can be divided into the following stages:

- Even though the Shan-Chen model is suitable for macroscopic simulations, the thermodynamical consistency in the Shan-Chen model can be improved in order to achieve the proper surface tension behaviour. There are a few possible ways to do it. One is to divide the surface tension term into two parts, where one part can be included into the equation of state (Lee and Fischer, 2006). Another approach is to integrate to the Shan-Chen model the free-energy approach (Sbragaglia et al., 2009), which can be utilized to obtain the proper thermodynamical behaviour.

- The eigenvalue analysis can be done in order to understand the role of the free parameters for the Shan-Chen model. It's a complicated task, because there is a pseudopotential density dependence, needed to be linearly approximated. However, the advanced techniques for stability analysis, such as the Miller theorem, mentioned by Kuzmin et al. (2009), can be used for simplification of equations obtained.

- Finally, the derived results can be applied for a droplet simulation on a arbitrarily inclined surfaces. Dynamic simulations for a droplet on surfaces are in need for the Shan-Chen model.

Appendix A

Sources

Everything presented in this work can be downloaded by issuing the following command in the linux environment:

svn co svn://136.159.105.148/home/shurik/work/development/SVN/Thesis/trunk Thesis

The material includes not only the Latex source of the thesis but the framework developed for parallel systems. All examples are implemented in this framework. The analysis of results were performed in Matlab and Mathematica files located at the same URL. The author really hopes that the work will help facilitate the development of the necessary skills for LBM newcomers to save their time on "reinventing" the wheel.

Bibliography

R. Adhikari, K. Stratford, M.E. Cates, and A.J. Wagner. Fluctuating lattice Boltzmann. *Europhys. Lett.*, 71(3):473–479, 2005.

B. Ahrenholz, J. Tölke, P. Lehmann, A. Peters, M. Krafczyk, and W. Durner. Prediction of capillary hysteresis in a porous material using lattice-Boltzmann methods and comparison to experimental data and a morhphological pore network model. 31(9): 1151–1173, 2008.

S. Ansumali, I.V. Karlin, and H.C. Öttinger. Minimal entropic kinetic models for hydrodynamics. *Europhys. Lett.*, 63lu(6):798–804, 2003.

S. Ansumali, I.V. Karlin, C.E. Frouzakis, and K.B. Boulouchos. Entropic lattice Boltzmann method for microflows. *Physica A*, 359:289–305, 2006.

P. Asinari. Semi-implicit-linearized multiple-relaxation-time formulation of lattice Boltzmann schemes for mixture modeling. *Phys. Rev. E*, 73(056705):1–24, 2006.

R. Benzi, S. Succi, and M. Vergassola. The Lattice Boltzmann Equation: Theory and Applications. *Phys. Rep.*, 222(3):145–197, 1992.

R. Benzi, L. Biferale, M Sbragaglia, S. Succi, and F. Toschi. Mesoscopic modeling of a two-phase ow in the presence of boundaries: The contact angle. *Phys. Rev. E*, 021509: 1–14, 2006.

P. L. Bhatnagar, E. P. Gross, and M. Krook. A Model for Collision Processes in Gases. I.Small Amplitude Processes in Charged and Neutral One-Component Systems. *Phys. Rev.*, 94(3):511–525, 1954.

S. Chapman and T.G. Cowling. *The mathematical theory of non-uniform gases.* Cambridge University Press, Cambridge, third edition, 1995.

B. Chun and A.J.C. Ladd. Interpolated boundary condition for lattice Botlzmann simulations of flows in narrow gaps. *Phys. Rev. E*, 75(066705):1–12, 2007.

P.J. Dellar. Bulk and shear viscosities in lattice Boltzmann equations. *Phys. Rev. E*, 64 (031203):1–11, 2001.

P.J. Dellar. Incompressible limits of lattice Boltzmann equations using multiple relaxation times. *J. Comput. Phys.*, 190:351–370, 2003.

P.J. Dellar. Lattice Kinetic Formulation for Ferrofluids. *J. Stat. Phys.*, 121:105–118, 2005.

D. d'Humières. Generalized Lattice-Boltzmann Equations. *Rarefied Gas Dynamics: Theory and Simulations. Prog. Astronaut. Aeronaut.*, 159:450–458, 1992.

D. d'Humières, I. Ginzburg, M. Krafczyk, P. Lallemand, and L.-S. Luo. Multiple-relaxation-time lattice Boltzmann models in three dimensions. *Phil. Trans. R. Soc. Lond. A*, 360:437–451, 2002.

M.M. Dupin, I. Halliday, and C.M. Care. Multi-component lattice Boltzmann equation for mesoscale blood flow. *J. Phys. A: Math. Gen.*, 36:8517–8534, 2003.

G. Falcucci, G. Chiatti, S. Succi, A.A. Mohamad, and A. Kuzmin. Rupture of a ferrofluid droplet in external magnetic fields using a single-component lattice Boltzmann model for nonideal fluids. *Phys. Rev. E*, 79(056706):1–5, 2009.

C. Flament, S. Lacis, J.-C. Bacri, A. Cebers, S. Neveu, and R. Perzynski. Measurements of ferrofluid surface tension in confined geometry. *Phys. Rev. E*, 53(5):4801–4806, 1996.

I. Ginzbourg and P.M. Adler. Boundary flow condition analysis for the three-dimensional lattice Botlzmann model. *J. Phys. France II*, 4:191–214, 1994.

I. Ginzbourg and P.M Adler. Surface Tension Models with Different Viscosities. *Transp. Porous Media*, 20:37–76, 1995.

I. Ginzburg. Generic boundary conditions for lattice Boltzmann models and their application to advection and anisotropic dispersion equations. *Adv. Wat. Res.*, 28:1196–1216, 2005a.

I. Ginzburg. Equilibrium-type and link-type lattice Boltzmann models for generic advection and anisotropic-dispersion equation. *Adv. Wat. Res.*, 28:1171–1195, 2005b.

I. Ginzburg. Lattice Boltzmann modeling with discontinious collision components: Hydrodynamic and Advection-Diffusion Equations. *J. Stat. Phys.*, 126(1):157–206, 2007.

I. Ginzburg. Consistent Lattice Boltzmann schemes for the Brinkman model of porous flow and infinite Chapman-Enskog expansion. *Phys. Rev. E*, 77(066704):1–12, 2008.

I. Ginzburg. Private communication, 2009.

I. Ginzburg and D. d'Humières. Multireflection boundary conditions for lattice Boltzmann models. *Phys. Rev. E*, 68(066614):1–30, 2003.

I. Ginzburg and K. Steiner. A free-surface lattice Boltzmann method for modelling the filling of expanding cavities by Bingham fluids. *Phil. Trans. R. Soc. Lond. A*, 360: 453–466, 2002.

I. Ginzburg, F. Verhaeghe, and D. d'Humières. Study of Simple Hydrodynamic Solutions with the Two-Relaxation-Times Lattice Bolzmann Scheme. *Commun. Comput. Phys.*, 3(3):519–581, 2008.

I. Ginzburg, D. D'Humieres, and A. Kuzmin. Note on the optimal stability of advection-diffusion Lattice Boltzmann models, and a comparison with nite-difference schemes. *J. Stat. Phys.*, submitted, 2009.

A.K. Gunstensen, D.H. Rothman, S. Zaleski, and G. Zanetti. Lattice Boltzmann model of immiscible fluids. *Phys. Rev. A*, 43(8):4320–4327, 1991.

Z. Guo, C. Zheng, and B. Shi. Discrete lattice effects on the forcing term in the lattice Boltzmann method. *Phys. Rev. E*, 65(046308):1–6, 2002.

X. He and L.-S. Luo. Theory of the lattice Botlzmann method: From the Boltzmann equation to the lattice Boltzmann equation. *Phys. Rev. E*, 56(6):6811–6817, 1997.

X. He, X. Shan, and G.D. Doolen. Discrete Boltzmann equation model for nonideal gases. *Phys. Rev. E*, 57(1):1–14, 1998.

F.J. Higuera and J. Jimenez. Boltzmann Approach to Lattice Gas Simulations. *Europhys. Lett.*, 9(7):663–668, 1989.

F.J. Higuera, S. Succi, and R. Benzi. Lattice gas dynamics with enhanced collisions. *Europhys. Lett.*, 9(4):345–349, 1989.

D.P. Jackson, R.E. Goldstein, and A.O. Cebers. Hydrodynamics of fingering instabilities in dipolar fluids. *Phys. Rev. E*, 50(1):298–307, 1994.

D. Kehrwald. *Numerical Analysis of Immiscible Lattice BGK*. PhD thesis, Fraunhofer-Institut für Techno- und Wirtschaftsmathematik, 2002.

M. Krafczyk, J. Tölke, and L.-S. Luo. Large-eddy simulations with a multiple-relaxation-time LBE model. *Int. J. Mod. Phys. B*, 1&2:33–39, 2003.

A. Kuzmin and A.A. Mohamad. Multirange Multi-Relaxation Time Shan-Chen Model with Extended Equilibrium. to be published, 2009.

A. Kuzmin, A.A. Mohamad, and S. Succi. Multi Relaxation Time Lattice Boltzmann model for multiphase flows. *Int. J. Mod. Phys. C*, 19(6):875–902, 2008.

A. Kuzmin, I. Ginzburg, and A.A. Mohamad. A role of the kinetic parameter on the stability of two-relaxation-times advection-diffusion lattice Boltzmann schemes. *Comp. Math. Appl.*, submitted, 2009.

P. Lallemand and L.-S. Luo. Theory of the lattice Boltzmann method: Dispersion, dissipation, isotropy, Galilean invariance, and stability. *Phys. Rev. E*, 61(6):6546–6562, 2000.

P. Lallemand and L.-S. Luo. Theory of the lattice Boltzmann method: Acoustic and thermal properties in two and three dimensions. *Phys. Rev. E*, 68(036706):1–25, 2003.

L. Landau and E. Lifshitz. *Fluid Mechanics*. Pergamon, Oxford, 1987.

O. Lavrova, G. Matthies, V. Polevikov, and L. Tobiska. Numerical modeling of the equilibrium shapes of a ferrofluid drop in an external magnetic field. *Proc. Appl. Math. Mech.*, 4:704–705, 2004.

R. Ledesma-Aguilar, A. Hernàndez-Machado, and I. Pagonabarraga. Three-dimensional aspects of fluid flows in channels. i.meniscus and thin film regimes. *Phys. Fluids*, 19 (102112):1–10, 2007.

T. Lee and P.F. Fischer. Eliminating parasitic currents in the lattice Boltzmann equation method for nonideal gases. *Phys. Rev. E*, 74(046709):1–7, 2006.

T. Lee and C.-L. Lin. Pressure evolution lattice-Boltzmann-equation method for two-phase flow with phase change. *Phys. Rev. E*, 67(056703):1–10, 2003.

L.-S. Luo. Unified theory of lattice Boltzmann models for non-ideal gases. *Phys. Rev. Lett.*, 81(8):1618–1621, 1998.

L.-S. Luo. Theory of the lattice Boltzmann method: Lattice Boltzmann models for nonideal gases. *Phys. Rev. E*, 62(4):4982–4996, 2000.

L.-S. Luo. A Survey of Some Recent Developments in LBE. In *ICMMES Shourt Courses*, 2009a.

L.-S. Luo. Lattice Boltzmann modelling of microchannel flow in slip flow regime. In *International Conference on Mesoscopic Methods in Science and Engineering*, 2009b.

L.S. Luo. Lattice Boltzmann Methods for Computational Fluid Dynamics, 2003.

M.E. McCracken and J. Abraham. Multiple-relaxation-time lattice-Boltzmann model for multiphase flow. *Phys. Rev. E*, 71(036701):1–9, 2005.

G.R. McNamara and G. Zanetti. Use of the Boltzmann Equation to Simulate Lattice-Gas Automata. *Phys. Rev. Lett.*, 61(20):2332–2335, 1988.

S. Mukherjee and J. Abraham. A pressure-evolution-based multi-relaxation-time high-density-ratio two-phase lattice-Boltzmann model. *Comput. Fluids*, 36:1149–1158, 2007.

R.W. Nash, R. Adhikari, and M.E. Cates. Singular forces and point-like colloids in lattice boltzmann. *Phys. Rev. E*, 77(026709):1–11, 2008.

R.R. Nourgaliev, T.N. Dinh, T.G. Theofanous, and D. Joseph. The lattice Boltzmann equation method: theoretical interpretation, numerics and implications. *Int. J. Multiph. Flow*, 29:117–169, 2003.

V.K. Polevikov. Methods for numerical modeling of two-dimensional capillary surfaces. *Comput. Meth. Appl. Math.*, 4(1):66–93, 2004.

C.M. Pooley and K. Furtado. Eliminating spurious velocities in the free-energy lattice Boltzmann method. *Phys. Rev. E*, 77(046702):1–9, 2008.

C.M. Pooley, H. Kusumaatmaja, and J.M. Yeomans. Contact line dynamics in binary lattice Boltzmann simulations. *Phys. Rev. E*, 78(056709):1–9, 2008.

C.M. Pooley, H. Kusumaatmaja, and J.M. Yeomans. Modeling capillary filling dynamics using lattice Boltzmann simulations. *Eur. Phys. J. Special Topics*, 171:63–71, 2009.

K.N. Premnath and J. Abraham. Simulations of binary drop collisions with a multiple-relaxation-time lattice-Boltzmann model. *Phys. Fluids*, 17(122105):1–21, 2005.

K.N. Premnath and J. Abraham. Three-Dimensional Multi-Relaxation Time (MRT) Lattice-Boltzmann Models for Multiphase Flow. *J. Comput. Phys.*, 224:539–559, 2007.

Y.H. Qian, D. d'Humières, and P. Lallemand. Lattice BGK Models for Navier-Stokes Equation. *Europhys. Lett.*, 17(6):479–484, 1992.

R.E. Rosensweig. *Ferrohydrodynamics*. General Publishing Company, 1997.

D.H. Rothman and J.M. Keller. Immiscible Cellular-Automaton Fluids. *J. Stat. Phys.*, 52(3/4):1119–1127, 1988.

R. Rubinstein and L.-S. Luo. Theory of the lattice Boltzmann equation: Symmetry properties of discrete velocity sets. *Phys. Rev. E*, 77(036709):1–11, 2008.

M. Sbragaglia, R. Benzi, L. Biferali, S. Succi, K. Sugiyama, and F. Toschi. Generalized lattice Boltzmann method with multirange potential. *Phys. Rev. E*, 75(026702):1–13, 2007.

M. Sbragaglia, H. Chen, X. Shan, and S. Succi. Continuum free-energy formulation for a class of lattice Botlzmann multiphase models. *Europhys. Lett.*, 86(24005):1–6, 2009.

B.R. Sehgal, R.R. Nourgaliev, and T.N. Dinh. Numerical simulation of droplet deformation and break-up by lattice-Boltzmann method. *Prog. Nucl. En.*, 34(4):471–488, 1999.

X. Shan. Analysis and reduction of the spurious current in a class of multiphase lattice Boltzmann models. *Phys. Rev. E*, 73(047701):1–4, 2006.

X. Shan and H. Chen. Simulation of nonideal gases and gas-liquid phase transitions by the lattice Boltzmann Equation. *Phys. Rev. E*, 49(4):2941–2948, 1994.

X. Shan, X.-F. Yuan, and H. Chen. Kinetic theory representation of hydrodynamics: a way beyond the Navier-Stokes equation. *J. Fluid Mech.*, 550:413–441, 2006.

S. Succi. *The Lattice Boltzmann Equation for Fluid Dynamics and Beyond*. Oxford University Press, Oxford, 2001.

M.R. Swift, W.R. Osborn, and J.M. Yeomans. Lattice Boltzmann Simulation of Nonideal Fluids. *Phys. Rev. Lett.*, 75(5):831–834, 1995.

M.R. Swift, E. Orlandini, W.R. Osborn, and J.M. Yeomans. Lattice Boltzmann simulations of liquid-gas and binary fluid systems. *Phys. Rev. E*, 54(5):5041–5052, 1996.

C. Teixeira, H. Chen, and D.M. Freed. Multi-speed thermal lattice Botlzmann method stabilization via equilibrium under-relaxation. *Comp. Phys. Commun.*, 129:207–226, 2000.

J. Thömmes, J. Becker, M. Junk, A.K. Vaikuntam, D. Kerhwald, A. Klar, K. Steiner, and A. Wiegmann. A Lattice Boltzmann Method for immiscible multiphase flow simulations using the Level Set Method. Technical report, Fraunhofer-Institut für Techno- und Wirtschaftsmathematik ITWM, 2007.

J. Tölke and M. Krafczyk. TeraFLOP computing on a desktop PC with GPUs for 3D CFD. *Int. J. Comput. Fluid Dyn.*, 22(7):443–456, 2008.

J. Tölke, S. Freudiger, and M. Krafczyk. An adaptive scheme using hierarchical grids for lattice Boltzmann multi-phase flow simulations. *Comput. Fluids*, 35:820–830, 2006.

G.E. Uhlenbeck, G.W. Ford, and E.W. Montroll. *Lectures in Statistical Mechanics*. American Mathematical Society, 1963.

S. Wolfram. *Theory and applications of cellular automata*. World Scientific Publication, 1986.

J.S. Wu and Y.L. Shao. Simulation of lid-driven cavity flows by parallel lattice Boltzmann method using multi-relaxation-time scheme. *Int. J. Numer. Meth. Fluids*, 46:921–937, 2004.

L. Wu, M. Tsutahara, L.S. Kim, and M.-Y. Ha. Three-dimensional lattice Boltzmann simulations of droplet formation in a cross-junction microchannel. *Int. J. Multiph. Flow*, 34:852–864, 2008.

H. Xi, G. Peng, and S.-H. Chou. Finite-volume lattice Boltzmann method. *Phys. Rev. E*, 59(5):6202–6205, 1999.

D. Yu, R. Mei, L.-S. Luo, and W. Shyy. Viscous flow computations with the method of lattice Boltzmann equation. *Progress in Aerospace Sciences*, 39:329–367, 2003.

Z. Yu, O. Hemminger, and L.-S. Fan. Experiment and lattice Boltzmann simulation of two-phase gas-liquid flows in microchannels. *Chem. Eng. Sci.*, 62:7172–7183, 2007.

P. Yuan and L. Schaefer. Equations of state in a lattice Boltzmann model. *Phys. Fluids*, 18(042101):1–11, 2006a.

P. Yuan and L. Schaefer. A Thermal Lattice Boltzmann Two-Phase Flow Model and Its Application to Heat Transfer Problems -Part 2. Integration and Validation. *J. Fluids Eng.*, 128:151–156, 2006b.

J. Zhang and D.Y. Kwok. Lattice Boltzmann Study on the Contact Angle and Contact Line Dynamics of Liquid-Vapor Interfaces. *Langmuir*, 20:8137–8141, 2004.

J. Zhang, B. Li, and D.Y. Kwok. Mean-field free-energy approach to the lattice Botlzmann method for liquid-vapor and solid-fluid interfaces. *Phys. Rev. E*, 69(032602):1–4, 2004.

R. Zhang and H. Chen. Lattice Boltzmann method for simulations of liquid-vapor thermal flows. *Phys. Rev. E*, 67(066711):1–6, 2003.

H.W Zheng, C. Shu, and Y.T. Chew. A lattice Boltzmann model for multiphase flows with large density ratio. *J. Comput. Phys.*, 218:353–371, 2006.

Q. Zou and X. He. On pressure and velocity boundary conditions for the lattice Botlzmann BGK model. *Phys. Fluids*, 9(6):1591–1598, 1997.